



**INSTITUTO SUPERIOR TÉCNICO**  
Universidade Técnica de Lisboa

**Synthesis, formulation and spray-drying of mixed oxides for the  
Chemical Looping Combustion process (CLC)**

**Diogo Lopes de Oliveira Marçal**

**Dissertação para obtenção do Grau de Mestre em  
Engenharia Química**

**Júri**

Presidente: Professora Doutora Maria Filipa Gomes Ribeiro (IST)

Orientadores: Professor Doutor José Manuel Félix Madeira Lopes (IST)

Doutor Mathieu Michau (IFPEN)

Vogais: Professora Doutora Ana Paula Vieira Soares Pereira Dias (IST)

Doutor Tiago Sozinho (IFPEN)

**Setembro de 2012**



# Acknowledgments

---

I feel lucky to be given the opportunity of having a professional experience in one of the most dignified investigation centers in the world. For making this experience possible, I would like to thank IST and IFPEN people involved in this matter.

I am thankful to Mathieu Michau for all the support and orientation during the internship and for the precious help with the report writing.

My special thanks to Ronald Comte for its priceless guidance and friendship throughout this six months. Without their knowledge, explanations and help this work would not be possible.

A great acknowledgement to Hugo Brunet and Thomas Regal for the support, friendship and collaboration during my work. I would like to thank Elodie Comte for the guidance and help during my work in the laboratory.

I am truly indebted and thankful to Victor Costa who received and gave us very important advices and support during the internship.

I am thankful to Professor José Madeira Lopes for the important advices for the manuscript and abstract writing.

I thank all my colleagues that came with me from IST, all the friends that I made at IFPEN and the Portuguese "family" in Lyon, who were my support during this new life experience.

Finally, I express my gratitude to my family and friends in Portugal, for the important long distance support.

# Resumo

---

Tendo em conta as crescentes preocupações com as alterações climáticas do nosso planeta, é urgente minimizar as emissões de CO<sub>2</sub>. Para concretizar esse objectivo, existe uma tecnologia bastante promissora. **Chemical Looping Combustion (CLC)** é uma oxi-combustão associada à separação e captura de CO<sub>2</sub> com baixa penalização energética. De um modo geral, CLC refere-se a um processo onde uma reação química ocorre em dois reactores distintos, nos quais circula um material sólido para conduzir uma reação química.

Para as unidades IFPEN CLC, o processo exige a utilização de um transportador de oxigénio sob a forma de partículas esféricas. Estas partículas são geralmente feitas a partir de produtos sintéticos.

A abordagem científica desenvolvida neste trabalho é baseada em interações físico-químicas entre uma fase activa e um ligante mineral inerte no interior do material final (partícula microesférica). A fase activa pode ser constituída por diversos óxidos metálicos e, no caso deste estudo, o ligante inorgânico corresponde a uma solução de alumina (boehmite peptizada).

Para este efeito, a técnica de pulverização Spray-drying foi estudada, uma vez que é um método adequado para a preparação de partículas esféricas. Operações unitárias, tais como síntese, filtração, lavagem, peneiração e calcinação foram utilizadas para testar quatro matérias-primas diferentes.

Uma das principais conclusões deste trabalho é a importância da reologia, formulação e atomização na morfologia, tamanho e textura das partículas obtidas. Foi concluído que se aumenta o tamanho das partículas e reduz-se a existência de defeitos microestruturais com o aumento da viscosidade da solução preparada.

**Palavras-chave:** Chemical looping combustion (CLC), Transportador de oxigénio, Síntese, Formulação, Spray-drying, Reologia

# Abstract

---

In the context of growing concerns with earth's climate changes, it is urgent to minimize CO<sub>2</sub> emissions. In order to do so, one combustion technology seems to be very promising.

**Chemical looping combustion (CLC)** is an oxy-combustion associated with inherent separation and capture of CO<sub>2</sub> with a low energy penalty. From a general point of view, CLC refers to a process where a chemical reaction takes place within two different reactors, and a reactive solid material circulates between both reactors to drive this chemical reaction.

Within IFPEN CLC units, the process requires use of an oxygen carrier elaborated in the form of coarse particles, generally composed by synthetic products.

The scientific approach developed in this work is based on physico-chemical interactions between an active phase and an inert mineral binder within the final material (microspherical particle). The active phase may correspond to various metal oxides and in our case the inorganic binder corresponds to an alumina sol (peptized Boehmite).

To this purpose, spray-drying technique was studied, as it is a method well suited for preparation of particles with high sphericity. Other unit operations such as synthesis, filtration, washing, milling, calcination and sieving were used to test four different raw materials.

One of the main conclusions of this work is that formulation, rheology and atomization parameters determine size, morphology and texture of particles. It was concluded that we could increase the size of the particles and decrease the existence of microstructural defects with the augmentation of viscosity.

**Keywords:** Chemical looping combustion (CLC), Oxygen Carrier, Synthesis, Formulation, Spray-drying, Rheology

# Table of Contents

---

<b>INDEX OF FIGURES.....</b>	<b>9</b>
------------------------------	----------

<b>INDEX OF TABLES.....</b>	<b>12</b>
-----------------------------	-----------

<b>1 INTRODUCTION.....</b>	<b>13</b>
----------------------------	-----------

<b>2 BIBLIOGRAPHIC STUDY.....</b>	<b>15</b>
-----------------------------------	-----------

<b>2.1 CO<sub>2</sub> capture and storage processes (CCS).....</b>	<b>15</b>
<b>2.2 Chemical-Looping Combustion (CLC).....</b>	<b>16</b>
2.2.1 CLC reactors design.....	18
2.2.2 Oxygen Carriers for CLC.....	19
2.2.3 Oxygen-carriers production.....	22
Formation of the metal and support matrix.....	22
Control of particle bulk morphology.....	24
Rigidity and curing.....	25
2.2.4 Spray-Drying.....	25
Process description.....	26
Critical Parameters.....	27
Design Considerations.....	28
<b>2.3 Rheology.....</b>	<b>35</b>

<b>3 EXPERIMENTAL SECTION.....</b>	<b>38</b>
------------------------------------	-----------

<b>3.1 Preparation of Raw Material.....</b>	<b>38</b>
3.1.1 Fe <sub>1.05</sub> Cu <sub>0.95</sub> AlO <sub>4</sub> .....	38
3.1.2 Mn Material.....	39
3.1.3 Main Equipments.....	39
Mixing Vessels.....	39
Batch Reactor.....	40
Filter Press.....	40
Spin Flash dryer.....	41
Ball Mill equipment.....	42
<b>3.2 Preparation and production of Oxygen Carriers.....</b>	<b>42</b>
3.2.1 Suspension preparation step.....	43
FeCuAl preparation.....	44
Mn <sub>x</sub> O <sub>y</sub> compound I (powder) and BMP (powder) preparation.....	44
Mn <sub>x</sub> O <sub>y</sub> compound II (suspension).....	45
Equipments.....	45
3.2.2 Atomization step.....	46
Pilot Spray Drying Tool (APV brand; Type PSD 55).....	47
3.2.3 Calcination step.....	48
Furnaces.....	49

3.2.4 Sieving .....	50
<b>3.3 Characterization Techniques .....</b>	<b>50</b>
3.3.1 Laser Granulometry .....	50
The Coulter™ LS230 laser granulometer .....	51
3.3.2 Rheology .....	51
3.3.3 Loss On Ignition.....	52
3.3.4 Scanning Electron Microscopy (SEM) .....	52
3.3.5 BET Surface and N <sub>2</sub> isotherms .....	54
3.3.6 Mercury Porosimetry .....	55
3.3.7 Bulk Density .....	55
3.3.8 Attrition resistance .....	56
<b><u>4 RESULTS &amp; DISCUSSION.....</u></b>	<b><u>57</u></b>
<b>4.1 Formulation and rheological behavior.....</b>	<b>57</b>
<b>4.2 Experimental Tests .....</b>	<b>58</b>
4.2.1 Tests on FeCuAl raw material .....	58
Test 120523 .....	62
Test 120524 .....	62
Test 120530 .....	63
Test 120601 .....	63
Test 120604 .....	63
Test 120605 .....	64
Test 120607 .....	66
Test 120611 .....	67
Test 120612 .....	67
Test 120612b .....	67
Test 120613 .....	69
Test 120614 .....	69
Test 120615 .....	69
Test 120618 .....	70
Test 120618b .....	71
Test 120618c .....	72
4.2.2 Tests on manganese oxide raw materials .....	73
Test 120711 .....	76
Test 120712 .....	76
Test 120716 .....	78
Test 120717 .....	79
Test 120718 .....	79
Test 120719 .....	81
Test 120730 .....	82
Test 120731 .....	84
<b><u>5 CONCLUSIONS &amp; PROSPECTS .....</u></b>	<b><u>91</u></b>
<b><u>6 REFERENCES.....</u></b>	<b><u>93</u></b>
<b><u>APPENDIX .....</u></b>	<b><u>96</u></b>

<b>Appendix A – Equipment characteristics .....</b>	<b>96</b>
Spray-Dryer APV .....	96
<b>Appendix B - Tests Results .....</b>	<b>97</b>
FeCuAl Synthesis.....	97
Granulometry of FeCuAl.....	97
Scanning Electron Microscopy Analysis.....	99
<b>Appendix C – Particle morphology in spray-drying .....</b>	<b>102</b>

# Index of Figures

FIGURE 1 - ATMOSPHERIC CO <sub>2</sub> CONCENTRATIONS MEASURED AT MAUNA LOA OBSERVATORY (1960-2010)[4] ..	12
FIGURE 2 - CO <sub>2</sub> CAPTURE PROCESSES [6] .....	14
FIGURE 3 - OXIDATION AND REDUCTION REACTIONS OF THE OXYGEN CARRIER .....	15
FIGURE 4 - CHEMICAL-LOOPING COMBUSTION GENERAL SCHEME [9],[10] .....	16
FIGURE 5. IFPEN IMAGES REPRESENTING THE CHEMICAL LOOPING COMBUSTION PROCESS AND A SCHEME ON CAPTURE & STORAGE OF CO <sub>2</sub> .....	17
FIGURE 6 – MASS RATIO OF ACTIVE OXYGEN FOR DIFFERENT METAL OXIDES [9] .....	19
FIGURE 7 – SCHEME OF THE IPEN SPRAY-DRYING EQUIPMENT.....	26
FIGURE 8 - ROTARY ATOMIZER [43], [44].....	28
FIGURE 9 - PRESSURE NOZZLE [44] .....	29
FIGURE 10 - TWO FLUID NOZZLE [46] .....	29
FIGURE 11 - ULTRASONIC NOZZLE [49].....	30
FIGURE 12 – USUAL PARTICLE SIZE DISTRIBUTION (PSD) OBTAINED FOR DIFFERENT TYPES OF ATOMIZERS [53] ..	31
FIGURE 13 - DIFFERENT TYPES OF SPRAY-DRYER CONFIGURATIONS [44].....	32
FIGURE 14 – EXAMPLE OF AN OPEN-CYCLE SPRAY-DRYER [54] .....	32
FIGURE 15 - EXAMPLE OF A CLOSED-CYCLE SPRAY-DRYER [54].....	33
FIGURE 16 - EXAMPLES OF A SEMI-CLOSED CYCLE SPRAY-DRYER [42] OUTRO ESQUEMA .....	33
FIGURE 17 - BEHAVIOR OF DIFFERENT TYPES OF FLUIDS [52] .....	36
FIGURE 18 – GENERAL SCHEME OF "FeCuAl" MATERIAL PRODUCTION.....	38
FIGURE 19 – IMAGE OF MIXING VESSELS USED FOR PREPARATION OF ACID AND BASIC SOLUTIONS .....	38
FIGURE 20 – BATCH REACTOR USED IN THIS WORK (VOLUME ABOUT 1 M <sup>3</sup> ) AND GENERAL SCHEME OF A STIRRED TANK REACTOR .....	39
FIGURE 21 – PICTURE OF THE INDUSTRIAL FILTER PRESS USED IN THIS WORK.....	40
FIGURE 22 – PICTURE OF THE SPIN FLASH DRYER EQUIPMENT USED IN THIS WORK.....	40
FIGURE 23 - BALL MILL EQUIPMENT USED IN THIS WORK .....	41
FIGURE 24 - SCHEME FOR PRODUCTION OF OXYGEN CARRIER PARTICLES .....	42
FIGURE 25 - PRINCIPLE SCHEME ASSOCIATED WITH AN IMAGE OF EQUIPMENTS USED FOR PREPARATION OF SUSPENSIONS .....	42
FIGURE 26 - EXAMPLE OF FORMULATION CALCULATION SHEET FOR THE EXPERIMENTAL TRIAL NAMED 120719 ..	44
FIGURE 27 – IMAGE OF ONE OF THE MIXING REACTORS USED IN THIS WORK .....	45
FIGURE 28 - EXAMPLE OF SPRAY-DRYING CONDITIONS FOR THE EXPERIMENTAL TEST 120719 .....	46
FIGURE 29 - SPRAY DRYING TOOL.....	47
FIGURE 30 - 700°C CALCINATION CURVE.....	48
FIGURE 31 - POLYVALENT MUFFLE FURNACE (FIG.A) AND HIGH TEMPERATURE CONVEYOR FURNACE (FIG.B).....	48
FIGURE 32 – IMAGES OF THE TWO SIEVING EQUIPMENTS USED IN THIS WORK .....	49
FIGURE 33 - SCHEMATIC DIAGRAM OF THE COULTER TM LS230 LASER GRANULOMETER [60].....	50
FIGURE 34 - PARALLEL PLATES CONFIGURATION AND RHEOMETER USED IN THIS WORK .....	51
FIGURE 35 - GENERAL SCHEME OF SCANNING ELECTRON MICROSCOPY, AND EQUIPMENT USED IN THIS WORK [62] .....	52
FIGURE 36 IFPEN JET CUP ATTRITION TEST.....	55
FIGURE 37 FLOW CURVES SHOWING SHEAR STRESS (PA) AND VISCOSITY (PA.S) VERSUS SHEAR RATE (S-1) FOR A "Mn SUSPENSION" .....	57
FIGURE 38 - GRANULOMETRY OF PRODUCTS FROM TEST 120523 AND 120524 AFTER SPRAY DRYING AND CALCINATION (700°C) .....	61
FIGURE 39 - GRANULOMETRY OF PRODUCTS FROM TEST 120601 AND 120604 AFTER SPRAY DRYING AND CALCINATION (700°C) .....	62
FIGURE 40 - GRANULOMETRY OF PRODUCTS FROM TEST 120605 AFTER SPRAY DRYING AND CALCINATION (700°C) .....	63
FIGURE 41 - GRANULOMETRY FOR THE RAW ATOMIZED PRODUCTS OF TEST 120604 AND 120605 .....	64
FIGURE 42 – PSD OF PRODUCTS FROM TEST 120604 AND 120605 AFTER SPRAY DRYING AND CALCINATION (700°C & 1200°C).....	65
FIGURE 43 - GRANULOMETRY FOR PRODUCT 120607 AFTER SPRAY-DRYING FOR PRESSURES OF 1 AND 1.5 BAR ...	65
FIGURE 44 - SEM IMAGES OF PRODUCT 120611 (SCALE BAR RESPECTIVELY OF 200, 100 AND 2 μM).....	66
FIGURE 45 - SEM IMAGES OF PRODUCT 120612B (SCALE BAR OF 200 AND 20 μM) .....	67
FIGURE 46 – CROSS-SECTION SEM IMAGES OF PRODUCTS 120611 AND 120612B .....	67
FIGURE 47 - SEM IMAGES OF PRODUCT 120615 (SCALE BAR OF 100 AND 20 μM) .....	68

FIGURE 48 - GRANULOMETRY OF PRODUCT 120615 AFTER SPRAY-DRYING WITH AIR PRESSURES OF 0.5, 1 AND 2 BAR.....	69
FIGURE 49 - GRANULOMETRY OF PRODUCT 120618 AFTER SPRAY-DRYING FOR PRESSURES OF 1.25, 2.5 AND 3 BAR .....	69
FIGURE 50 - GRANULOMETRY OF PRODUCT FROM TEST 120618B AFTER SPRAY DRYING AND CALCINATIONS (700°C+1200°C).....	70
FIGURE 51 - GRANULOMETRY OF PRODUCT FROM TESTS 120618 & 120618B AFTER SPRAY DRYING AND CALCINATIONS (700°C+1200°C).....	71
FIGURE 52 - SEM IMAGES SHOWING WHITE FILAMENTS OBSERVED ON THE SURFACE OF SOME FeCuAl PRODUCTS .....	71
FIGURE 53 - OPTICAL MICROSCOPY IMAGES FOR CALCINED PRODUCT BEFORE AND AFTER SIEVING (TEST 120712) .....	75
FIGURE 54 - SEM PHOTOS OF PRODUCT 120712 (SCALE BAR OF 200 AND 10 μM).....	76
FIGURE 55 – MORPHOLOGY OF DRIED SPHERES (A: HOLLOW; B: SOLID) AND REPRESENTATION OF POSSIBLE STRUCTURES. ....	77
FIGURE 56 - OPTICAL MICROSCOPY IMAGE FOR PRODUCT 120716 AFTER CALCINATION AND SIEVING .....	77
FIGURE 57 - GRANULOMETRY OF PARTICLES PRODUCED FROM TESTS WITH Mn <sub>x</sub> O <sub>y</sub> COMPOUND I.....	78
FIGURE 58 - OPTICAL MICROSCOPY IMAGES SHOWING EVOLUTION OF PRODUCT 120718 DURING ITS ELABORATION .....	79
FIGURE 59 - GRANULOMETRY OF SPRAY-DRIED PRODUCT 120718 FOR PRESSURES OF 2, 3 AND 4 BAR .....	80
FIGURE 60 - FIGURE 45 - SEM IMAGES OF PRODUCT 120719 (SCALE BAR OF 200 AND 100 μM).....	80
FIGURE 61 - OPTICAL MICROSCOPY IMAGES SHOWING EVOLUTION OF PRODUCT 120730 DURING HIS ELABORATION .....	81
FIGURE 62 - PARTICLE SIZE DISTRIBUTION OF PARTICLES PRODUCED FROM Mn <sub>x</sub> O <sub>y</sub> COMPOUND II (CONCENTRATED SOLUTION) .....	82
FIGURE 63 - TAPPED POWDER DENSITY OF PARTICLES PRODUCED FROM Mn SOLUTION IN FUNCTION OF AL BINDER CONTENT .....	83
FIGURE 64 - SEM IMAGES OF PARTICLES FROM TEST 120731 (SCALE BAR OF 200μM) .....	84
FIGURE 65 – SEM IMAGES OF PARTICLES ELABORATED RESPECTIVELY FROM Mn <sub>x</sub> O <sub>y</sub> COMPOUND I (POWDER) , Mn <sub>x</sub> O <sub>y</sub> COMPOUND II (SOLUTION) AND BMP (POWDER) AND TESTS 120712, 120719 AND 120731 (SCALE BAR OF 200μM).....	84
FIGURE 66 – SEM IMAGES OF PARTICLES FROM Mn <sub>x</sub> O <sub>y</sub> COMPOUND I , Mn <sub>x</sub> O <sub>y</sub> COMPOUND I AND BMP (TEST 120712, 120719 AND 120731 - SCALE BAR OF 100μM).....	85
FIGURE 67 - PARTICLE SIZE DISTRIBUTION OF PARTICLES PRODUCED FROM BMP (TEST 120731).....	86
FIGURE 68 - GRANULOMETRY OF PARTICLES PRODUCED FROM Mn RAW MATERIAL (120716, 120730 AND 120731) .....	86
FIGURE 69 - SEM IMAGES OF FeCuAl AND Mn <sub>x</sub> O <sub>y</sub> PARTICLES SUMMARIZING TRIALS OF THIS WORK (SCALE BAR OF 200μM).....	87
FIGURE 70 - SPECIFIC SURFACE AREA IN FUNCTION OF RAW MATERIAL USED AND BINDER ON CHARGE RATIO (SBET – M <sup>2</sup> /G).....	88
FIGURE 71 - SEM IMAGES REPRESENTING GOOD FINDINGS ON OXYGEN CARRIER PARTICLES ELABORATED DURING THIS INTERNSHIP .....	91
FIGURE 72 - SPRAY-DRYER APV SPECIFICATIONS SHEET AND REPRESENTATION OF A TWO FLUID NOZZLE (PNEUMATIC) WITH EXTERNAL MIX.....	95
FIGURE 73 - PARTICLE SIZE DISTRIBUTION FOR PRODUCT 120530 CALCINED AT 700°C.....	96
FIGURE 74 - PARTICLE SIZE DISTRIBUTION FOR PRODUCT 120607 CALCINED AT 700°C.....	96
FIGURE 75 - PARTICLE SIZE DISTRIBUTION FOR PRODUCT 120611 CALCINED AT 700°C.....	97
FIGURE 76 - PARTICLE SIZE DISTRIBUTION FOR PRODUCT 120612B CALCINED AT 700°C.....	97
FIGURE 77 PARTICLE SIZE DISTRIBUTION FOR PRODUCT 120615 CALCINED AT 700°C.....	97
FIGURE 78 - PARTICLE SIZE DISTRIBUTION FOR PRODUCT 120618C CALCINED AT 700°C.....	97
FIGURE 79 - SEM PHOTOS OF PRODUCT 120523 .....	98
FIGURE 80 - SEM IMAGES OF PRODUCT 120524.....	98
FIGURE 81 - SEM IMAGES OF PRODUCT 120530.....	98
FIGURE 82 - SEM IMAGES OF PRODUCT 120601.....	98
FIGURE 83 - SEM IMAGES OF PRODUCT 120604.....	99
FIGURE 84 - SEM IMAGES OF PRODUCT 120605.....	99
FIGURE 85 - SEM IMAGES OF PRODUCT 120607.....	99
FIGURE 86 - SEM IMAGES OF PRODUCT 120618.....	99
FIGURE 87 - SEM IMAGES OF PRODUCT 120618B.....	100

FIGURE 88 - SEM IMAGES OF PRODUCT 120618C .....	100
FIGURE 89- EXAMPLES OF PARTICLE MORPHOLOGY OBTAINED ON IFPEN SPRAY DRYER.....	101
FIGURE 90- ELEMENTS OF UNDERSTANDING ON MORPHOLOGY CHANGES THAT OCCUR DURING SPRAY DRYING .	101

# Index of Tables

---

TABLE 1 - ADVANTAGES AND DISADVANTAGES OF CLC REACTORS DESIGN [8].....	18
TABLE 2 - OXYGEN CARRIERS COMPARISON [3],[9],[17],[18][19],[20],[22].....	20
TABLE 3 - OXYGEN CARRIERS COMPARISON [3],[17],[19],[20],[23],[24],[25],[26],[27],[28],[29],[30],[31],[32].	21
TABLE 4 - DIFFERENT METHODS OF CATALYSTS PREPARATION [14].....	24
TABLE 5 - SPRAY DRYING PARAMETERS DEPENDENCE [39].....	28
TABLE 6 - ADVANTAGES AND DISADVANTAGES OF DIFFERENT TYPES OF ATOMIZERS [41],[42],[44],[45],[50],[51],[52].....	31
TABLE 7 - SUMMARY TABLE OF FeCuAl FORMULATION TESTS.....	60
TABLE 9 - SUMMARY TABLE OF MANGANESE TESTS FORMULATION.....	74
TABLE 11 - RESULTS OF ATTRITION TESTS.....	88
TABLE 12 - DATA CONCERNING FeCuAl SYNTHESIS.....	97

# 1 Introduction

---

Nowadays CO<sub>2</sub> is the largest contributor to the GreenHouse Gas (GHG) effect and this is the result of two factors: firstly CO<sub>2</sub> represents the largest GHG emissions, about 75%, and secondly because CO<sub>2</sub> residence time in atmosphere is about 300 years, much greater than other GHG [1]. In 2010 the CO<sub>2</sub> atmospheric concentration was about 390 ppm [2], a value much higher than some decades ago, and that fact could be very dangerous, because the increase of CO<sub>2</sub> atmospheric concentration leads to increase of global temperature and to a lot of other climatic problems such as drought and flood, sea level rise, changes in crops, food and water supply, etc. It is considered that to avoid catastrophic changes on earth, the CO<sub>2</sub> atmospheric concentrations must not exceed 450 ppm [3], so it is extremely necessary to reduce our increasing emissions. Figure 1 presents the CO<sub>2</sub> atmospheric concentrations after 1960 measured at Mauna Loa Observatory.

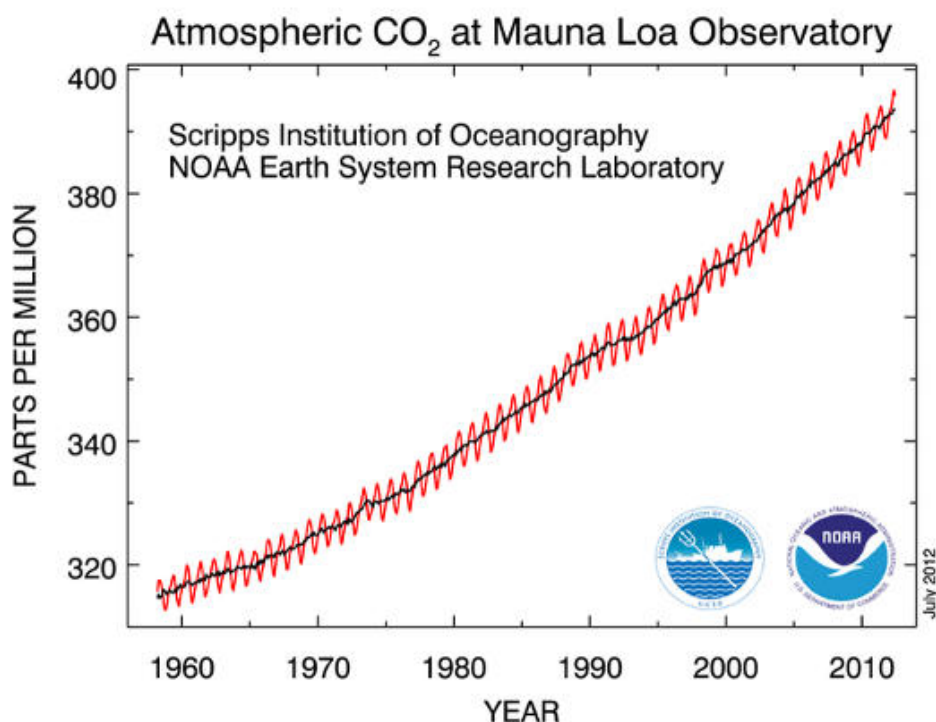


Figure 1 - Atmospheric CO<sub>2</sub> concentrations measured at Mauna Loa Observatory (1960-2010)[4]

There are some different ways to reduce the CO<sub>2</sub> emissions such as reduction of energy consumption by increasing energy efficiency, decrease the use of carbon fuels, increase the use of renewable energy sources, increase the use of nuclear energy, but also promote natural CO<sub>2</sub> sequestration and enhance CO<sub>2</sub> capture and storage (CCS). None of these ways are the real solution to solve the GHG emissions problem, so it is necessary to proceed and develop all of them.

According to Intergovernmental Panel on Climate Change (IPCC) and International Energy Agency (IEA) the capture and storage of CO<sub>2</sub> could account for 19% of the total CO<sub>2</sub> emissions reduction needed to stabilize climate change at reasonable cost [3]. This fact led to a great development of CCS technologies during the last years.

In the present work, considering various CO<sub>2</sub> capture technologies, we will try to develop materials for a particular one: the chemical looping combustion named "CLC process". For this purpose we will synthesize and elaborate different inorganic particles composed by mixed oxides and especially designed or shaped to act as fluidizable oxygen carriers within the CLC process developed at IFPEN.

The subject of this study is based on chemical engineering and materials science at a pilot scale thanks to industrial equipments. Therefore, this report will mainly deal about chemical synthesis and formulation, but also development and characterization of oxide materials.

One of the goals will be the improvement of size, shape and thermo-mechanical resistance of these materials in order to develop an innovative formulation/composition and produce particles at a semi-industrial scale to supply raw material for IFPEN CLC units.

## 2 Bibliographic Study

This section intends to present the most relevant aspects of Chemical Looping Combustion (CLC) process, but also oxygen-carriers production, as formulation, rheology and spray-drying of concentrated oxides suspensions developed in this work.

### 2.1 CO<sub>2</sub> capture and storage processes (CCS)

CO<sub>2</sub> capture and storage processes involve three steps: capture, transport and storage. The capture step contributes with about 75% of the process cost, [5] which make it a very important issue. There are three main groups of CO<sub>2</sub> capture processes:

- Post-combustion processes
- Pre-combustion processes
- Oxy-fuel combustion processes

In post-combustion processes, CO<sub>2</sub> is separated from a CO<sub>2</sub>-rich gas stream, such as a flue gas from a conventional power plant. In pre-combustion processes, CO<sub>2</sub> is captured from a gas mixture with H<sub>2</sub> at high pressure and medium CO<sub>2</sub> content. In that case the feed gas contains CO<sub>2</sub>, H<sub>2</sub> and also other components such as CO, H<sub>2</sub>S and other sulfur compounds. In oxy-fuel combustion processes, a concentrated stream of CO<sub>2</sub> can be produced by the exclusion of N<sub>2</sub> before or during the combustion/conversion process, which avoids the need of CO<sub>2</sub> separation and results in a reduction of NO<sub>x</sub> emissions, but has the disadvantage of additional cost for the O<sub>2</sub> separation from air [5]. Below it can be viewed a scheme of the major CO<sub>2</sub> capture processes (figure 2).

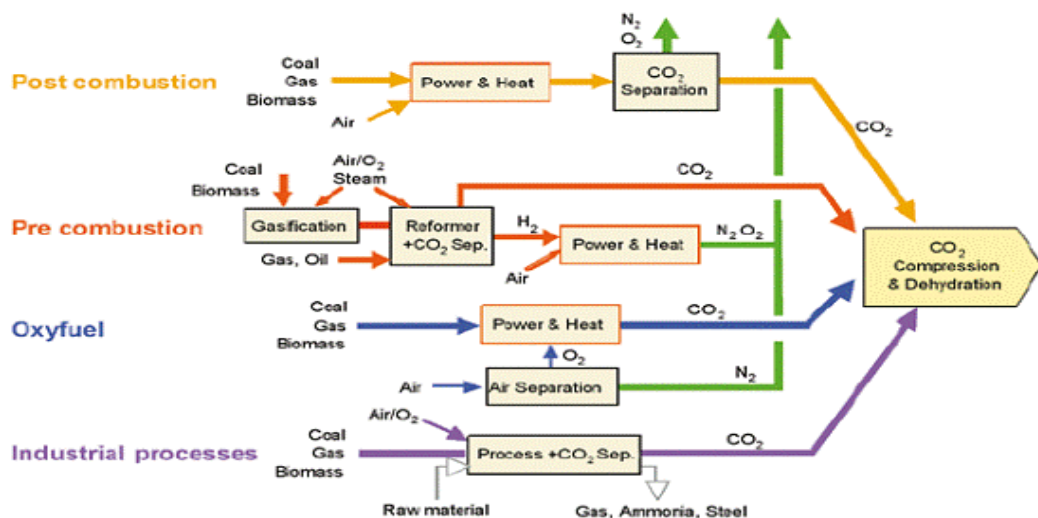


Figure 2 - CO<sub>2</sub> capture processes [6]

Chemical Looping Combustion (CLC) is an important CO<sub>2</sub> capture technology which can have applications including combustion and hydrogen production. CLC is often classified as an oxy-fuel process, but could be more adequately considered as an unmixed combustion process, like fuel cells processes [7]. It consists basically in an oxygen transfer between air and fuel, using an oxygen-carrier material that allows the combustion without an air-fuel contact. The reactions occur in two fluidized bed reactors.

This technology is considered as a low-cost option for CO<sub>2</sub> capture because it is two times cheaper than pre-combustion or classic oxy-fuel processes [3], and also as a combustion process that does not need CO<sub>2</sub> separation and generates little energy penalty.

The location of CO<sub>2</sub> storage is also an important matter of the capture process. Currently deep saline aquifers offer the largest CO<sub>2</sub> storage capacities and also have the advantage of proximity between the source and the storage site [8]. Another option could be the storage in hydrocarbon reservoirs, which have the advantage of generating a low operating cost process. On the other hand this choice also has some disadvantages such as limited storage capacities and long distances from CO<sub>2</sub> emission sites [8]. Finally, unmineable coal beds seem to be a good alternative for carbon sequestration reservoirs, but due to their limited storage capacities and problems with injection, they not yet been used [8].

## 2.2 Chemical-Looping Combustion (CLC)

Chemical-Looping Combustion, as previously stated, generally consists in an oxygen transfer between air and fuel in a dual fluidized bed system where an oxide is employed as a material providing the oxygen for combustion. This transfer occurs in two reactors, one of them is an air reactor and the other one a fuel reactor. The oxygen transfer is made by a solid oxygen carrier, normally composed of metal oxides, hence avoiding the air-fuel contact.

First the fuel is oxidized to CO<sub>2</sub> and H<sub>2</sub>O by a metal oxide which is reduced to a lower oxidation degree. In this step the produced gas contains CO<sub>2</sub>, H<sub>2</sub>O and also some fractions of CO and H<sub>2</sub> if there is partial oxidation of fuel. After water condensation and purification, a highly concentrated CO<sub>2</sub> stream is obtained that is ready for transport and storage steps. This first step occurs in the fuel reactor in a generally endothermic reaction, which can be made exothermic, depending on the fuel and oxygen carrier choice. Normally, when CH<sub>4</sub> is used this reaction is endothermic, whereas with H<sub>2</sub> or CO is usually exothermic [3].

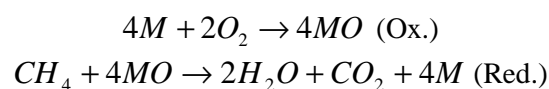


Figure 3 - Oxidation and reduction reactions of the oxygen carrier

The metal or reduced metal oxide is then oxidized with air and, when the material is regenerated, a new cycle starts. This step occurs in the air reactor and this reaction is always exothermic, producing a flue gas with  $N_2$  and unreacted  $O_2$  from air. A basic scheme of the CLC process is shown in figure 4.

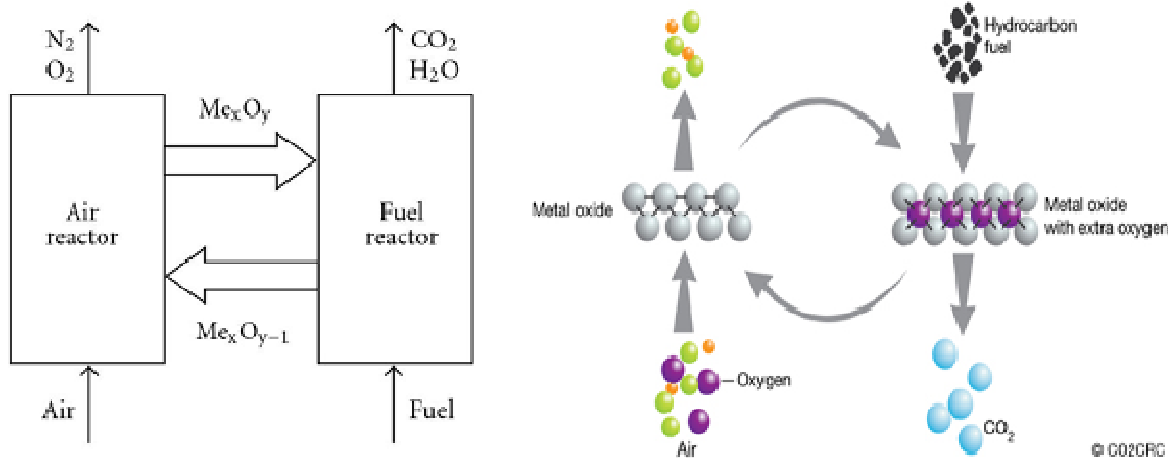


Figure 4 - Chemical-Looping Combustion general scheme [9],[10]

CLC with gaseous fuels has been widely investigated [11],[12],[13], but in recent years, the adaption of CLC systems to solid fuels has been investigated, due to the abundance of this kind of fuels. With solid fuels it is possible to either introduce directly the fuel into the fuel reactor, performing gasification in-situ (in-situ Gasification CLC, iG-CLC), or first produce syngas in a gasifier and proceed as with gas fed CLC processes (Syngas-CLC) [3].

The critical parameters in a CLC reactor design are the solids inventory, the circulation rate of oxygen carriers, the dimensions of reactors and also the pressure drop [9]. Besides the fuel choice, CLC success depends strongly on oxygen carrier choice, its composition and elaboration method but also on its durability along Red/Ox cycles.

We can see below (figure 5) two IFPEN images respectively showing a chemical looping combustion scheme and a detailed scheme for capture and storage of  $CO_2$ .

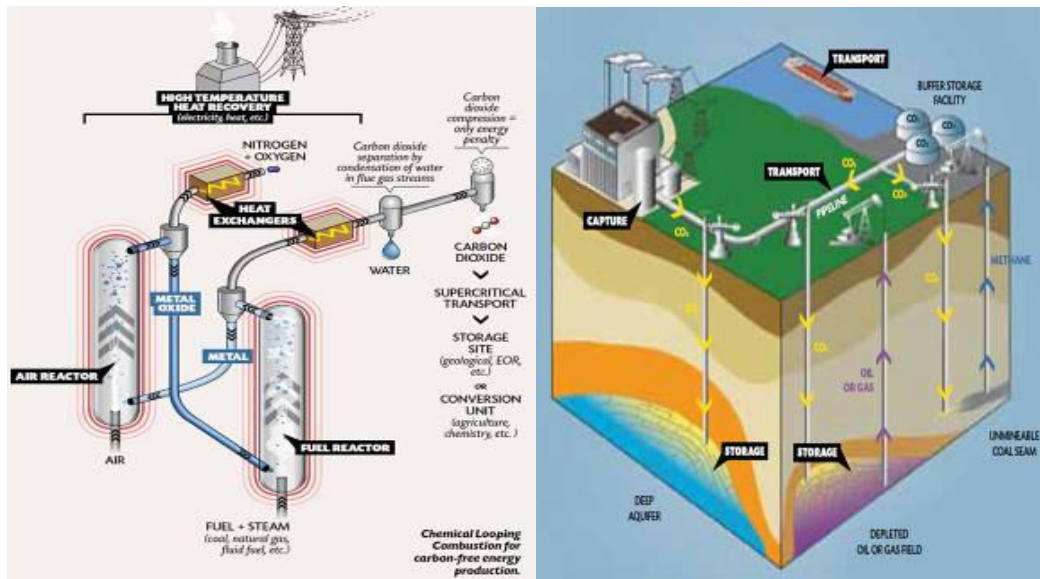


Figure 5. IFPEN images representing the chemical looping combustion process and a scheme on capture & storage of CO<sub>2</sub>

## 2.2.1 CLC reactors design

A CLC unit is composed, as previously stated, of two linked reactors that can be circulating fluidized bed, fixed bed or rotary reactor. Circulating fluidized beds (CFB) reactors are the most studied and most components required for industrialization of CLC in CFB have already been developed and validated at industrial scale for other applications [8]. Table 1 shows a summary of some advantages and disadvantages of these types of CLC reactors.

Table 1 - Advantages and disadvantages of CLC reactors design [8]

Design	Advantages	Disadvantages
<b>Circulating Fluidized Bed (CFB)</b>	Continuous operation Good heat and mass transfer Fast reactions Low quantity of solid used	Attrition Difficulty in fines separation Size (expansion of the refractory material and the shell)
<b>Fixed Bed</b>	No attrition or other mechanical degradation No dust in the gas leaving the reaction	Heat transfer poorly defined Problem of valves at reactor exit Slow kinetics Refractory material subject to high variations in gas temperature
<b>Rotary Reactor</b>	Continuous operation No dust in the gas leaving the reaction Small size	Heat transfer poorly defined Difficult to make a perfect seal between the zones and also between the moving and fixed parts

## 2.2.2 Oxygen Carriers for CLC

The oxygen-carrier choice is a fundamental step of the CLC process. Indeed, this material must match some specific characteristics such as good oxygen transport capacity, thermodynamically favorable reactions, high reactivity for oxidation and reduction, attrition resistance to minimize losses of elutriated solids, low tendency for carbon deposition, suitable size and good fluidization properties, limited cost and environmentally friendly characteristics. [3],[14].

An oxygen-carrier is basically a pure metal oxide or a metal oxide combined with a support that is often an inert material. This material may provide a higher surface area for reactions, act as a binder for increasing the mechanical strength and attrition resistance but also act as an ion conductor enhancing the ion permeability in the solid particles [15].

It is possible to use a wide range of metals such as Iron, Copper, Nickel, Manganese or Cobalt. Each of them has some advantages and disadvantages and one of the ways to improve the oxygen-carriers characteristics is to mix some of these metals or/and add other compounds.

Ni/NiO is the best performing material for natural gas but stays problematic due to its cost and toxicity [16]. Moreover Nickel oxide cannot thermodynamically convert the fuel to 100% CO<sub>2</sub> and H<sub>2</sub>O [17].

Copper-based oxygen carriers have some advantages such as high reaction rates, high oxygen transfer capacity, no thermodynamic restrictions for complete fuel conversion to CO<sub>2</sub> and H<sub>2</sub>O, both reactions are exothermic which avoids the need of heat supply in the reduction reactor. We also have to mention the fact that it is cheaper and its use generates less environmental problems than metals such as Ni and Co [3],[9]. The major disadvantage of Cu-based oxygen carriers is about the low melting point (1089°C) which is correlated with agglomeration problems [17].

Iron-based carriers are much cheaper and environmentally friendly than Nickel and Cobalt materials and also iron is not toxic. Despite this aspect, Fe-based carriers have weak redox characteristics [3]. The mass ratio of active oxygen is very high for the iron system Fe<sub>2</sub>O<sub>3</sub>-Fe, as seen on figure 6, but due to thermodynamic limitations it is not possible to reduce iron further than Fe<sub>3</sub>O<sub>4</sub> and still achieve complete conversion to CO<sub>2</sub> and H<sub>2</sub>O [18].

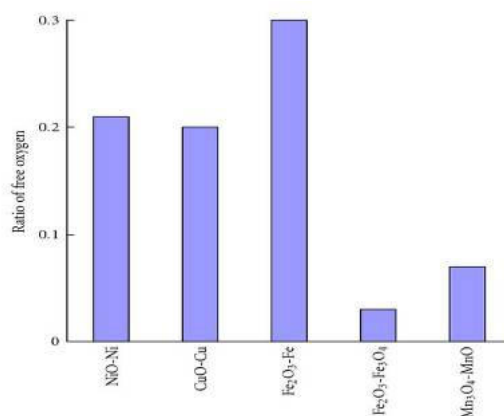


Figure 6 – Mass ratio of active oxygen for different metal oxides [9]

Manganese is also a cheap material but depending on its various forms, it can present a certain toxicity. Mn-based carriers have higher oxygen transport capacity than Fe and have no major disadvantages so it seems to be a good choice for CLC [17].

Like for the active phase of oxygen carriers, a wide range of supports or inert matrices have been studied. Al<sub>2</sub>O<sub>3</sub> as a support can lead to good reactivity, high mechanical strength and also thermal stability [19]. ZrO<sub>2</sub> is considered to be the best inert material for manganese oxides considering reactivity and mechanical strength [9]. On the other hand Al<sub>2</sub>O<sub>3</sub> is not a good support for manganese oxides due to formation of a MnAl<sub>2</sub>O<sub>4</sub> phase during sintering, which does not react with fuel and oxygen [20]. Other common supports that could be used are MgAl<sub>2</sub>O<sub>4</sub>, SiO<sub>2</sub> and TiO<sub>2</sub>.

As previously mentioned, it is possible to use more than one metal oxide to create an oxygen-carrier with better characteristics. As an example, the spinel Fe<sub>1,05</sub>Cu<sub>0,95</sub>AlO<sub>4</sub> is considered to be the best working spinel formulation [21] and will be studied in this work. The main characteristics of this oxygen carrier are a high oxygen transfer capacity, a high oxidation rate, but a low reduction rate compared with other oxygen-carriers such as Ni-based materials.

Table 2 presents a summary of the main families of oxygen carriers for CLC, concerning performance, cost and HSE (Health, Safety & Environment).

Table 2 - Oxygen Carriers Comparison [3],[9],[17],[18][19],[20],[22]

Oxygen carriers	Performance	Cost	HSE (Health Safety & Environment )
<b>Fe-based</b>	–	++	++
<b>Mn-based</b>	+	++	–
<b>Cu-based</b>	+	+	++
<b>Ni-based</b>	++	--	--
<b>Co-based</b>	++	--	--

Table 3 presents the result of a research done in many publications about CLC oxygen carriers. Some of the fields of the table are not filled due to lack of information.

Table 3 - Oxygen Carriers Comparison [3],[17],[19],[20],[23],[24],[25],[26],[27],[28],[29],[30],[31],[32]

Metal Oxide	Inert	Performance	Cost	HSE (Health Safety & Environment )
NiO	YSZ	++	--	++
	Al <sub>2</sub> O <sub>3</sub>	+	+	+
	γ-Al <sub>2</sub> O <sub>3</sub>	-	-	-
	α-Al <sub>2</sub> O <sub>3</sub>	++	-	-
	MgAl <sub>2</sub> O <sub>4</sub>	++	-	-
	CaAl <sub>2</sub> O <sub>4</sub>	++	-	-
	NiAl <sub>2</sub> O <sub>4</sub>	++	-	-
	γ-Al <sub>2</sub> O <sub>3</sub> -MgO	++		
	SiO <sub>2</sub>	+		
	TiO <sub>2</sub>	++		
CuO	ZrO <sub>2</sub>	-		
	Al <sub>2</sub> O <sub>3</sub>	+	+	
	γ-Al <sub>2</sub> O <sub>3</sub>	+	+	++
	SiO <sub>2</sub>	++		
	TiO <sub>2</sub>	++		
Fe <sub>2</sub> O <sub>3</sub>	ZrO <sub>2</sub>	+		
	Al <sub>2</sub> O <sub>3</sub>	+	++	++
	MgAl <sub>2</sub> O <sub>4</sub>	++		
	SiO <sub>2</sub>	-		
	TiO <sub>2</sub>	+		
FeTiO <sub>3</sub> (ilmenite)		+	++	
Mn <sub>3</sub> O <sub>4</sub>	ZrO <sub>2</sub>	++		-
	Al <sub>2</sub> O <sub>3</sub>	--	++	-
	Mg-ZrO <sub>2</sub>	++		-
	SiO <sub>2</sub>			-
	TiO <sub>2</sub>			-
Mn <sub>2</sub> O <sub>4</sub>	Al <sub>2</sub> O <sub>3</sub>	--		
La <sub>0,8</sub> Sr <sub>0,2</sub> Co <sub>0,2</sub> Fe <sub>0,8</sub> O <sub>3-5</sub>		-		-
CoO	YSZ	++	--	
	Al <sub>2</sub> O <sub>3</sub>	--	--	
CoO-NiO	YSZ	+++	--	-
	Al <sub>2</sub> O <sub>3</sub>		--	-
CaSO <sub>4</sub>		+		
Fe <sub>2</sub> O <sub>3</sub> -MnO <sub>2</sub>	ZrO <sub>2</sub>	++		

### 2.2.3 Oxygen-carriers production

Oxygen-carriers could be produced by several different methods and the choice is a very important step because it has a great influence on the final product characteristics such as size, shape, microstructure (crystallized or amorphous), stability and mechanical strength [33]. One of the main procedures for oxygen-carriers synthesis can be divided into three steps [14]:

- Formation of metal and support matrix
- Control of particle bulk morphology
- Rigidity and curing

For the metal-support matrix formation a lot of different methods can be used. Below there is a brief explanation about some of these methods.

#### **Formation of the metal and support matrix**

The methods used to form the metal and support matrix are:

- Mechanical Mixing;
- Freeze Granulation;
- Dry impregnation or Incipient Wet Impregnation;
- Wet Impregnation;
- Dissolution and Co-Precipitation ;
- Sol-Gel Synthesis;
- Solution Combustion

Mechanical Mixing consists in the direct mixing of metal oxide, support and binding agents that may be added to give more strength to the matrix. Before mixing, it is necessary to dry the metal oxide and support powders. This is an economical method that can give a satisfactory yield. This method results in a less homogeneous material compared with other techniques. This method is not suitable to metals that sinter at low temperatures, such as copper [23].

Freeze Granulation is commonly used to synthesize small spherical particles. The procedure consists in mixing metal oxide and support in distilled water with a small amount of dispersant that improves the mixture homogeneity. The mixture is then grinded in a ball mill to obtain fine powder

slurry and a binder is added to increase the mechanical strength of the particle. The mixture is then dried using the freeze-drying technique and sieved to obtain a well defined particle size. Chemical reactivity of particles is highly influenced by metal oxide and binder interaction. Freeze granulation, like mechanical mixing, cannot be used with copper oxygen-carrier synthesis because of sintering [20].

Dry Impregnation and Incipient Wet Impregnation methods are often used to impregnate valuable materials in the porous network of a support material. The support is exposed to a metal salt solution having the same volume as the whole pore volume and finally the product is calcined. The major disadvantages of these methods are high costs associated to synthesis and tedious procedures. For a copper-based material it is a good option to choose one of these methods due to decrease of copper sintering [14].

Wet Impregnation is similar to the method shown above but in this case the amount of metal solution is higher. The support is soaked in a metal solution (generally a nitrate) and after a low-temperature calcination the nitrates decompose into NO<sub>x</sub> and insoluble oxides. In this case, copper-based oxygen-carriers have shown good reactivity, stability and mechanical resistance [23]. However wet impregnation results in formation of an outer shell of metal oxide, which has a weak bond with the support and tends to attrite after initial cycles [14].

Co-precipitation uses three precursors: a metal salt solution, a support precursor solution and a precipitating agent. The first step consists in mixing the metal salt solution and the support precursor solution. Then, a precipitating agent is added to the solution and precipitation of metal and support hydroxides occurs. The precipitating agent is added only after the solutions mixing to avoid sequential precipitations caused by possible differences in component solubility [34].

During co-precipitation, the pH should be adjusted and kept constant which could be achieved by regulating the flow of precipitating agent [34]. One disadvantage of co-precipitation is the formation of large volumes of salt-containing solutions during the in precipitation and washing stages [35]. In order to improve the interactions between metal and support and to remove impurities, multiple washing steps could be carried out with different characteristics obtained for the final product.

In this work, co-precipitation was the chosen method for synthesis of the Fe<sub>1,05</sub>Cu<sub>0,95</sub>AlOOH oxyhydroxide, which is the precursor to the spinel phase.

Sol-Gel Synthesis is characterized by an excellent control over the physical parameters of final particles but along with this control comes high cost and difficulty in procedures.

The precursors, usually metal alkoxides, are mixed together and submitted to a series of hydrolysis and condensation reactions in water to form an amorphous metal oxide gel. This gel is then cured by calcination. Sol-gel synthesis provides a homogeneous mixture and a good control over the

microstructure. The pore size of the product can be controlled with the degree of aggregation or flocculation of colloidal precursors.

Solution Combustion consists in mixing metal nitrates and support in water with a combustible agent (glycine). Then the solution is heated to vaporize water and when the majority of water is driven out, the solution is ignited and a metal-oxide-based material is obtained. After that step the oxygen carrier material is grinded in a mill and finally calcined.

Particles obtained by this method show good reactivity for numerous CLC cycles as well as a high crushing strength [36]. One of the disadvantages of this method is the high attrition rates and low performance of extruded particles [36]. Table 4 presents different methods of catalysts preparation focusing in different aspects such as cost, attrition resistance, homogeneity and others.

**Table 4 - Different methods of catalysts preparation [14]**

Property	Technique						
	Mechanical Mixing	Freeze Granulation	Dry Impregnation or IWI	Wet Impregnation	Dissolution or Coprecipitation Method	Sol-Gel Process	Solution Combustion
Economic Feasibility	++	+	-	-	+	--	+
Metal/Support Loading	++	++	--	--	-	+	-
Homogeneity	--	--	n/a	n/a	+	++	+
Attrition Resistance	-	-	+	-	-	+	--
Iron Based Looping medium	++	++	+	+	++	++	++
Nickel Based Looping medium	++	++	+	+	++	++	+
Copper Based Looping medium	--	--	++	+	-	-	-

++ highly suitable, + suitable, - not suitable, -- highly not suitable, n/a not applicable.

### **Control of particle bulk morphology**

Several methods can be used to shape metal and support matrices for preparation of CLC particles such as ball-mill grinding, granulation, pelletization and extrusion. These methods result in different products that differ in microstructure, homogeneity and properties.

Ball-mill grinding is used to obtain fine powders. To get them, a dried metal-support powder is mixed with a small amount of distilled water and sometimes dispersants. The ball mill residence time depends upon the size and homogeneity that are desired for the final product.

Another method to obtain CLC particles is granulation. This process is adapted to produce small granules. There are many different types of granulation processes, such as fluidized bed granulation, mixer granulation, freeze granulation or spray drying. Spray-drying is one of the most common granulation methods used for CLC particles [14] and, as the technology used in this work, it will be explained in more detail in chapter 2.2.4. The main advantages of this technology are the large

feed rate that can be used, the fact that this is a continuous process adapted to full automatic control and also the fact that particles obtained by this method can have a nearly spherical shape [37].

Pelletization consists in a high pressure compression of dried or humid powder. Binding agents can be added to increase the physical strength of the material [14].

The extrusion method is mainly used to prepare extrudates. the first step is the mixture of metal-support matrix with distilled water to obtain a paste that is then forced through an extrusion die and cut into small pellets.

### **Rigidity and curing**

Curing of particles is performed using drying and calcination processes. Drying processes have the objective to remove water or solvents from the particles. Calcination is often used to completely remove water from a material and to burn out organic agents such as temporary organic binders, or used to oxidise a material (under air), resulting in microstructural and/or phase changes (depending on calcination temperature), generally associated with an increase of the density and mechanical strength of the particle.

The temperature of the calcination step is much higher than that of the drying step, and it is close to the required sintering temperature [14]. During calcination, the metal salts in the particle are converted to metal oxides and various gaseous phases can be produced. This action induces additional interactions between support and metal phases, giving more mechanical strength to a particle [14]. It is generally considered that the higher the sintering temperature, the higher the mechanical strength of the final material [24].

After drying and calcination steps, a classic procedure consists in separating the product particles in different size ranges by a sieving process, and selecting the appropriate fraction.

## **2.2.4 Spray-Drying**

Spray-Drying is a powder production method which is used in many fields such as food, pharmaceutical, ceramic, polymer and chemical industries [38]. Some examples of spray-drying products are low-fat milk, beer concentrate, blood plasma, peptides and dyes. The raw material could be a solute and its solvent, an emulsion, or a suspension [39]. In terms of size and shape, spray-drying can give results comparable to other methods, such as crystallization, precipitation, freeze drying and extrusion.

## **Process description**

The objective of spray-drying is basically to transform a feed from a fluid state into a dried particulate form. This objective is achieved by spraying the feed into an hot drying medium, normally hot air, which results in water evaporation.

The process generally involves five main steps: suspension preparation, atomization, droplet-air contact, droplet drying and separation.

First, in the suspension preparation step, the feedstock is concentrated before introduction into the spray dryer.

The atomization step consists in creation of the optimum conditions for solvent evaporation, usually water, to produce particles with the desired characteristics (size, shape, morphology, moisture content, etc...). At this stage it is very important to control the droplet production, which should be well distributed and homogeneously mixed with the hot gas stream (mainly air).

Droplet size management is also very important to avoid the appearance of operational problems such as wall build-up, particles deformation, surface defects, large particle size distribution... The droplets must not be too large, which could generate incompletely dried particles, but also must not be too small because the product recovery would be difficult [37].

In the droplet-air contact stage, the atomized liquid is brought into contact with the hot gas, which should result in evaporation of the water initially present at the droplets boundaries [37].

Droplet drying consists in evaporation of the remaining moisture. This step has two different stages of evaporation: during the first stage, evaporation takes place at a relatively constant rate because there is sufficient moisture in the droplet to replace liquid that is evaporated on the surface. During the second stage there is not enough moisture to replace the evaporated liquid, so the evaporation rate decreases and starts to depend on moisture diffusion through the shell.

Finally, the last stage of the spray-drying process consists in separating the particles from the hot air flow. For this step, it is possible to use various equipments such as cyclones, filter bags or electrostatic precipitators to achieve the separation. In industrial processes wet scrubbers are often used to trap ultrafine particles fraction in order to purify and cool the exhaust air before sending it to the atmosphere [37].

One of the major concerns for spray-drying technology is the production of fine and ultrafine particles that may represent some risks for the environment and for human health. It can also lead to product losses and to changes in the physical properties of the final product such as solubility in water [33]. The fines produced may be recycled to the atomizing chamber or sent to a gas treating equipment (cyclone, wet scrubber...).

A scheme of the IFPEN spray-drying equipment working with a pneumatic nozzle (two fluid) and a fountain configuration (mixed flow) is shown in figure 7.

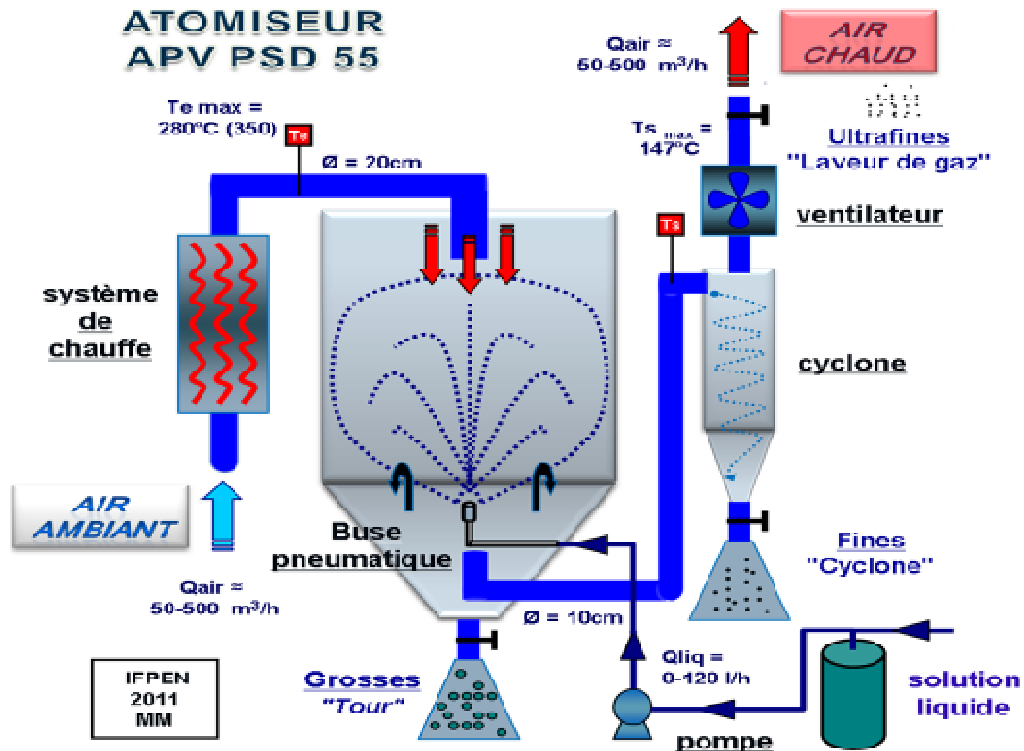


Figure 7 – Scheme of the IPEN spray-drying equipment

### Critical Parameters

In the spray-drying process, there are some critical parameters that must be very well controlled: inlet air temperature, outlet air temperature, liquid flow rate, feed viscosity, solid content, surface tension of the liquid feed, volatility of the solvent, and many other parameters depending on equipment, devices and configurations used (nozzle diameter, air nozzle pressure, wheel atomizer speed, ..)[37]. Some of these parameters can be easily and directly controlled on the equipment such as inlet air temperature, feed flow rate, nozzle diameter , but according with the raw material/product involved, other ones may be difficult to manage because of interdependent relations.

To achieve the desired particle characteristics or accelerate the whole process, different procedures can be tested such increase air inlet temperature that results in a faster moisture evaporation, but it is not possible to increase so much this value because if feed is subjected to high temperatures, some properties of the final product could be degraded (solubility, shape, ..) [40]. On the other side it is also necessary to take care about temperature differences, between inlet and outlet, because larger values could result in a large amount of residual moisture [39]. A high drying gas flow

(ie high aspirator rate / fan speed) could also result in a large amount of residual moisture because of a shorter residence time, so it is recommended to use an appropriate gas stream [39].

The use of a high temperatures liquid feed could also increase the process efficiency because with a higher temperature, it is easier to dry the solution by bringing more energy to the system [37]. Other process improvements could be the use of high volatility solvents or as an example of operating cost reduction the use of a nozzle material that has high resistance to abrasion and corrosion, such as tungsten carbide [37]. Considering process cost, the outlet temperature is an important parameter to control, taking into account the feed properties, equipment dimensions and its configuration. Indeed it is a difficult parameter to control because it depends strongly on inlet air temperature, aspirator flow rate, feed flow rate, atomizing devices and physico-chemical properties of the material being sprayed [39].

A summary table with influence of some parameters on the most important characteristics of the final product.

**Table 5 - Spray Drying parameters dependence [39]**

parameter dependence	aspirator rate ↑	air humidity ↑	inlet tempe- rature ↑	spray air flow ↑	feed rate ↑	solvent ins- tead of wa- ter	concen- tration ↑
outlet tempera- ture	↑↑ less heat losses based on total inlet of energy	↑ more energy stored in humidity	↑↑↑ direct proportion	↓ more cool air to be heated up	↓↓ more solvent to be evaporated	↑↑↑ less heat of energy of solvent	↑↑ less water to be evaporated
particle size	-	-	-	↓↓↓ more energy for fluid dispersion	(↑) more fluid to disperse	(↓) less surface tension	↑↑↑ more remaining product
final humidity of product	↑↑ lower partial pressure of evaporated water	↑↑ higher partial pressure of drying air	↓↓ lower relative humidity in air	-	↑↑ more water leads to higher particel pressure	↓↓↓ no water in feed leads to very dry product	↓ less water evaporated, lower partial pressure
yield	↑↑ better separation rate in cyclone	(↓) more humidity can lead to sticking product	(↑) eventually dryer product prevent sticking	-	(↓↑) depends on application	↑↑ no hygroscopic behaviour leads to easier drying	↑ bigger particles lead to higher separation

### **Design Considerations**

One of the most important design specifications of a spray-drying equipment is the atomizer or atomizing device because it has a high influence on Particle Size Distribution (PSD) and yield characteristics. Whatever the feed solution, the main objective is to achieve high spraying rates that

results in high energy efficiency of the process. There are various devices used for spraying the liquid feed at the entrance of the atomization chamber:

- Rotary atomizers;
- Pressure nozzles;
- Two-fluid nozzles;
- Ultrasonic nozzles

A rotary atomizer (fig.8) consists in an atomization wheel that rotates at high speed. The liquid feedstock is introduced at the wheel center and is distributed over the surface, flowing to periphery and then liquid disintegrates into droplets when it leaves the wheel. Some of the advantages of this type of device are: possibility of changing the particle size by changing the wheel speed, low pressure feed system and few blockage problems [41],[42]. On the other hand this kind of atomizer could bring some problems such as high capital cost due to mechanical maintenance, production of large quantities of fines and difficulty to use with highly viscous materials [41],[42].



**Figure 8 - Rotary Atomizer [43], [44]**

Pressure nozzles (fig.9) are actually the most commonly used atomizing device. This type of nozzle has some features, such as swirl configuration, that cause rotation of the liquid, which allows conversion of potential energy to kinetic energy by forming a thin film with high-speed at the nozzle exit. As this film leaves the nozzle, it is disintegrated, forming firstly ligaments, then droplets. Some of the advantages of this device are a low cost, a wide range of flow rates and modularity on particle size by adjusting feed pressure [41]. However pressure nozzles have some disadvantages such as a very little turndown ratio and a susceptibility to erosion because of the high pressures involved [45].



**Figure 9 - Pressure nozzle [44]**

Another type of nozzle is the two fluid nozzle (also called pneumatic nozzle) (fig.10) that is a good choice for pilot dryers due to its versatility concerning feed and air flows and droplet size [45]. The liquid enters the nozzle at a relatively low pressure and can be mixed with compressed gas (mainly air) internally or externally. Liquid atomization occurs thanks to the energy of compressed gas, which results in a high cost operation. However this kind of device is able to atomize highly viscous feeds and also can produce very fine particles [42]. As an example, one of the applications of this device is the production of particles required for inhalation products within the pharmaceutical industry [44].



**Figure 10 - Two fluid nozzle [46]**

Ultrasonic nozzle (figure 11) is a more recent type of atomizing device that consists basically in breaking a thin film of liquid into fine droplets by action of a vibrating surface. This mechanism could be explained by two hypotheses: capillary wave and cavitation. Capillary wave hypothesis is based on Taylor instability criteria [47]. Cavitation hypothesis is generally applied to high frequency and high-energy or intensity systems. In this hypothesis a liquid film is sonicated, forming cavitation bubbles that further collapse and generate high intensity hydraulic shocks. These hydraulic shocks initiate disintegration of the liquid film and cause direct ejection of droplets [48].



Figure 11 - Ultrasonic nozzle [49]

The major advantages and disadvantages of different types of atomizers are presented in table 6.

Table 6 - Advantages and disadvantages of different types of atomizers [41],[42],[44],[45],[50],[51],[52]

	<b>Advantages</b>	<b>Disadvantages</b>
<b>Rotary Atomizer</b>	Particle size adjustment by changing wheel speed Low pressure liquid feed No blockage problems Great Flexibility	High capital cost Difficulty with high viscosity fluids Large quantities of fines Cannot be used with horizontal dryers
<b>Pressure Nozzle</b>	Wide range of flow rate and particle size Suited for co-current and counter-current flow	Little turndown ratio Susceptible to erosion because of high pressures
<b>Two-fluid Nozzle</b>	Ability to produce very fine particles Ability to atomize high viscosity fluids High variety of particle sizes by changing air pressures and nozzle diameter	Not economic for high capacity units (air consumption) More complex flow control
<b>Ultrasonic Nozzle</b>	Compatible with almost any liquid Ultra-low flow compatibility Reduce atmosphere contamination No clogging risk	Requires high electrical power

Figure 12 intends to present the usual particle size distribution obtained with the different types of nozzles, presented on table 6.

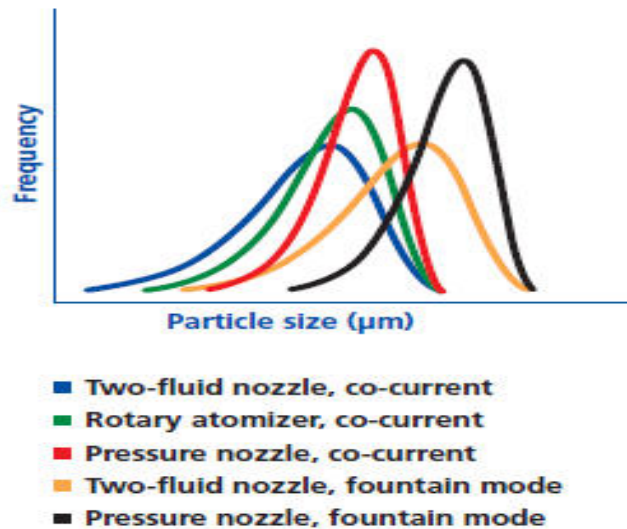


Figure 12 – Usual particle size distribution (PSD) obtained for different types of atomizers [53]

With regards to flow directions of liquid droplets and hot gas (mainly air), a spray-dryer can have different configurations including co-current, counter-current and mixed-flow.

In a co-current spray dryer, the liquid feed and the hot air enter together and with the same direction. Spray evaporation is quick and air temperature decreases rapidly with vaporization of water. This kind of configuration is preferred for heat-sensitive products because the hottest drying air contacts the droplets at their maximum moisture content [41]. The great advantage of this configuration is the fact that the product does not suffer from heat degradation because the droplet temperature stays low during most of the evaporation process [41]. Often, co-current dryers are used in dairy and other heat-sensitive food products [42].

In a counter-current design, the liquid feed and the drying air are introduced by opposite sides. The fluid enters at the top of the chamber and the drying air enters at the bottom of the dryer. Counter-current dryers offer a quicker evaporation than co-current equipments and also a higher energy efficiency [42]. This design is only suitable for thermally stable products due to contact between the driest particles and hot air at the bottom of the dryer [39],[41]. This configuration is commonly used to produce soaps and detergents [42].

Mixed flow dryers combine parts of both configurations described above. The hot air stream enters the drying chamber at the top and the fluid stream enters at the bottom. The product goes up against the hot air and falls by gravity into a container at the bottom. This kind of dryer is not appropriate for heat-sensitive products for the same reason as the counter-current dryer [42].

Figure 13 shows the different types of spray-dryer configurations, concerning the type of current.

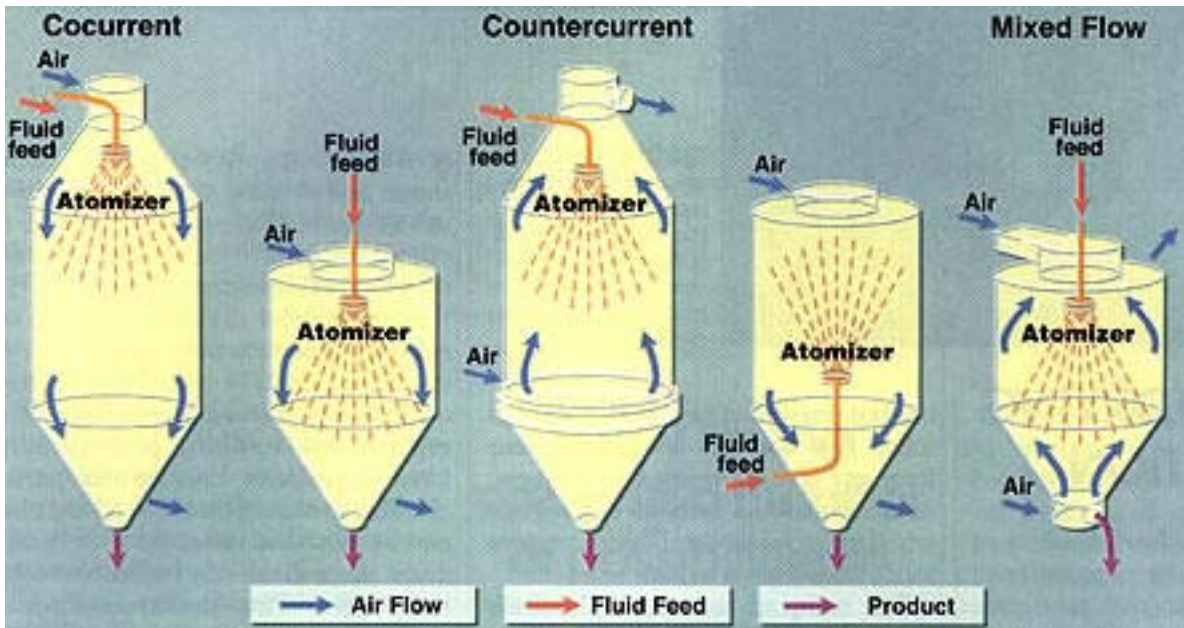


Figure 13 - Different types of spray-dryer configurations [44]

A spray dryer could also be classified according to its cycle. Open-cycle, closed-cycle and semi-closed cycle are the possible options, and the main difference between them is the gas circulation in the system.

Open-cycle dryer is the most commonly used configuration [42]. The air is captured from the atmosphere and heated, and after passing through the chamber it is released to the atmosphere. Figure 14 presents an example of an open-cycle spray-dryer.

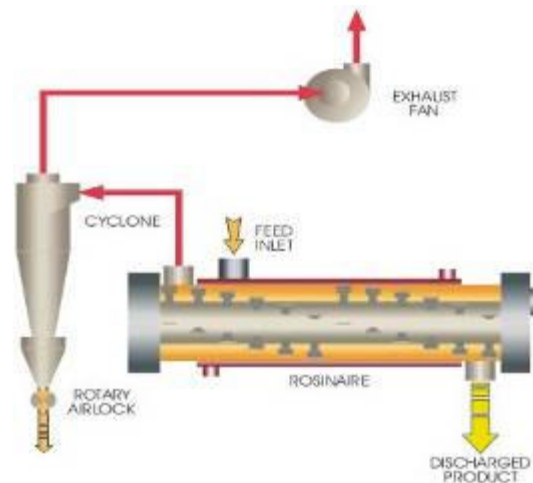


Figure 14 – Example of an open-cycle spray-dryer [54]

Closed-cycle dryers (figure 15) are used when flammable solvents, toxic or oxygen sensitive products are processed [39]. In this configuration, the drying gas, normally an inert gas [42], is continually recycled and reused.

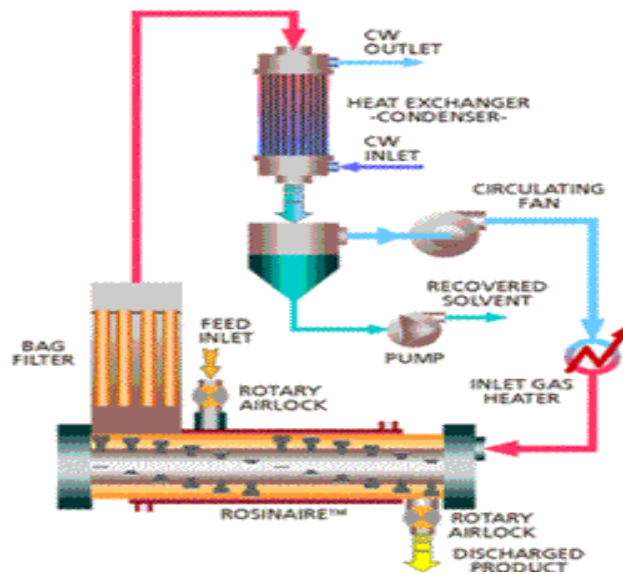


Figure 15 - Example of a closed-cycle spray-dryer [54]

A semi-closed-cycle dryer (figure 16) is a cross between open- and closed-cycle dryers [42]. In this kind of configuration there are many variations, and the most important is the self-inertizing design. For this design, a direct-fired heater is used and air that enters into the system is limited to that required for the combustion. The gas is recycled through the dryer and it has a very low oxygen content, which makes it suitable for materials that cannot be exposed to oxygen, due to explosive hazard or product degradation [41].

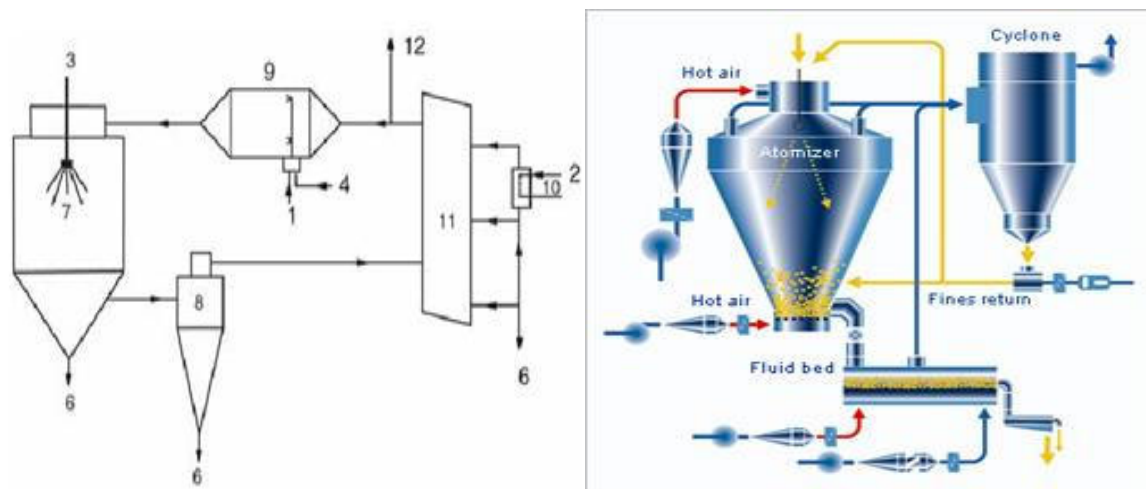


Figure 16 - Examples of a semi-closed cycle spray-dryer [42] outro esquema

Spray dryers can also vary in the number of stages. Single stage designs are used in the majority of spray- dryers [41] and in this case, moisture is reduced to a target value in just one pass through the dryer. In two stage designs, moisture is reduced in two steps. The second stage may be performed in a fluidized bed dryer or a vibrating bed dryer [41]. This kind of design allows the use of lower temperatures, which is suited for heat-sensitive products [41].

Spray dryers can also be displayed in two different positions: vertical or horizontal. Vertical dryers are commonly larger and the residence time of sprayed droplets is longer, which allows the use of higher flow nozzles [42]. Horizontal dryers are normally small and the particle residence time is relatively short, requiring the use of lower flow nozzles [42].

## 2.3 Rheology

Rheology is the science of deformation and flow, which means that it studies the behavior of solids, liquids and materials that have some characteristics of liquids and others from solids, when they are submitted to an external force.

This study consists in applying some force on the substance and then measure the evolution of viscosity with time (using a rheometer or viscometer). This measured viscosity corresponds to the resistance of a material to flow, and for different values of applied strength, various flow curves are obtained. These flow curves can be represented in viscosity as a function of shear rate or in shear stress as a function of shear rate.

Two main modes of deformation exist: stretching and shearing deformation. These two categories can be divided in uniaxial and biaxial for stretching, and simple or torsional for shearing deformation [55].

The apparent viscosity is obtained by the quotient between shear stress, a force per unit of area, and shear rate, a change in strain with time.  $\eta = \frac{\tau}{\dot{\gamma}}$

Many materials show characteristics of both ideal solids and viscous liquids, and they are called viscoelastic solids or liquids, depending on the predominant characteristics [55].

Different categories exist to classify materials in terms of rheological behavior after they are submitted to an external force. The main categories of matter are either Newtonian fluids or non-Newtonian fluids.

A Newtonian fluid is a fluid that obeys Newton's laws, which means that the apparent viscosity is independent of the shear rate. In this kind of materials, viscosity does not depend on shear rate but it could depend on time. Some examples of this kind of fluids can be silicon oil or low concentration suspensions [56]. Such fluids are called ideal or normal fluids [52], and they generally correspond to relatively simple liquid such as water. In practice the majority of materials obey Newton's laws over limited ranges of shear rate [55].

Non-Newtonian fluids are more common and inside this group, fluids show a large variety of behaviors. Such fluids are characterized by a variation of viscosity with shear rates. Normally this group can be subdivided in two groups: time dependent fluids and time independent fluids. Beyond this division, non-Newtonian fluids can be shear-thinning (pseudoplastics), shear-thickening (dilatants) and also Bingham plastics. Another important consideration for this kind of fluid is the existence (or not) of a yield stress.

Shear-thinning materials are characterized by a decreasing viscosity with an increasing shear rate. Examples of this type of fluid are polymers and dispersions [56]. On the other hand, shear-thickening materials show an increase of viscosity with increasing shear rate. An example could be corn flour [56]. A Bingham plastic is similar to a Newtonian fluid, with the difference that this kind of material has a yield stress, meaning that it needs a minimum shear stress to start flowing, and then it has a Newtonian fluid behavior. Examples of Bingham plastics fluids are pastes, paints and food products such as mayonnaise, ketchup and margarine [57]. Both shear-thinning and shear-thickening materials can have (or not) a yield stress.

Another important concept in rheology is thixotropy. A thixotropic material has a time-dependent response, due to a change of viscosity with time, at the same shear rate. This kind of fluids is always shear-thinning or shear-thickening, but shear-thinning and shear-thickening are not all thixotropic [56].

Figure 17 intends to present the rheological behavior of the most important fluids.

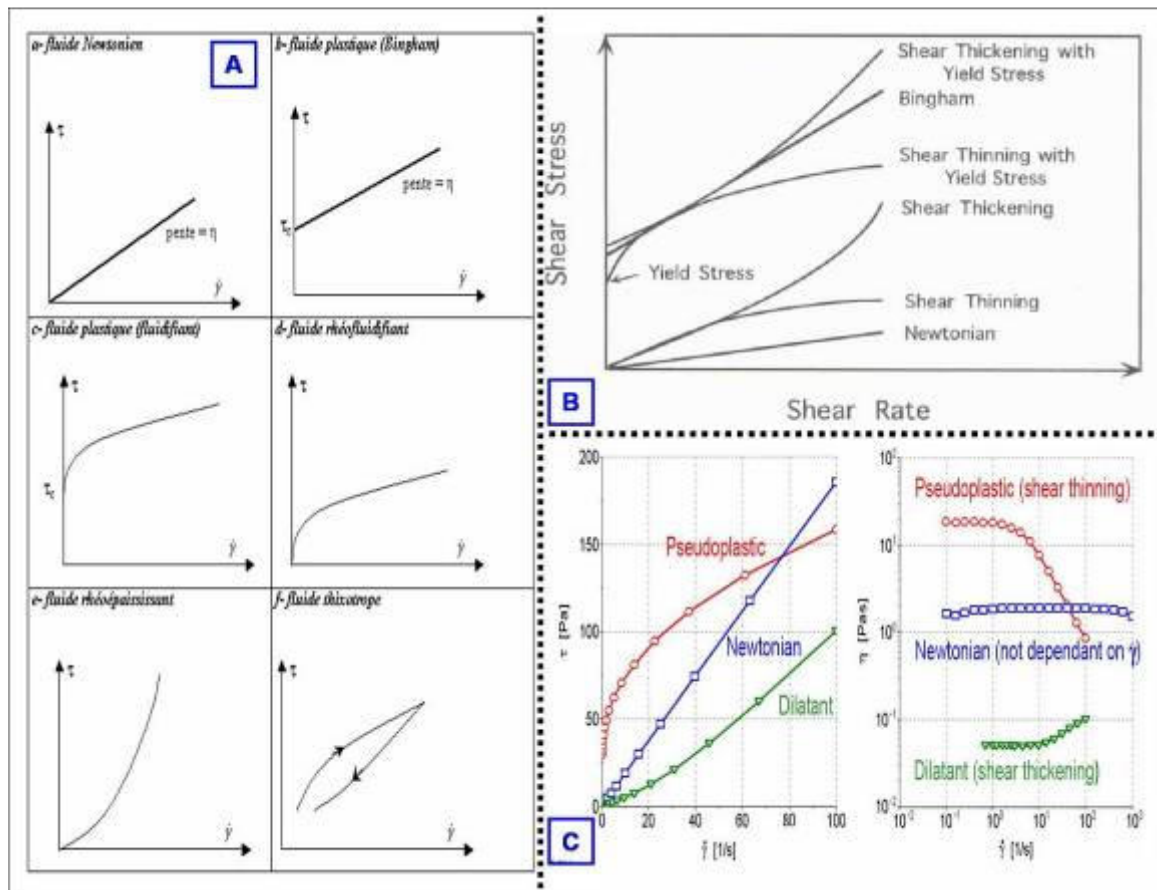


Figure 17 - Behavior of different types of fluids [52]

## 3 Experimental Section

---

This section describes experimental procedures used to elaborate the oxygen carriers, the main equipments and also the characterization techniques utilized to analyze the final particles.

### 3.1 Preparation of Raw Material

In this experimental work, four different raw materials were used, namely  $\text{Fe}_{1.05}\text{Cu}_{0.95}\text{AlO}_4$  material,  $\text{Mn}_x\text{O}_y$  compound I (powder),  $\text{Mn}_x\text{O}_y$  compound II (suspension) and BMP (black magic powder for confidentiality reasons) . Different preparation methods were chosen or applied to each raw material which are briefly explained below.

#### 3.1.1 $\text{Fe}_{1.05}\text{Cu}_{0.95}\text{AlO}_4$

The  $\text{Fe}_{1.05}\text{Cu}_{0.95}\text{AlO}_4$  spinel structure named "FeCuAl" powder for simplicity was produced from nitrate solutions of Iron, Copper and Aluminum that are commercially available. First the three nitrate solutions were mixed in the correct stoichiometric proportions in a stirred tank reactor. The co-precipitation occurred in a batch reactor between the nitrate mixture and a NaOH solution as precipitating agent. The inlet flows of solutions were regulated to maintain the pH at the desired value (about 8-9). It is also important to control the temperature due to the enthalpy of the reaction, by either heating or cooling the reactor. Another important factor in the reactor is to achieve sufficient agitation to get a good homogeneity in phases mixing and also to prevent the formation of a gel state.

At the end of the reaction, the mixture was sent to an industrial filter-press in order to recover the precipitated phase and remove an important percentage of the synthesis water containing various impurities. The filtration step was followed by a washing step in order to clean the precipitated phase from sodium nitrate salts and impurities. This operation was performed with a volume of hot water two times larger than the synthesis volume and then the precipitate product was compacted with pressurized air (9 bar) to give a brown, cohesive and pasty material also called "cake".

After the filter press operation, the cake was collected and sent into a spin flash dryer , which is a rapid granulation dryer working at about 300°C . After this step the obtained powder had a mean diameter of 20 $\mu\text{m}$ , with a polyedric shape and a moisture content about 30 wt%.

The dried product obtained with the spin flash dryer was mixed with water and then ball-milled to form a concentrated suspension with particles size between 1 and 5  $\mu\text{m}$  and with a solid content of about 40 to 60 wt%.

A basic scheme for the production of the "FeCuAl" powder is shown in figure 18.

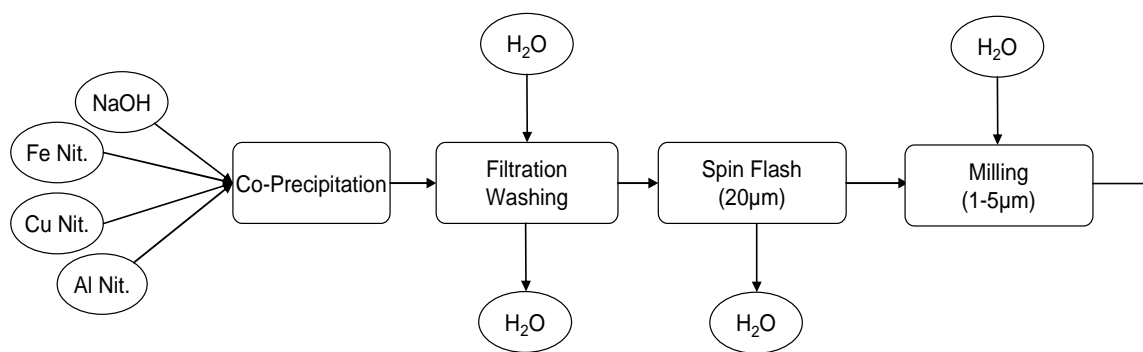


Figure 18 – General scheme of "FeCuAl" material production

### 3.1.2 Mn Material

All the three Manganese products used in this work as raw material were commercially available. For confidentiality, we can just specify that each product exhibits a well suited particle size, in order to be formulated with other agents for preparation of concentrated suspensions.

### 3.1.3 Main Equipments

For the preparation of the various raw materials, the main industrial equipments that were used are mixing vessels, a batch reactor, a filter-press, a spin flash dryer and also a ball-mill equipment, which are briefly described below.

#### Mixing Vessels

To prepare the nitrate solution and to feed the reactor with acidic and basic solutions at controlled flows, we used two mixing vessels regulated in temperature and containing two propeller stirrers. Figure 19 shows the mixing vessels utilized in this work.

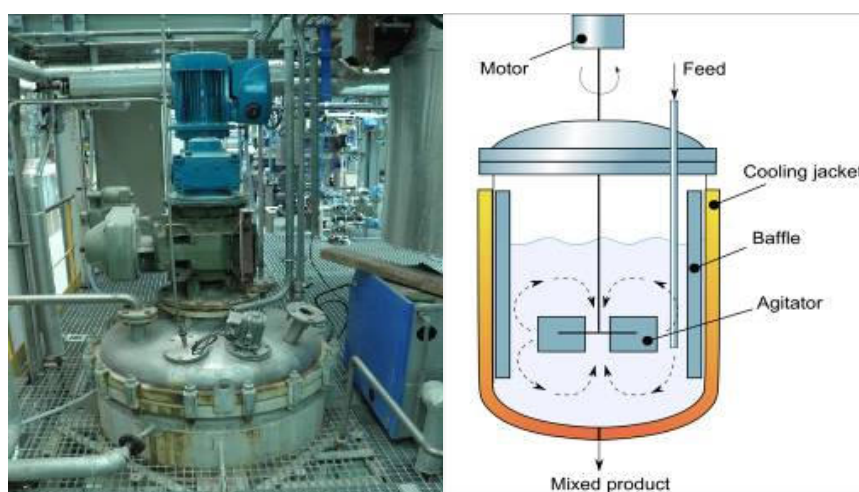


Figure 19 – Image of mixing vessels used for preparation of acid and basic solutions

## **Batch Reactor**

The synthesis was performed in a cylindrical batch reactor with a total volume of about 1000 L. This equipment contains two propeller stirrers in order to well agitate the mixture (solution and precipitate). Depending on volume and concentration of the mixture, the stirring power could be regulated to prevent settling.

As mentioned before, the inlet flow of reagents could be regulated with a control panel to maintain the pH at the desired value. Figure 20 presents the reactor used in this work and a general scheme of a stirred tank reactor.



**Figure 20 – Batch Reactor used in this work (volume about 1 m<sup>3</sup>) and general scheme of a stirred tank reactor**

## **Filter Press**

At the end of reaction, the slurry mixture is sent to a filter press equipped with 24 plates, where a filter cake was formed under pressure created by a peristaltic pump connected at the bottom of the batch reactor. The filter cake remains sandwiched between the plates, and the synthesis solution passes through the cloth filtering medium and exits via corner orifices.

The filtration step was followed by washing of the filter cake, with a volume of water two times larger than the volume of the synthesis solution. Then the filter cake is compressed between the plates under air pressure to give a cohesive and agglomerated material. This final cake was recovered by separating the plates, and then positioned on a conveyor connected to the spin-flash drying unit.

Figure 21 presents the industrial filter press used in the filtration step.



Figure 21 – Picture of the industrial Filter Press used in this work

### **Spin Flash dryer**

A spin flash dryer, as shown on figure 22, was used to finely cut and quickly dry the cake into small particles with a final mean diameter of about 20 $\mu$ m and reduced moisture content. This unit is constituted of an open chamber where the cake falls, and equipped at the bottom with a screw conveyor, which transports small pieces of product into the drying chamber. Then the product is divided in a closed chamber by a rotating tool (cutting knives) and continuously dried by a hot air stream with a temperature of about 250-300 $^{\circ}$ C. This chamber is connected with a separation cyclone associated with a container where the coarse particles fall. Finally the finest particles are driven with humid hot air and then separated by a wet scrubber.

This granulation and drying equipment contains a control panel where it is possible to set the inlet and outlet temperatures, the rotating tool speed and the differential pressure between inlet and outlet in order to manage the hot air flow. The speed of the screw conveyor can be automatically regulated but it is also an important parameter to manually adjust as another way to achieve the desired characteristics (modulate final size and moisture content).



Figure 22 – Picture of the Spin Flash dryer equipment used in this work

### **Ball Mill equipment**

After the drying step, particles were grinded in a ball-mill unit to form smaller particles with a mean diameter ( $dv_{50}$ ) lower than 2  $\mu\text{m}$ . The powder obtained from spin-flash drying was introduced with water in a small agitated reactor and then this suspension was forced to pass through the ball-mill unit using a pump in recirculation mode. The quantity of water and powder added to the reactor was regulated to control solid content and achieve a moderate viscosity.

The particles were grinded by action of small inorganic hard beads (made of Silica and Zirconium dioxide material) that are forced to move and rotate quickly with the powder in the grinding chamber. This operation generates shocks and very intense contacts between the grinding medium and the product particles, resulting in reduction of their mean particle size. This process continues until the desired particle size is achieved. Figure 23 presents the ball mill equipment used for this work.



**Figure 23 - Ball Mill equipment used in this work**

## **3.2 Preparation and production of Oxygen Carriers**

The oxygen carriers produced in this experimental work are based on an original approach where particles of active material (charge) are precisely associated and bonded with an inorganic binder within the final material. The main goal is the design of inorganic microspheres with a controlled size ranging from 100 to 300 $\mu\text{m}$  and also with a high attrition resistance.

In our case we prepared and used an aqueous alumina sol (made of bohemite peptized with nitric acid) as a binding agent. All our trials were conducted with the same general production scheme, which started with a preparation step, where water and various chemical agents were mixed together with the raw material (charge). One of the objectives was to manage homogeneity and viscosity of the resulting suspension to allow for its pumping and atomization in the spray-drying unit. After this atomization step, as a way to give the required resistance for the CLC process, the particles were

submitted to additional thermal treatments. The complementary drying and calcination steps were performed in two furnaces, the first one working up to 700°C and the second one, designed for sintering and densification, working up to 1200°C. Between these two calcination stages, a sieving by mechanical sieving tools was performed to eliminate the fine particles (highly sensitive to high temperatures) and to obtain a final product fraction with the required size distribution.

A simplified scheme of the general procedure employed for the production of the oxygen carrier particles is shown in figure 24.

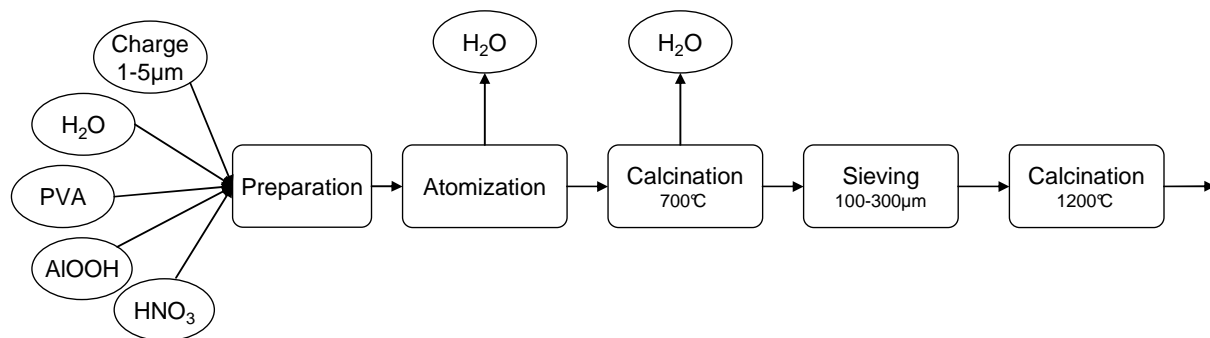


Figure 24 - Scheme for production of oxygen carrier particles

### 3.2.1 Suspension preparation step

The suspension preparation step was the only part of particles production that changed depending on the different raw material used. We describe below short protocols for elaboration of viscous and concentrated suspensions adapted to spray-drying. Figure 25 shows a principle scheme and an image of classic equipments used for the preparation step.

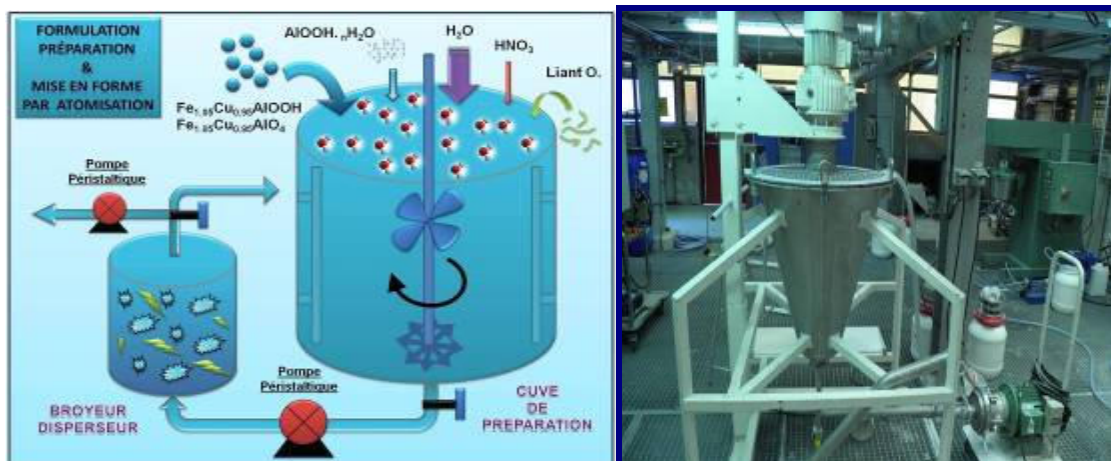


Figure 25 - Principle scheme associated with an image of equipments used for preparation of suspensions

### **FeCuAl preparation**

For raw material based on the spinel structure “FeCuAl”, the experimental protocol was:

- Addition of water into reactor , turn on agitation and recirculation mode;
- Addition of Nitric Acid;
- Addition of the inorganic binder (boehmite AlOOH) under powerful agitation for about 5-10 minutes to allow the peptisation mechanism ( chemical and mechanical fragmentation) ;
- Slow addition of FeCuAl charges under powerful agitation for about 5-10 minutes;
- Addition of organic binder (PVA: polyvinyl alcohol polymer).

For some tests, after adding the organic binder, various silica particles and/or coarse FeCuAl particles (not ball-milled) were added to reach a higher viscosity, due to shear-thickening effects. In the characterizations & results section (page 61) we can see a summary table describing all tests and all additional products added to suspensions.

### **Mn<sub>x</sub>O<sub>y</sub> compound I (powder) and BMP (powder) preparation**

For these two types of raw materials the experimental protocol was:

- Addition of water into reactor , turn on agitation and recirculation mode ;
- Addition of Nitric Acid;
- Addition of the inorganic binder (boehmite AlOOH) under powerful agitation for about 5-10 minutes to allow the peptisation mechanism ( chemical and mechanical fragmentation) ;
- Slow addition of 50 w% of charge under powerful agitation for about 5-10 minutes;
- Addition of organic binder (PVA : polyvinyl alcohol polymer)
- Slow addition of the remaining 50 w% of charge under powerful agitation for about 5-10 minutes, and if necessary addition of nitric acid to decrease viscosity and stabilize the suspension

### Mn<sub>x</sub>O<sub>y</sub> compound II (suspension)

This concentrated Manganese suspension already contains some water (plus other additives) and is quite fluid, so the decision was taken to not incorporate additional water in the final suspension. The experimental protocol for this case was:

- Addition of charge into reactor and turn on agitation and recirculation mode;
- Addition of Nitric Acid;
- Addition of organic binder (PVA : polyvinyl alcohol polymer);
- Addition of the inorganic binder (boehmite AlOOH) under powerful agitation for about 10-15 minutes to allow the peptisation mechanisms and if necessary addition of nitric acid to adjust pH and decrease viscosity , as a way to stabilize the suspension

Below, on figure 26, we present for Mn<sub>x</sub>O<sub>y</sub> compound I (powder) an example of the formulation calculation sheets that resume all parameters considered for the preparation of a suspension.

<b>BILAN QUANTITES BRUTES A PESER (g)</b>			
H2O	0	Masse sèche Oxyde (g)	3537,0
Charge Mn <sub>x</sub> O <sub>y</sub>	40000	Masse sèche Mn <sub>x</sub> O <sub>y</sub> (g)	28000,0
Charge Oxyde	0	Teneur en Oxyde (w%)	11,2
Charge Al-Si	0	Teneur en Mn <sub>x</sub> O <sub>y</sub> (w%)	88,8
Liant AlOOH	4500	Ratio L/C (AlOOH/ Mn <sub>x</sub> O <sub>y</sub> )	12,6
Liant Si(OH) <sub>4</sub>	0	Ratio L/C [(Si(OH) <sub>4</sub> +AlOOH+Al-Si) / Mn <sub>x</sub> O <sub>y</sub> ]	12,6
Liant Al-Si	0	Ratio L/C global [(AlOOH+Si(OH) <sub>4</sub> +Al-Si) / ΣM <sub>x</sub> O <sub>y</sub> ]	12,6
Acide	650	Taux d'acide p/ AlOOH (w%)	12,50
Liant Organique	5000	Taux d'acide p/ masse sèche totale (w%)	1,34
Dispersant	0	Taux de PVA p/ masse sèche totale (w%)	3,03
<b>SOMME</b>	<b>50150,0</b>	Taux dispersant p/ masse sèche totale (w%)	0,00
		<b>VOLUME TOTAL CUVE ESTIME (L)</b>	<b>25,0</b>
		MASSE TOTALE INTRODUITE (g)	50150,0
		MASSE SECHE INTRODUITE (g)	32979,0
		EAU LIBRE TOTALE (g)	17171,0
		TENEUR EN SOLIDE/ E.S. (w%)	65,76

Figure 26 - Example of formulation calculation sheet for the experimental trial named 120719

### Equipments

For the preparation of feed suspensions, four different reactors were used with a total volume ranging from 6 to 60L. They are equipped with various stirring devices but we always keep the objective of achieving a good homogeneity for suspension and a suitable flow for the recirculation mode or inside the pipes before the spray-dryer.

One of the reactors is represented on figure 27. This reactor contains two propeller stirrers, four counter-baffles and is normally connected with a pump that allows the product recirculation and with another pump that is connected with the spray drying equipment.



Figure 27 – Image of one of the Mixing reactors used in this work

### 3.2.2 Atomization step

The atomization step, like the preparation of suspensions, is also very important for the quality of products obtained at the end of the process. Therefore it is really necessary to determine and use the optimum operating conditions that allow to completely dry the particles and also to form particles with the desired shape and size.

For each experimental trial, some operating conditions such as inlet temperature, air nozzle pressure or pump flow were changed due to different characteristics of the feed suspension, and also to avoid some common problems such as clogging of pipes, wetting of walls and roof of the atomization chamber.

In the chapter about Characterizations & Results we can see a summary table resuming the experimental conditions for all spray-drying tests performed during this study.

Below, figure 28 shows in dark blue an example of operating conditions, specifically chosen for the experimental trial called 120719.

DETAIL DES CONDITIONS OPERATOIRES D'ATOMISATION					
Mesure pH	5,76	Visco (cP@ 100s-1)	1950	P°ligne (bar)	1
Config.	fontaine	Syst. Ato.	Buse pneu.	Type de buse	mel. ext.
D. buse (mm) / V turb (rpm)	3 (120)		P°air (bar)	3	
T entrée (°C)	180		Qair (0-100% ou hz)	100%	
Ql (L/h)	9		T sortie (°C)	120	
V Ato. (L)	55,2	Durée (mn)	150	Etat paroi	-
Masse G. (g)	14605	Masse F. (g)	1550	% F.	9,59%
d50 G. (µm)		SPAN G(d90-d10/d50)		d50 F. (µm)	

Figure 28 - Example of spray-drying conditions for the experimental test 120719

### Pilot Spray Drying Tool (APV brand; Type PSD 55)

The atomization of the CLC suspensions was performed in a APV-Anhydro PSD 55 spray-drying tool (figure 29). This pilot equipment can operate in co-current or mixed flow mode which allows choosing placement of the nozzle, either at the top (roof mode).or at the bottom of the drying chamber (fountain mode).

The liquid suspension is pumped to a nozzle then atomized or pulverized in small droplets through the chamber. We precisely control the pump flow in order to regulate the outlet air temperature, and therefore the moisture content in particles. Ambient air enters in an electrical heating device where its temperature increases up to 350°C, prior to entering the drying chamber and contacting droplets of suspension. The powder and hot and humid drying air leave the chamber at the conical bottom part and particles are conveyed either to a main container for the largest particles (coarse particles collected at the bottom of the chamber) or to a cyclone device, from where fine particles fall to a second container. Then hot air is discharged at the top of the cyclone and goes through a gas wet scrubber to eliminate the ultrafine particles that could be dangerous for the environment [58].

An image of the spray-drying tool used in this work can be viewed on figure 29.

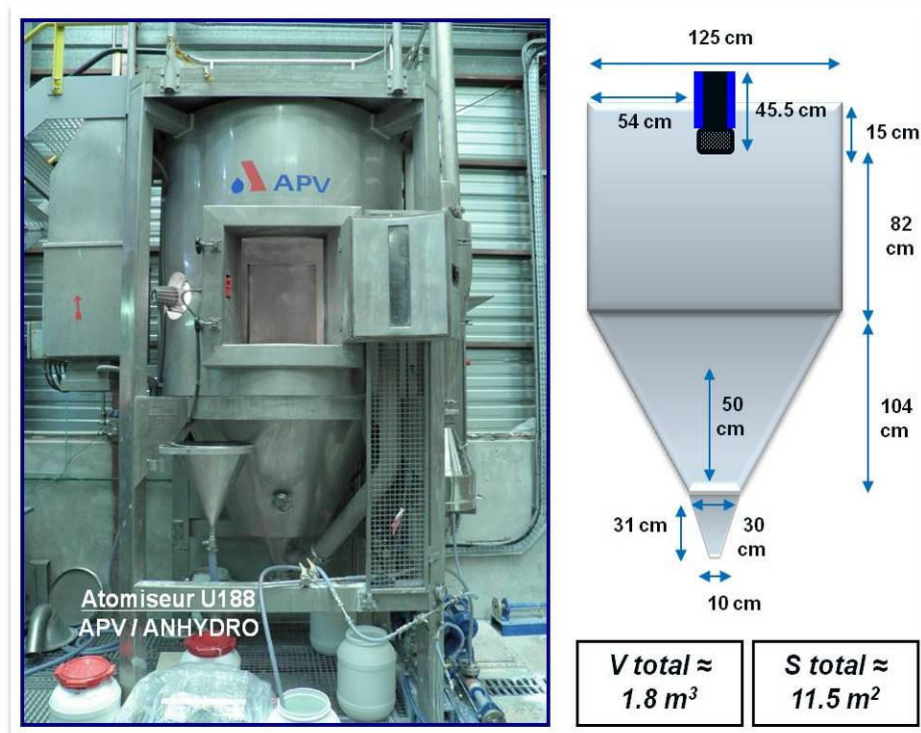


Figure 29 - Spray Drying Tool

### 3.2.3 Calcination step

Calcination under air, as mentioned before, is an important step to completely remove water, burn out organic components and fully oxidise mineral phases (boehmite is then transformed in a transition or  $\alpha$  alumina). Depending on the temperature, this thermal treatment may generate an increase in density and mechanical strength of the particles. So in our case we intend to consolidate the particles and make them more resistant to stresses and attrition occurring at high temperatures of the CLC process.

For this study it was planned to perform two calcinations steps, one with a final temperature of about 700°C and the other one at 1200°C. However it was not possible to do that due to technical problems with the high temperature furnace, so all the products were treated at 700°C but only 3 products were calcined at a higher temperature.

To avoid a heat shock and consequently the possible breakage of particles, a moderate calcination ramp was used (1°C/mn), including three levels of stabilized temperature respectively at 80°C (to remove residual free water), 300°C (to burn out organic phases) and 700°C (to transform in oxide), as can be seen below on figure 30.

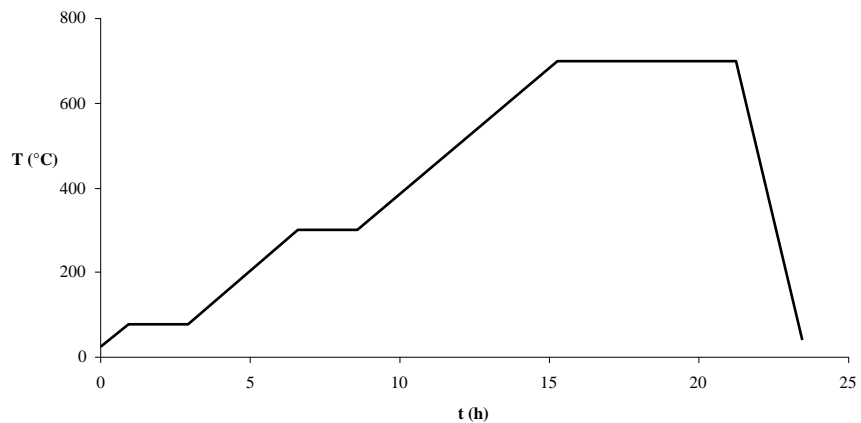


**Figure 30 - 700°C Calcination Curve**

For the second calcination at 1200°C, we cannot choose a calcination ramp because the furnace is constructed with a moving carpet and particles can only be submitted to one fixed temperature.

### **Furnaces**

Two furnaces were used for the calcination step, one of them for calcinations at 700°C and the second one for calcination at 1200°C. The first one (figure 31-A) is a polyvalent muffle furnace, which may be programmed to perform a ramp like that described in figure 30, including four compartments and a ventilation system. The second one (figure 31-B) is a high temperature conveyor furnace with a length of about 8 m, with a heating compartment of about 2m followed by a cooling zone of about 6 m. The heating area has a constant high temperature, so the ceramic containers must be pre-heated before entering the furnace to avoid a heat shock and a possible breakage.

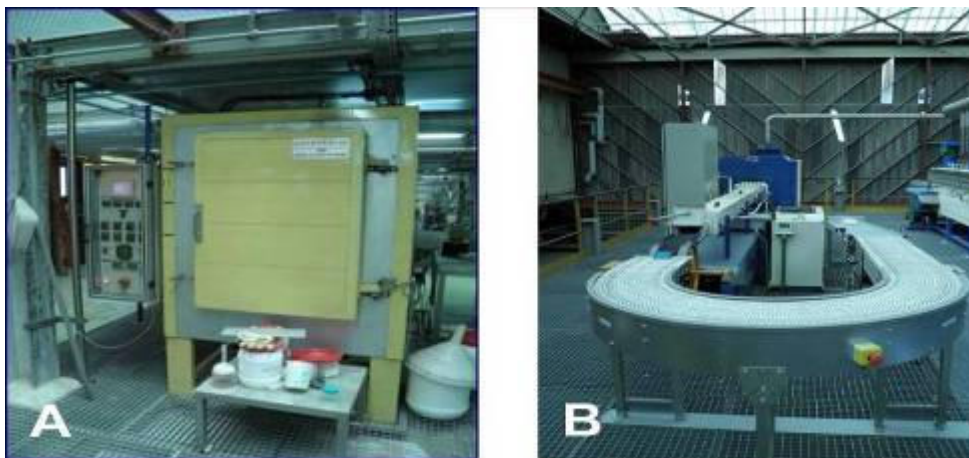


**Figure 31 - Polyvalent muffle furnace (fig.A) and high temperature conveyor furnace (fig.B)**

### 3.2.4 Sieving

The objective of this study was to obtain particles with a size ranging between 100 and 300  $\mu\text{m}$ . That's why, after the calcination step at 700°C, the product was sieved to remove all the smaller (<100 $\mu\text{m}$ ) and bigger particles (>300 $\mu\text{m}$ ). For productivity considerations two equipments, were used, one of them equipped with 100 and 315  $\mu\text{m}$  sieves and the other one with 75 and 250  $\mu\text{m}$  sieves. The first equipment is a simple laboratory sieving device on which it's possible to regulate the vibration power and the duration (figure 32-A). The second one (figure 32-B) is a pilot sieving equipment that includes a vibration and also an ultrasonic system that avoids blockage, fouling and clogging of the sieves and allows to have a fast and high performance process. However only one sieve can be used each time, so to get the right fraction (100-300 $\mu\text{m}$ ) for each main powder, two passages are needed.

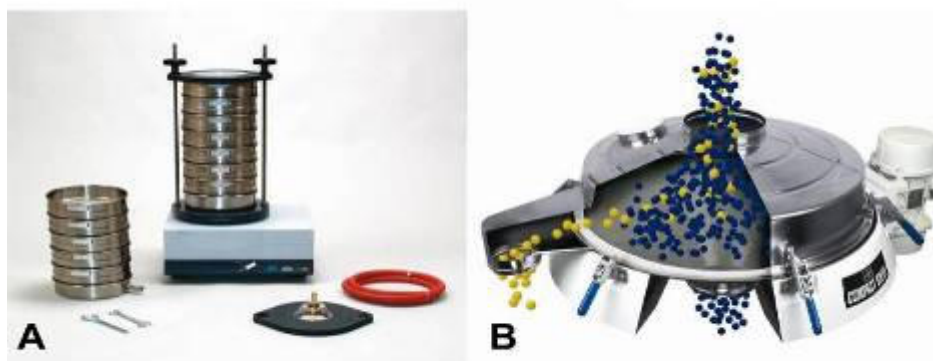


Figure 32 – Images of the two sieving equipments used in this work

## 3.3 Characterization Techniques

In this section, all the techniques used to characterize our products are briefly described.

### 3.3.1 Laser Granulometry

Laser Granulometry is a characterization method that is used to measure a particle size distribution. This method is based on the principle that there is a direct relationship between the size of particles and the degree to which they diffract light. There are two particularly important theories when it comes to laser granulometry, namely the Fraunhofer theory and the Mie theory. Differences between the two rely on the fact that the Fraunhofer theory is applicable for large particles (compared to wavelength), since diffusion and adsorption phenomena are not considered. The Mie theory is more appropriate for small particles, as it takes into account diffusion and adsorption effects around the particles and in the analytical medium. [59]

### **The Coulter™ LS230 laser granulometer**

The Coulter™ LS230 laser granulometer measures particles size by laser diffraction, based on the Fraunhofer diffraction theory. It measures particles sizes ranging from 0.4µm to 2000 µm. A schematic diagram of the granulometer can be seen in figure 33. [60]

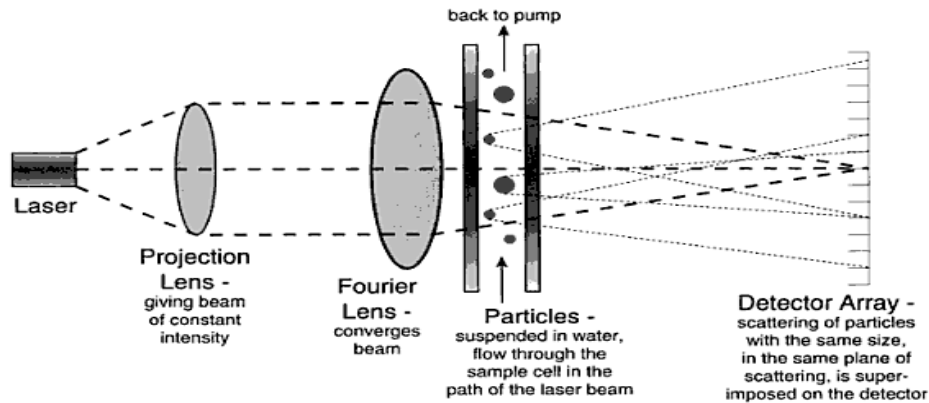


**Figure 33 - Schematic diagram of the Coulter™ LS230 laser granulometer [60]**

The basic operating procedure requires a small amount of sample to be added to a water reservoir in the fluid module (wet dispersion). The granulometer is operated via a PC running a specialized Particle Characterization software. A large number of sample preparation and instrument run conditions can be used.

An ultrasonic treatment, either before or during sample run may aid disaggregation of the sample, although some particles may disintegrate if they are sonicated for too long.

A range of statistical parameters can be generated by the instrument software, including average, median, mode, span, standard deviation, variance and cumulative percentile values.

### **3.3.2 Rheology**

A rheometer is a laboratory device used to measure the way in which a liquid, suspension or slurry flows in response to different applied forces. It is used for those fluids which cannot be defined by a single value of viscosity and therefore require more parameters to be set and measured than in the case of a viscometer.

Rheological measurements were performed in a Dynamic Stress Rheometer (Rheometrics RS200), with a parallel plates configuration (figure 34). H represents the gap between two plates, which depends on the amount of fluid sandwiched between both surfaces.

Typically the upper plate is rotated and the force on the plate is measured. The movement of the plate is resisted by a thin piece of metal which twists - known as a torsion bar. The known

response of the torsion bar and the degree of twist give the shear stress, while the rotational speed and plate dimensions give the shear rate.



Figure 34 - Parallel plates configuration and rheometer used in this work

The viscosity was also measured with a Brookfield Viscosimeter that gives a value of viscosity at a certain shear rate (about  $100\text{s}^{-1}$ ) moment. Those measurements only gave qualitative informations (Brookfield Viscosimeter is not adapted to non-Newtonian fluids) and were used as an indicator to conduct the experimental tests, particularly with regards to the limits of operating conditions for mixing and pumping.

### 3.3.3 Loss On Ignition

Loss On Ignition means the mass of material lost during a thermal treatment. It consists in strongly heating a sample of the material at a specified temperature, allowing volatile substances to escape, until its mass ceases to change.

This simple test typically consists in accurately weighing a few grams of the material in a tarred, pre-ignited crucible then placing it in a temperature-controlled furnace for a set time at the required temperature, cooling it in a controlled (e.g. water-free, CO<sub>2</sub>-free) atmosphere, and measuring the final mass. The process may be repeated to ensure that mass-change is complete.

This parameter is very important because it gives an idea of the real value of water content in particles and residual moisture after drying. As its value increases, it means that the quantity of volatile substances in the material is higher and that the percentage of solid product decrease.

### 3.3.4 Scanning Electron Microscopy (SEM)

A scanning electron microscope (SEM) is a type of electron microscope that images a sample by scanning it with a high-energy beam of electrons in a raster scan pattern. The electrons interact

with atoms that make up the sample producing signals that contain information about the sample's surface topography, composition, and other properties such as electrical conductivity.

By using electrons instead of light, SEM produces a magnified image larger than optical microscopy. Scanning electron microscopes have a large depth of field and much higher resolution than traditional optical microscopes. Because it uses electromagnets instead of lenses, researchers have much more control in degree of magnification, but analysis is often limited to small samples.

The beam of electrons is produced at the top of the microscope by an electron gun. The electron beam follows a vertical path through the microscope chamber, with a vacuum atmosphere. The beam travels through electromagnetic fields and lenses, which focus it towards the sample. Once the beam hits the sample, electrons and X-rays are ejected from it. [61]

Detectors collect X-rays, backscattered electrons and secondary electrons and convert them into a signal that is sent to a sensitive screen that produces the final image. [61] A scheme of a SEM and the equipment used in this work can be seen in figure 35.

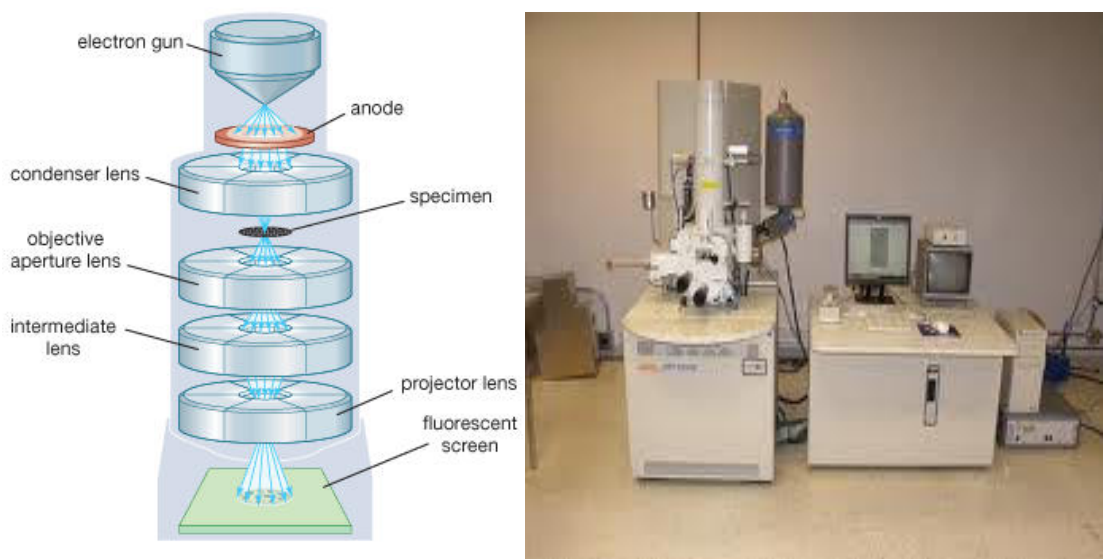


**Figure 35 - General scheme of Scanning Electron Microscopy, and equipment used in this work [62]**

Because SEM operates under vacuum conditions and uses electrons to form an image, special preparations of the sample must be performed. All water must be removed from samples, as water would vaporize in vacuum. Also, since all metals are conductive, they don't require any preparation before being analyzed. On the other hand, all non-metals need to become conductive, which is made by covering the sample with a thin layer of conductive material (generally Au or Pt). This is made with a sputter coater. [63]

The sputter coater is a plasma device that uses an electric field and argon gas. The sample is placed into a chamber under vacuum conditions. An electric field causes an electron to be removed from the argon, making the atoms positively charged. Argon ions become attracted to a negatively charged target (gold foil). Then, the argon ions knock atoms from the surface of the gold foil. These atoms are ejected onto the sample surface, producing a thin gold coating. [63]

Sample preparation, for the purposes of this work, should be performed as follows: the sample (powder) must be placed in a graphite tablet (or graphite paste) and metalized, in order to allow the passage of electrons. The samples were analyzed in a JEOL JSM 6340F microscope.

### 3.3.5 BET Surface and N<sub>2</sub> isotherms

N<sub>2</sub> adsorption analysis tools allow determination of the textural parameters of porous solids such as surface area expressed in m<sup>2</sup> / g (real accessible area, ie on the material surface and including pores surface), the available pore volume (expressed in cm<sup>3</sup>/g) , pore size (given in nm) and distribution of pore sizes.

Therefore the products synthesized are characterized by their surface area (measurement of surface area, S<sub>BET</sub>), their mesoporous volume and their average pore diameter (analysis by mercury porosimetry). Both methods are based on adsorption of a gas or a liquid, on the surface of a solid that differs by its scope. Indeed, the volume of nitrogen adsorption analysis is applicable to microporous and mesoporous materials. It covers a range of pore diameters smaller than 50 nm. On the other side mercury porosimetry (Hg) is adapted to analysis of mesoporous and macroporous materials, covering various pore diameters ranging from 3 nm up to a hundred microns.

For the determination of specific surface area the adsorption isotherms of N<sub>2</sub> were measured using an ASAP2000 apparatus. The product mass (about 200 mg) was measured on a Mettler AG204 balance. Before measuring the isotherm, the compound to be analyzed must undergo a degassing step by vacuum drying for 3 hours, which eliminates any product adsorbed on its surface (water or other gas molecules).

The shape of the isotherm provides qualitative information on the type of material analyzed (microporous, mesoporous). The isotherm is constructed with 64 points, within the interval of pressure from 730 to 770 mmHg. The apparatus gave the pore volume distribution and the surface area versus the pore diameter. The specific surface was measured by BET method and the pore volume distribution by Kelvin relation, following the adsorption of N<sub>2</sub>.

### **3.3.6 Mercury Porosimetry**

Porosimetry is an analytical technique used to determine various quantifiable aspects of a material's porous nature, such as pore diameter, total pore volume, surface area, bulk and absolute densities, pore size distribution and to investigate the tortuosity, permeability, fractal dimension and compressibility of porous materials.

The technique involves the intrusion of a non-wetting liquid (often mercury) at high pressure into the material through the use of a porosimeter. In our case mercury porosimetry consists in pushing mercury into the pores of the samples and it is then possible to relate the volume of mercury injected at a given pressure to the pore diameter. By the application of various levels of pressure to a sample immersed in mercury it is possible to characterize a material's porosity. Indeed based on the external pressure needed to force the liquid into a pore against the opposing force of the liquid's surface tension, the pore size can be determined.

This technique is based on the fact that mercury does not wet most substances and, therefore, will not penetrate pores by capillarity unless it is forced to do so. Entry into pore spaces requires the application of external pressure to balance the capillary pressure drop. By assuming that the pores are cylindrical, and this is a major drawback of the method, the applied pressure can be related to the pore diameter, knowing surface tension and contact angle of mercury

For meso- and macro-porous materials, the pore size distribution is determined by measuring the volume of mercury forced into the pores under pressure. The measurement of pore size distributions in the range of 3,75-7500 nm are performed with a mercury pressure porosimeter at pressures ranging from 0,1 to 200 MPa. The pore sizes are precisely calculated using pore volume and surface area data.

### **3.3.7 Bulk Density**

Bulk density is an important property of powders, granules and other divided materials, especially those used as catalyst supports in refining industries. Bulk density is defined as the mass of many particles of the material divided by the total volume they occupy. This total volume includes particle volume, inter-particle void volume and internal pore volume. The bulk density is not an intrinsic property of a material and it can change depending on how the material is handled. For powders or pellets, density is primarily defined as the weight of a material per unit volume. The test consists in a simple process where the powder is "freely settled". Experimentally, a funnel is positioned above a measuring container or cylinder. The funnel is filled with the sample and allowed to freely flow into the measuring container. The material excess on top of the container is removed off with a straight tool. The sample and the cylinder is then weighed and the weight / volume can be determined.

### 3.3.8 Attrition resistance

An attrition test is a test carried out to measure the resistance of a granular material to wear. Classic examples of a material subjected to an attrition test are stones used in road construction, indicating the resistance of the material to being broken down under road traffic. Heterogeneous catalysts such as FCC particles are also subjected to attrition tests to determine their mechanical strength and physical performance in industrial reactors.

The test itself involves agitating the particles, typically by tumbling within a drum, vibration, or with jets of gas to simulate a fluidized bed. After a specified time, the material is sieved and the sieved material weighed to measure the proportion of material which has been reduced to below a certain size (referred to as 'fines'). The specifics of the test are defined by various standards as applicable to the purpose in question, such as those defined by ASTM or PSRI. Figure 36 presents the IFPEN Jet cup attrition test equipment.



Figure 36 IFPEN Jet cup attrition test

In our case, according to PSRI standards we used a jet cup attrition test which is a common method for evaluating particle attrition in fluidized beds. An attrition index, calculated from jet cup data, is used to compare with one or more reference materials.

For our materials, attrition resistance will be expressed with the attrition factor (A%) established for particular CLC conditions (Gas flow and duration). We can see on figure 36 some images of the device used at IFPEN

Considering fine particles as the powder fraction inferior to 20 $\mu$ m, the attrition rate can be determined as follow:

$$A (\%) = \% \text{ fines produced} - \% \text{ fines at the beginning}$$

# 4 Results & Discussion

---

This chapter intends to present and discuss the results obtained during preparation of the CLC particles.

The first part is related to the formulation of feed suspensions and to their rheological behavior.

In the second part, all tests are presented and analyzed, with some comments on experimental procedures and we also briefly describe the most relevant points or events that occurred.

Then for each trial we describe and comment the characterization results.

Finally for each experimental test, the main characteristics concerning preparation, treatment and properties of final products are summarized on table 7 and 8.

## 4.1 Formulation and rheological behavior

Generally concentrated suspensions of hard particles can be described as a viscoplastic fluid, i.e. a shear thinning fluid with a yield stress. Thus, one basic approach describing the flow behavior and the rheological properties of our suspensions can be done by using the Herschel-Bulkley model (tendency to display power law rate dependence). A Herschel-Bulkley fluid can be described mathematically as follows:

$$\tau = \tau_0 + k\gamma^n$$

Where  $\tau$  (MPa) is the shear stress,  $\tau_0$  (MPa) is the bulk yield stress; k (Pa.s-n) is the consistency/viscosity index;  $\gamma$  (1/s) is the shear rate and n is the power law exponent.

Concerning the rheological behavior, for all raw materials used, it was determined that the great majority of suspensions present a shear thinning behavior. Shear thinning fluids which are non-Newtonian fluids, are identifiable when their viscosities decrease, as the applied shearing stress increases. Therefore according to the chosen representation, it can be seen on figure 37 that the shear stress increases with an increase in shear rate (while viscosity decreases). For this particular flow curve we can see that the value of yield stress is about 50 Pa but it is also important to remark that the rheological behavior is quite similar to that of a Bingham fluid.

DM\_MM\_100712\_ES45\_5p\_test 1

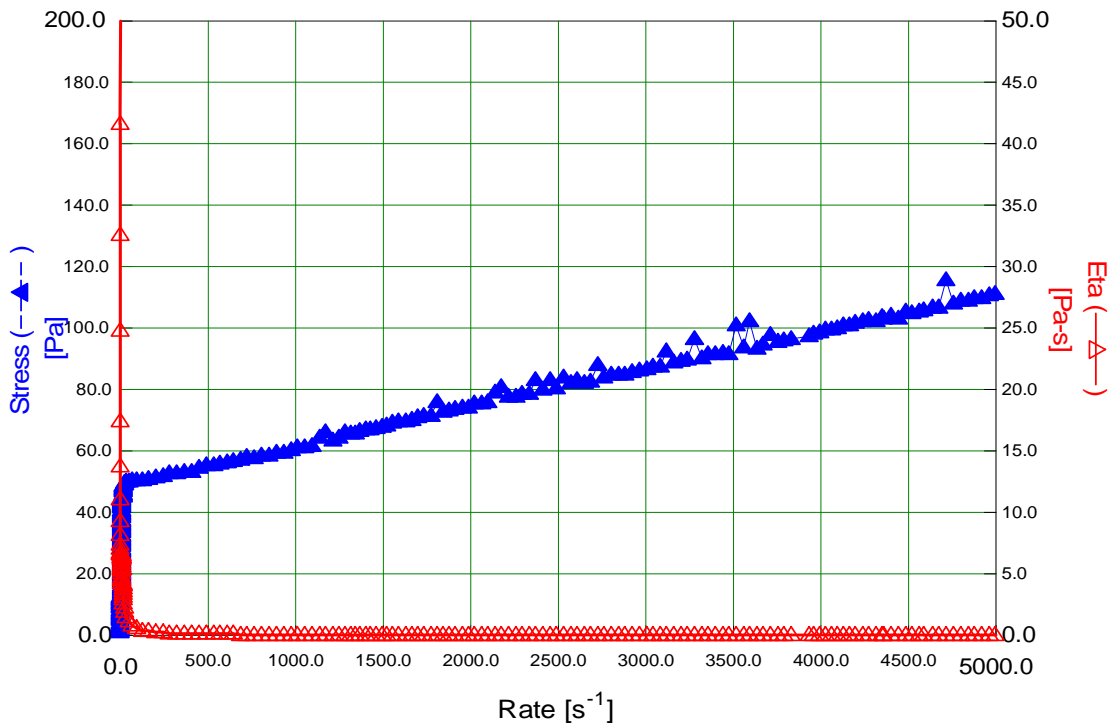


Figure 37 Flow curves showing shear stress (Pa) and viscosity (Pa.s) versus shear rate (s-1) for a "Mn suspension"

## 4.2 Experimental Tests

### 4.2.1 Tests on FeCuAl raw material

Sixteen tests were made using "FeCuAl" as raw material. However only thirteen products were recovered due to different problems.

It's important to note that Tests 120612 and 120613 were accidentally mixed in the sieving step and that the corresponding product was lost during calcination at 1200 °C because of a technical problem with the high temperature furnace. The suspension produced during test 120614 was extremely viscous and our pump was not sufficiently powerful to transport it toward the pneumatic nozzle positioned into the atomization chamber.

Table 7 presents preparation and formulation characteristics of each suspension, operating conditions of spray-drying and also particles size and total mass of the final product. The last column presents an internal assessment of each test considering particle size, product mass, but also operating conditions & costs.

As can be seen, only few products achieve the objective concerning the particles size requirement, but tests 120611, 120612b and 120615 still represent satisfactory results. Regarding preparation conditions, table 7 shows that operational reactors and pipes were frequently adapted due to a poor performance of certain equipments to perform this kind of test.

Table 8 describes for each test the post-treatment steps and also presents results from granulometry, porosimetry and density analysis.

Table 7 - Summary table of FeCuAl formulation tests

Test	Catasepa	Charge	d50 p.p. / susp. (µm)	Solid Content (w%)	Al binder/ Charge (w%)	Org. binder (w%) / type	pH / H+ (w% p/AlOOH)	To (Cp) / Visco (Cp@100s-1)	Preparation Conditions	Ato. Cond. Ti - To (°C) / Ql (L/h) / Rpm Vent.	Nozzle (mm) / P°air (bar)	d50 G (µm)	d90 G (µm)	Mass G (g)	Balance / €
<b>Goal</b>	-	<b>MxOy</b>	<b>2 / 8</b>	<b>&gt;45</b>	<b>10</b>	<b>3 / 120k</b>	<b>4 / 4</b>	<b>10000 /1000</b>	<b>New lignes CLC/FT</b>	<b>280-120 / 20/2000</b>	<b>Buse 120/ 3</b>	<b>200</b>	<b>250</b>	<b>-</b>	<b>++++</b>
120523	110271	FeCuAlOOH 1µ	1,77 / -	30,11	10,2	3,1 /Opt.60	- / 3	-	R50+ISI	280-120/28,5/2000	Buse 100 / 3,5	36	59	4520	+
120524	110273	FeCuAlOOH 1µ	1,9 / -	30,8	10,3	6/Opt.60	- / 3	-	R50+ISI	195-103/18/2900	Buse 120 / 2,5	21	51	2760	+
120530	110278	FeCuAlOOH 1µ + G 20µ	1,54 ; 20 / -	30,01	12,0	4,6/Opt.60	- / 4	-	R50+ISI	150-90/11,5/2000	Buse 120 / 2	90	152	889	+++
120601	110281	FeCuAlOOH 1µ + G 20µ	1,61 ; 20 / -	28,5	9,7	4,4/Opt.60	- / 4	1300	R6L+ISI	165-90 / 12 /2000	Buse 120 /1,5	101	190	1067	+++
120604	110283	FeCuAlOOH 1µ + G 20µ	1,61 ; 20 / -	32,4	10,2	4,8/Opt.60	- / 4	3200	R50 + SPX15 + GMC +ISI	175-85 / 12 /2000	Buse 120 / 1,5	78	121	2712	++
120605	110287	FeCuAlOOH 1µ + G 20µ	1,61 ; 20 / -	32,8	10,1	4,9/Opt.60	- / 4	-	R50 + SPX15 + ISI	185-85 / 16 /2000	Buse MT /5	81	114	2366	++
120607	110294	FeCuAlOOH 1µ	1,61 / -	32,1	12,7	3,7/Opt.60	- / 4	800	R6L + ISI13 & PCM	140-90 / 7 /2000	Buse 120 / 1	91	159	1059	+++
120611	110296	FeCuAlOOH 1µ + G 20µ + Si(OH)4 vieilli	1,61 ; 20 ; 50 / -	45,3	10,2	3,9/Opt.60	- / 5,5	800	R6L + ISI13 & PCM	155-85 / 7(3,5) /2000	Buse 120 /1,5	132	213	1411	++++
120612	110557 (110297)	FeCuAlOOH 1µ	1,61 / -	46,1	8,2	3,1/Opt.60	- / 12,8	400	R6L + ISI13 & PCM	155-90 / 7(3,5) /2000	Buse 120 / 1,75	84	207	867	+++
120612b	110298	FeCuAlOOH 1µ + G 20µ	1,61 ; 20 / -	52,1	5,7	2,2/Opt.60	- / 12,6	1100	R6L + ISI13 & PCM	165-90 / 7(4) /2000	Buse 120 /1,5	137	294	2046	++++
120613	110557 (110299)	FeCuAlOOH 1µ + G 20µ	1,61 ; 20 / -	51,5	16,2	2,2/Opt.60	- / 4	1600	R6L + ISI13 & PCM	155-90 / 7 (6) /2000	Buse 120 / 3	154	242	603	++++
120614	110300	FeCuAlOOH 1µ	1,61 / -	44,2	20,3	3,8/Opt.60	- / 4	3000	R6L + ISI13 & PCM	160-110 / 12 (6) /2000	Buse 120 /3	-	-	-	
120615	110301	FeCuAlOOH 1µ + Si(OH)4 vieilli	1,61 ; 50 / -	37,4	13,3	3,2/Opt.60	- / 5,5	900	R6L + ISI13 & PCM	140-80 / 7,5 (3,5) /2000	Buse 120 / 0,5	132	227	1095	++++
120618	110303	FeCuAlOOH 1µ + Si(OH)4 vieilli	1,61 ; 50 / -	33,6	12,3	5,5/Opt.60	- / 5,5	1700	T9 + ISI13 & PCM	140-78 / 7,5 (4) /2000	Buse 120 /4	103	134	1750	++
120618b	110304	Si(OH)4 vieilli + SiO2 aero 90	1,61 ; 50 ; / -	34	12,0	5,3/Opt.60	- / 5,4	2000	T9 + ISI13 & PCM	140-85 / 6 (3) /2000	Buse 120 / 3,5	55	90	360	+
120618c	110305	Si(OH)4 vieilli + SiO2 aero 90	1,61 ; 50 ; / -	33,4	13,0	5,6/Opt.60	- / 7,8	-	T9 + ISI13 & PCM	140-85 / 6 (5) /2000	Buse 120 /3	88	132	1756	++

Table 8 - Summary table of analysis on FeCuAl tests

Test	Catasepa	LIMS	Thermal Treatments (°C)	Sieving	Mass after Calcination/Sieving(g)	d50 / d90 (µm)	SPAN	Attrition test (w%)	Sbet (m <sup>2</sup> /g)	Vpt (ml/g)	Vp macro (ml/g)	Dp macro (nm)	DRT (kg/m <sup>3</sup> )
Goal	-	-	700/1200°C	75-250 µm		150/200	1	<10	>20	> 0,1	>0,05	>500 nm	>2000
120523	110271	1203290	700	100-315	1328	138/276	1,806	-	37,5	0,45	0,29	221,5	790
120524	110273	1203293	700	100-315	385	56/278	4,945	-	36	0,55	0,39	336,34	830
120530	110278	1203283	700	75-250	470	42/132	3,032	-	66	0,55	0,3	258,28	810
120601	110281	1203284	700	75-250	235	94/214	2,131	-	47	0,39	0,21	236,31	920
120604	110283	1203291	700	75-250	500	78/165	1,863	-	33,5	0,39	0,2	171,15	990
120605	110287	1203289	700/1200	75-250	?	129/335	2,229	-	0	0,02	0,02	2734,6	2110
120607	110294	1203285	700	75-250	365	45/151	3,129	-	27	0,36	0,21	1333,5	940
120611	110296	1203281	700	75-250	485	55/294	5,199	-	33	0,38	0,22	1374,1	840
120612	110557 (110297)	-	700/1200	75-250	0	-	-	-	-	-	-	-	-
120612b	110298	1203280	700	75-250	425	39/167	4,09	41,7	12	0,34	0,26	1160,2	930
120613	110557 (110299)	-	700/1200	75-250	0	-	-	-	-	-	-	-	-
120614	110300	-	-	-	-	-	-	-	-	-	-	-	-
120615	110301	1203282	700	75-250	440	47/170	3,484	-	41	0,41	0,23	1470,5	860
120618	110303	1203287	700/1200	75-250	250	142/298	1,659	-	0	0,01	0,01	1504,1	2170
120618b	110304	1203288	700/1200	75-250	35	82/140	1,133	-	0	0,02	0,02	2434	-
120618c	110305	1203286	700	75-250	390	79/185	1,945	-	57	0,37	0,19	462,53	940

### **Test 120523**

For this test the suspension was prepared in a 50L reactor (R50). The product was then directly conveyed thanks to a peristaltic pump toward the spray drying equipment. This first test did not operate very well due to a limited knowledge about ideal operating conditions with this new raw material. The most relevant event was the wetting of walls of the atomization chamber due to a high viscosity of suspension which resulted in the loss of some product.

### **Test 120524**

In this test we used the same equipment as in test 120523. The feed pipes clogged twice and the walls of the chamber were wet which resulted in a humid final product. Figure 38 presents the particle size distribution of the products 120523 and 120524 after spray-drying and calcination.

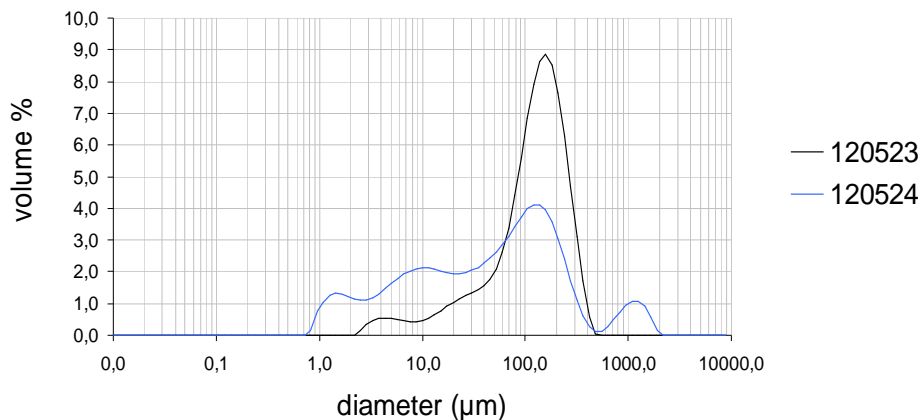


**Figure 38 - Granulometry of products from test 120523 and 120524 after spray drying and calcination (700°C)**

Between tests 120523 and 120524, the major differences of formulation and spray-drying conditions were the content of organic binder, respectively about 3 and 6 w% (expressed versus total solid content) and also the fan speed, respectively about 2000 rpm and 2900 rpm, that modulates the hot air stream. In figure 38 we can observe that Particle Size Distribution (PSD) for test 120523 presents a classic shape which is not the case for test 120524. For this test the wide range of particle size values (multimodal distribution) and presence of a lot of small particles could be explained by higher ventilator speed, which causes more shocks and breaking of some particles. In table 8 it's possible to see that product 120524 has a higher density value probably due to the higher content of organic binder that provides more cohesive particles by reinforcing interactions and bonding strength between raw materials. With a higher density, particles have normally a higher mechanical strength. We can suppose that if the fan speed was the same for both tests, we could have obtained a better PSD for test 120524.

### **Test 120530**

The equipment and configuration used in this test were the same as in test 120523. The pipe clogged twice because the suspension was highly viscous and walls of the chamber were wet as soon as the spray-drying started despite a lower liquid flow than in other tests.

### **Test 120601**

This suspension was prepared in a small reactor with a volume of 6L connected to the spray-dryer with a peristaltic pump. For this we used a shorter pipe, about 5 times shorter than that previously used, to see if the problem of blockages and clogging was caused by the pipe length. However the pipe clogged four times, which allows us to conclude that the problem was not caused by the length of the feeding line. The walls of the chamber were wet, but despite those problems, the production yield was much higher than in previous tests.

### **Test 120604**

In this test, the fifty liter reactor (R50) was used again, and a peristaltic pump coupled with a colloidal mill were added to the line to create a continuous recirculation mode. Our objective was to homogenize and stabilize the suspension in order to avoid clogging of pipes. This objective was partially achieved because of two clogging at the nozzle boundaries due to a high viscosity. The walls of the spray-dryer were wet due to high viscosity and a low inlet temperature when product entered in the atomization chamber. Figure 39 presents the particle size distribution of products 120601 and 120604 after spray-drying and calcination.

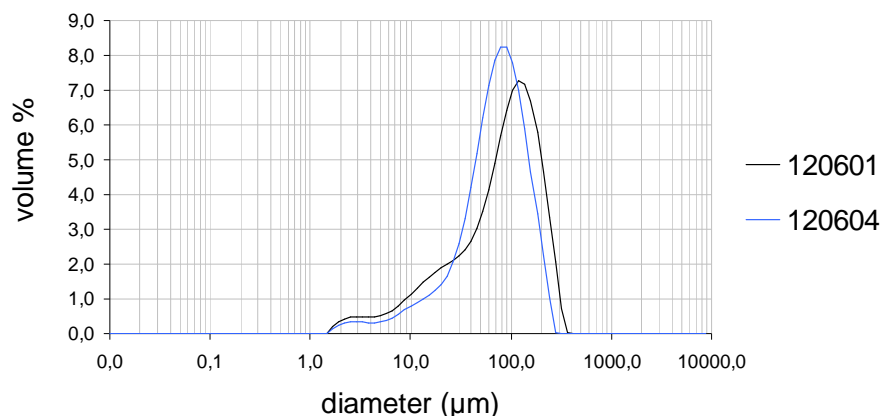


**Figure 39 - Granulometry of products from test 120601 and 120604 after spray drying and calcination (700°C)**

Tests 120601 and 120604 used a finely milled raw material (FeCuAl particles with size about 1µm) and also FeCuAl charges obtained after spin flash drying step (particles with size about 20 µm).

The major difference during preparation of these two tests was the solid content of suspension, respectively about 28,5 and 32,4 wt% which results in viscosity respectively of 1300 and 3200 cP (1000cP is equal to 1mPa.s). In figure 39 it can be observed that product 120601 presents bigger particles, and on the other hand 120604 presents a slightly narrower peak on PSD. Concerning the particle diameters, higher values for 120601 are quite surprising but could be explained by the use of a colloidal mill during preparation of 120604. It may reduce the size of aggregates present in the suspension, and thus reduces the droplets size.

We assume that the higher density obtained for particles of test 120604 (table 8) results from a higher solid content in the suspension.

### **Test 120605**

This test had the same configuration than test 120604 with the difference that the colloidal mill was removed for preparation, and the nozzle was changed for spray drying (trial of a multi-holes nozzle). Due to a high suspension flow at the beginning, the walls of the chamber were wet and a lot of agglomerates were collected in the final product.

On table 8 we can see that after sieving and calcinations at 700 and 1200 °C, the biggest particle diameters were obtained for this test,. The SPAN (polydispersity index =  $d_{90}-d_{10}/d_{50}$ ), a measure of monomodality of this PSD is about 2,2, a value slightly higher than our target (~1). Also, more than 50% of the particles have a diameter comprised between 100 and 300 µm. Figure 40 presents the granulometry of product 120605 after spray-drying and calcination.

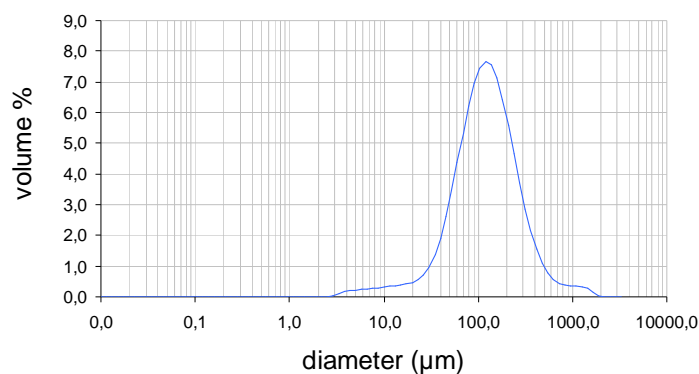


**Figure 40 - Granulometry of products from test 120605 after spray drying and calcination (700°C)**

Concerning the preparation step, tests 120604 and 120605 were quite similar, except in test 120605, the colloidal mill was taken out from the continuous recirculation mode. During spray-drying, for test 120605 the classic nozzle was changed to a multi hole nozzle and air pressure was also increased from 1,5 bar to 5 bar. Moreover product 120604 was calcined only at 700°C while product 120605 was calcined at 700 then at 1200°C which make these particles difficult to compare.

Figure 41 presents particle size distribution of both tests immediately after spray-drying. Both products have a similar value of  $d_{50}$  around 80  $\mu\text{m}$  (ie 50%>80 $\mu\text{m}$  & 50%<80 $\mu\text{m}$ ). However the value for peak mode, which represents the diameter for the main fraction of particles, is higher for product 120604. The blue curve (120605) has one higher peak around 80  $\mu\text{m}$  but has also a small peak around 30  $\mu\text{m}$ , which could be explained by the type of nozzle used for this test and the higher air pressure. Indeed this kind of nozzle has 6 holes oriented in different directions that may cause formation of fine particles due to an increase of collisions between particles but also with the chamber walls. This phenomenon may be accentuated by the air pressure increase conferring more velocity to the particles.

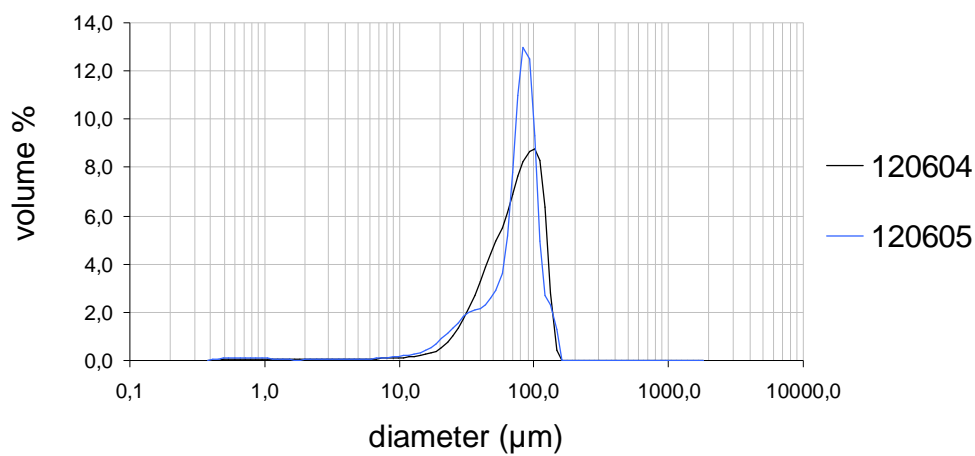


**Figure 41 - Granulometry for the raw atomized products of test 120604 and 120605**

Figure 42 presents the particle size distribution of the product obtained after calcinations at 700 $^{\circ}\text{C}$  for 120604 and 1200 $^{\circ}\text{C}$  for 120605. It is interesting to observe that after calcination, product 120605 presents a mean particle diameter higher than that of 120604. Test 120604 has a lot of particle diameters comprised between 1 and 20  $\mu\text{m}$  while 120605 has a considerable fraction of particles with a diameter higher than 300  $\mu\text{m}$  which may suggest formation of agglomerates with a thermal treatment at 1200 $^{\circ}\text{C}$ .

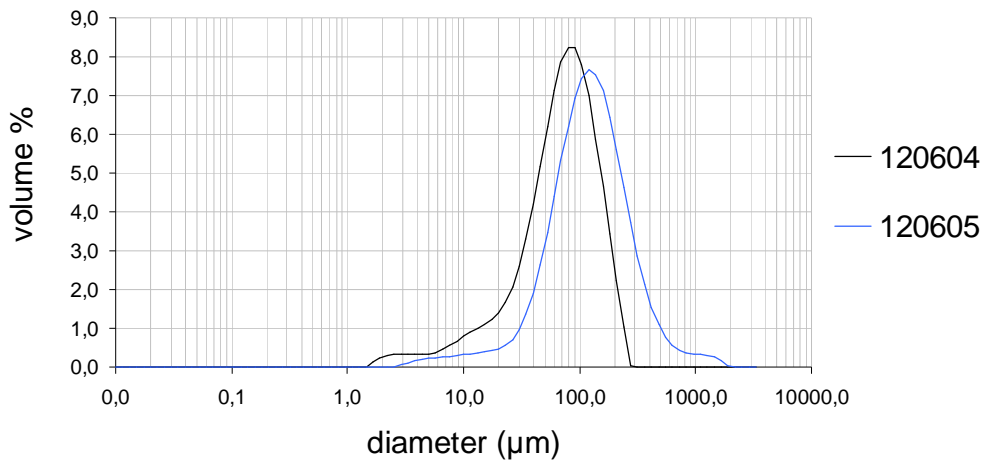


Figure 42 – PSD of products from test 120604 and 120605 after spray drying and calcination (700°C & 12 00°C)

### Test 120607

The suspension was prepared with the small 6L reactor already used in test 120601. Since for the majority of tests, the chamber walls were wet due to high viscosities and a difficult control between inlet flow, air pressure and ventilator speed, a positive displacement pump was introduced to feed the nozzle. This kind of pump allows having an almost constant flow which could prevent wetting problems that may appear with a pulse peristaltic pump. This test was conducted without major problems.

Figure 43 presents the particle size distribution of raw particles obtained after spray-drying with different air pressures. In this case we can verify that pressure has a low but significant influence on the final product size, with a higher particle diameter for lower pressure values.

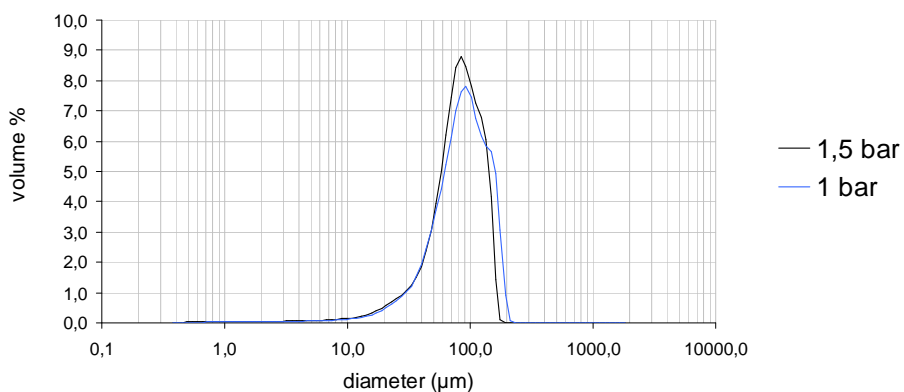


Figure 43 - Granulometry for product 120607 after spray-drying for pressures of 1 and 1.5 bar

### **Test 120611**

In this case we used the same equipments and lines as those for test 120607. No relevant occurrences were observed.

Concerning particle diameters (132  $\mu\text{m}$ ) and mass of product recovered at the end of spray-drying, this test could be considered as one of the best using FeCuAl as raw material; Besides, using SEM analysis we can observe (figure 44) that the majority of particles presents a diameter smaller than 60  $\mu\text{m}$  and also a non spherical aspect .

These observations may be explained by a low performance of sieving process that does not cut the fines fraction in the final product and/or deteriorate the shape and break big particles.

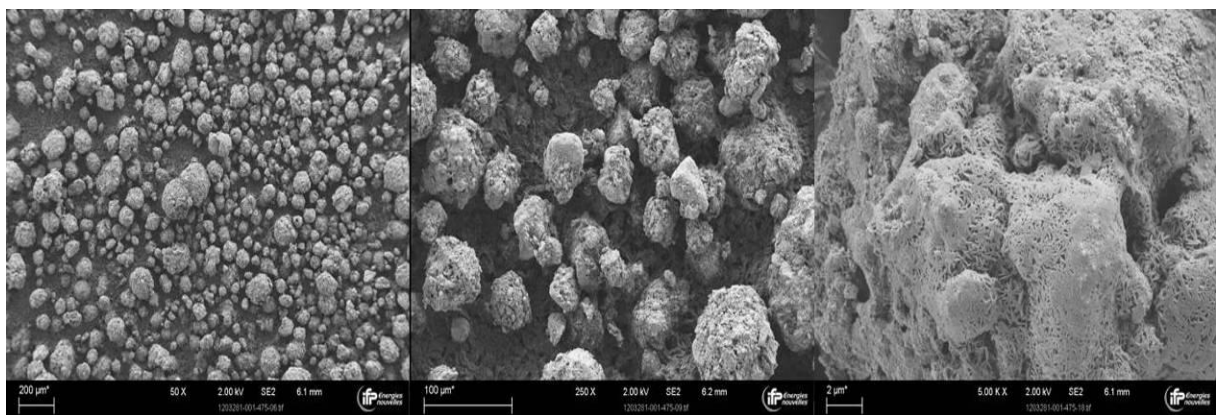


Figure 44 - SEM images of product 120611 (scale bar respectively of 200, 100 and 2  $\mu\text{m}$ )

### **Test 120612**

In this case we used the same equipments and lines as those for test 120607. The product obtained had a very irregular shape and had an high moisture content. This result could be caused by the lower content of mineral binder (peptized boehmite) and a lower viscosity. Therefore the binding phase between particles of raw material is less pronounced and the product is more sensitive to shocks and mechanical stress. As it was said before, this product was unfortunately mixed with 120613 during the sieving step due to a labeling error.

### **Test 120612b**

In this case we use the same equipments and lines that test 120607. Some of the sprayed suspension impacted walls of the atomization chamber which resulted in a product with irregular shape and not completely dry. Otherwise this test was the one, using FeCuAl as raw material, with the highest solid content resulting in higher viscosity and particle size collected. Nevertheless the lower content of mineral binder has lead to a poor mechanical cohesion in the bulk material, generating

sensitivity to shocks, some deterioration and a polyhedral shape for final products. That's why table 8 shows lower particle diameters for this product and also a higher SPAN.

SEM images show a lot of fine particles, but some spherical particles with a diameter around 150  $\mu\text{m}$ . The second image in figure 45 reveals an irregular surface which may result of the particle deterioration but could also be due to the presence of non-milled coarse grains (20 $\mu\text{m}$ ) mixed with small grains (1 $\mu\text{m}$ ) of raw material

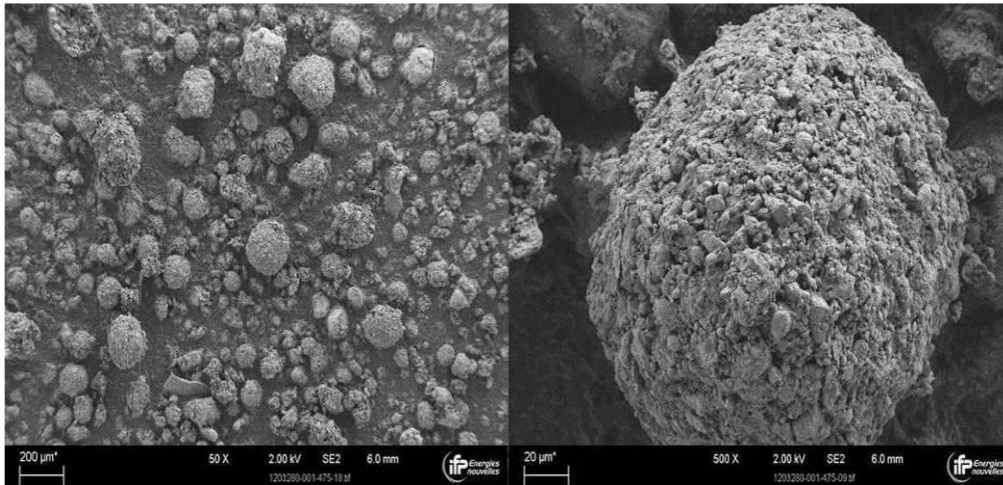


Figure 45 - SEM images of product 120612b (scale bar of 200 and 20  $\mu\text{m}$ )

Figure 46 shows a polished section analysis of tests 120611 and 120612b. In dark gray we can see a phase composed of Aluminum and Oxygen. This phase is present in the particle periphery and as can be seen in these images, product A (120611) shows a larger presence of Al and O rich phase than in product B (120612b). This observation was expected because in product A formulation, the alumina binder (peptized boehmite) is introduced with a weight ratio of 10% (ratio= dry mass of binder / dry mass of charges) whereas it's only 5,7 w% for product B.

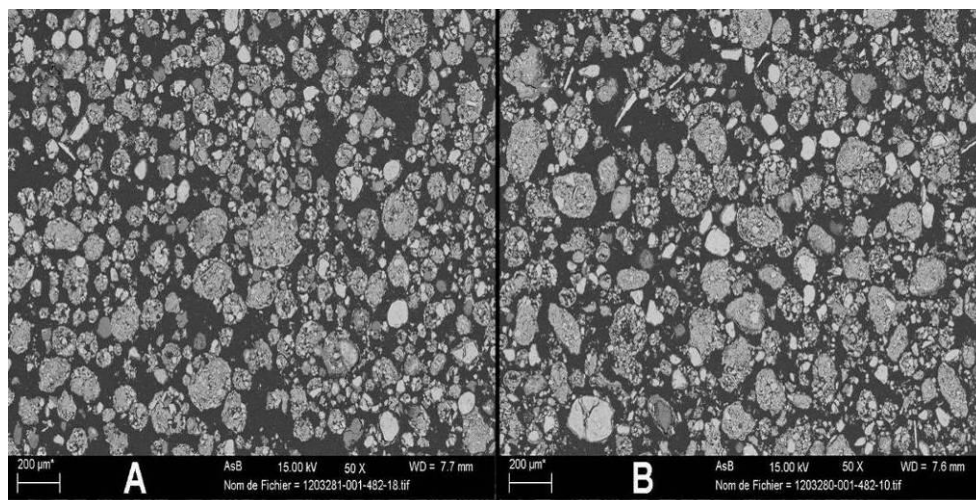


Figure 46 – Cross-section SEM images of products 120611 and 120612b

### **Test 120613**

In this case we used the same equipments and lines as those for test 120607. Due to the high viscosity of suspension, many product droplets impacted and wetted the walls of the atomization chamber and because of that a lot of product was not recovered. After spray-drying this product presents good values for  $d_{50}$  &  $d_{90}$  respectively of 154 and 242  $\mu\text{m}$ , however this product was unfortunately mixed with 120612 and lost after calcination at 1200°C due to furnace malfunction .

### **Test 120614**

In this case we used the same equipments and lines as those for test 120607. The suspension had a very high viscosity (3000 cP) which generated six clogging of pipes. Therefore, liquid product did not arrive at the atomizing nozzle, so absolutely no product was recovered. The high content of mineral binder (20,3w%), nearly two times higher than the usual content, was the cause for this higher viscosity and the impossibility to continuously pump and atomize the suspension.

### **Test 120615**

In this case we used the same equipments and lines as those for test 120607 and no major occurrences were observed.

Besides high diameters obtained after spray-drying, we can see in table 8 that the granulometry of the final particles presents a SPAN (polydispersity index) higher than the required value but also a low value of  $d_{50}$  that can be seen in figure 47. This image reveals also that particles have a very irregular shape with only few of them with a near spherical shape. We assume that small polyhedral particles and irregular morphologies result from cracks and breakage of big spherical particles.



Figure 47 - SEM images of product 120615 (scale bar of 100 and 20  $\mu\text{m}$ )

For test 120615, we present below on figure 48, the particle size distributions of products obtained at different air pressures and inlet suspension flows (expressed in % against full capacity of pump which is not really estimable during experimental trials due to an electric regulation). It is possible to verify that for lower air pressures, the size of particles is higher and also that influence of small variations of inlet suspension flow is almost negligible.

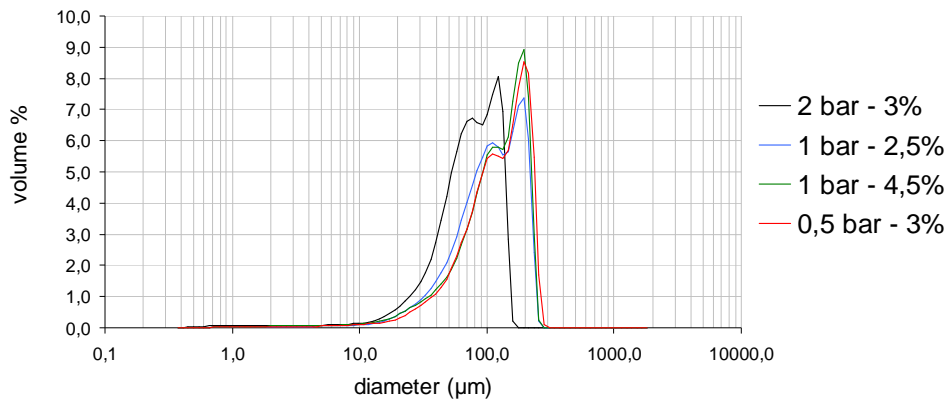


Figure 48 - Granulometry of product 120615 after spray-drying with air pressures of 0.5, 1 and 2 bar

### **Test 120618**

In this test we prepared a batch with a bigger volume of suspension in order to obtain more product. The suspension was prepared in the T9 mixing tank and then progressively transferred to the small reactor (6L) already used in previous tests. No major occurrences were observed. Figure 49 shows three particle size distributions obtained for different air pressures and inlet suspension flows.

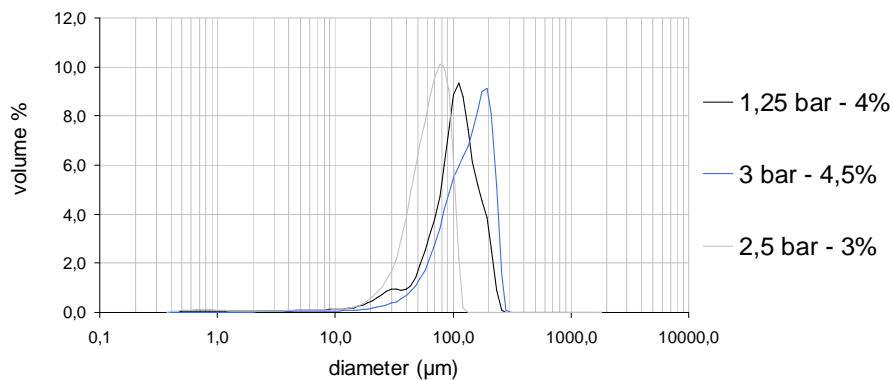


Figure 49 - Granulometry of product 120618 after spray-drying for pressures of 1.25, 2.5 and 3 bar

It is surprising to observe that the highest air pressure results in particles with bigger diameters which is opposite to the traditional trend for spray-drying. We assume that this particular result may stem from a difference in inlet flow or from the fact that these trials were achieved with a

unique mother suspension that may have undergone some ageing during the experiments (variation of viscosity due to water evaporation, particle settling, ..).

### **Test 120618b**

In this test, some colloidal silica (< 2w%) was added to the suspension of test 120618 that remained inside the mixing tank. With the addition of this product, the viscosity of the solution decreased. No major problems occurred during realization of the test.

The particle size distribution obtained after sieving and calcination at 700 and 1200°C can be viewed in figure 50. Of all tests performed with FeCuAl as raw material, this is the one with the lowest value of SPAN, which means that we got the narrowest range of particle sizes. However, a small peak can be seen close to 10 µm, certainly due to some breakage of big particles during sieving and/or analysis.

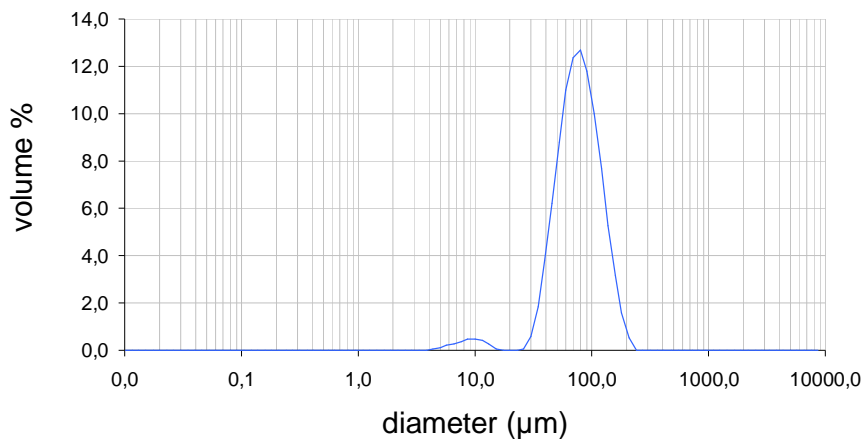


**Figure 50 - Granulometry of product from test 120618b after spray drying and calcinations (700°C+1200° C)**

The only difference in formulation and composition between tests 120618 and 120618b, is the presence of a colloidal silica material in the second one. This product was added to the previously prepared suspension (test 120618) to impart a slight shear-thickening behavior which resulted in a viscosity increase from 1700 to 2000 cP. In figure 51 it is possible to see that both particle size distributions present a good SPAN, especially test 120618b. The distribution curve of test 120618 is wider than the other one, however it is shifted on the right, meaning that particles have a higher mean diameter.

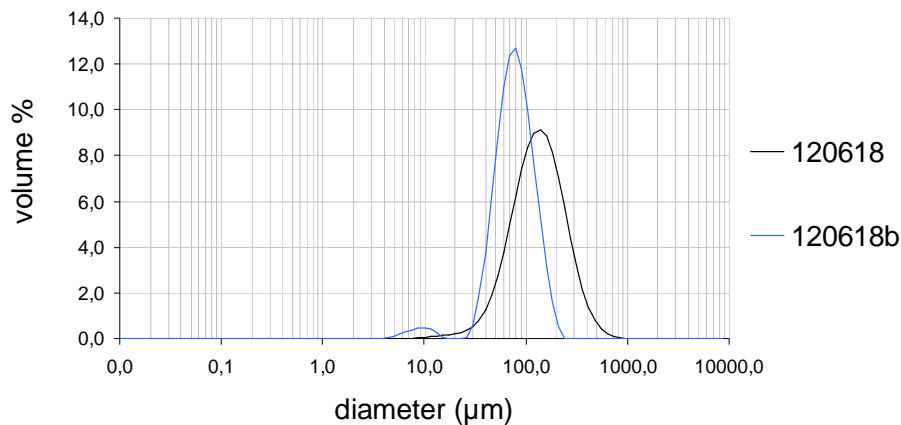


Figure 51 - Granulometry of product from tests 120618 & 120618b after spray drying and calcinations (700°C+1200°C)

### **Test 120618c**

In this test, two kinds of colloidal silica (powder & solution) were added to suspension 120618b as a way to achieve a higher viscosity and obtain bigger particles than in previous tests. No major problems occurred during realization of the test.

Besides some important aspects such as granulometry, morphology, density, porosimetry, it is also interesting to discuss the observation of few white "filaments" that emerged on the surface of FeCuAl products. This occurrence (figure 52) was observed on some products sent to analysis, on milled charges, and also on deposits that remained in the reactor, filter press and spin flash equipment, after a few days of air exposure only. These filaments appeared in different shapes such as spheres, platelets and needles. A microanalysis of this material (SEM/EDS) revealed the presence of sodium, aluminum, oxygen and traces of silica and chlorine and we assume that it may correspond to recrystallization of impurities such as salts (sodium nitrate / sodium hydroxyde). This observation may suggest that a very small fraction of reactants was not consumed during synthesis or that the washing step has to be improved due to limitations on our equipments, i.e. preferential pathways on filter press, resulting in high level of impurities such as  $\text{NaNO}_3$ .

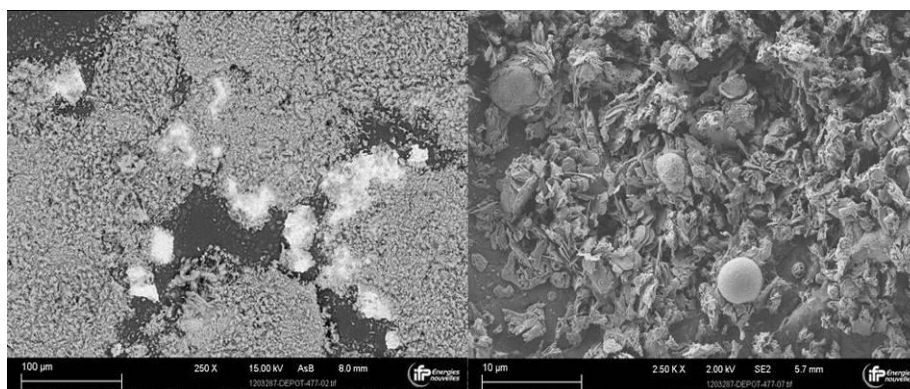


Figure 52 - SEM images showing white filaments observed on the surface of some FeCuAl products

For charges based on the  $\text{Fe}_{1.05}\text{Cu}_{0.95}\text{AlO}_4$  spinel phase, results show that we can produce coarse particles with a diameter ( $d_{v50}$ ) varying from 40 to 145  $\mu\text{m}$ , but with a poor spherical aspect (microspheres and polyhedric micro-granules), a weak bulk cohesion between the mixed phases, and presence of some microstructural defects such as pinholes and cracks.

#### 4.2.2 Tests on manganese oxide raw materials

Eight tests were performed using Manganese oxide products as raw materials. Four of them were made with  $\text{Mn}_x\text{O}_y$  compound I (powder), however in one of these tests no product was recovered due to clogging problems. Three tests were performed with  $\text{Mn}_x\text{O}_y$  compound II (solution), and the last one with BMP compound (powder).

All the products described below received the same post-treatments, namely a calcination at 700°C followed by a sieving step with sieves comprised between 100 & 315 $\mu\text{m}$ . Due to technical problems on our high temperature furnace, the planned thermal treatment at 1200°C was not possible for these products.

Table 9 shows the most relevant parameters concerning formulation & suspension composition, but also operating conditions of spray-drying and also particles size and total mass of the final product. The last column presents an internal qualitative assessment of each trial, considering particle size, product mass, but also operating conditions & costs. Regarding size of particles, except for one test (120719), these trials didn't reach the expected results. However production yields, expressed according to total collected mass of spray-dried product, were much better than those obtained for FeCuAl tests.

Table 10 describes, for each trial, the post-treatment steps and presents also results from granulometry, porosimetry and density analysis.

Table 9 - Summary table of Manganese tests formulation

Test	Catasepa	Charge	Solid Content (w%)	Al binder/ Charge (w%)	Org. binder (w%) / type	pH / H+ (w% p/AlOOH)	To (Cp) / Visco (Cp@100s-1)	Preparation Conditions	Ato. Cond. Ti - To (°C)/ QI ( L/h) / Rpm Vent.	Nozzle (mm) / P°air (bar)	d50 G (µm)	d90 G (µm)	Mass G (g)	Balance / €
<b>Goal</b>	-	<b>MxOy</b>	<b>&gt;45</b>	<b>10</b>	<b>3 / 120k</b>	<b>4 / 4</b>	<b>10000/1000</b>	<b>New lignes CLC/FT</b>	<b>280-120 / 20/2000</b>	<b>Buse 120 / 3</b>	<b>200</b>	<b>250</b>	<b>-</b>	<b>++++</b>
120711	111213	Mn3O4 4,15µ	45,1	5,2	3,1 /Opt.60	5,4 / 11	4550	T9+GMC+SPX15+R 6L+ISI+PCM	170-85 / 13(5) /2000	Buse 120 / 3,5	75	119	85	+
120712	111214	Mn3O4 4,15µ	45,1	5,2	3,1 /Opt.60	5,9 / 6,9	3600	T9+GMC+SPX15+R 6L+ISI+PCM	220-110 / 22(6,5) /2000	Buse 120 / 4	108	146	3155	+++
120716	111215	Mn3O4 4,15µ	45,7	8,0	3 /Opt.60	5,4 / 13	3640	T9+GMC+SPX15+R 6L+ISI+PCM	245-110 / 21,5(8,5) /2900	Buse 120 / 4	99	145	3745	+++
120717	111220	Mn3O4 4,15µ	45,9	10,0	3 /Opt.60	5,4 / 11,7	>???	T9+GMC+SPX15+R 6L+ISI+PCM	-	-	-	-	-	
120718	111216	Solution 70% Mn3O4 2,3µ	65	10,4	3,4 /Opt.60	5,7 / 13	2100	R50L+SPX15+??+I SI+PCM	180-115 / 10(5,5) / 2900	Buse 120 / 2	105	141	8820	++++
120719	111217	Solution 70% Mn3O4 2,3µ	65,8	12,6	3 /Opt.60	5,8 / 13	1950	R50L+SPX15+??+I SI+PCM	180-120 / 9(3,5) / 2900	Buse 120 / 3	133	160	14605	++++
120730	111218	Solution 70% Mn3O4 2,3µ	66	15,0	3 /Opt.60	5,5 / 12,5	2550	R50L+SPX15+??+I SI+PCM	185-120 / 10(4,5) / 2900	Buse 120 / 4	89	115	14200	+++
120731	111219	BMP 5µ	49,5	8,1	2,6 /Opt.60	4,3 / 3,5	25	R6L+ISI+PCM	200-130 / 6(4) / 2900	Buse 120 / 3	95	140	305	+

Table 10 - Summary table of Manganese tests characterization

Test	Catasepa	LIMS	Thermal Treatments (°C)	Sieving	d50 / d90 (µm)	SPAN	Attrition test (w%)	Sbet (m <sup>2</sup> /g)	Vpt (ml/g)	Vp macro (ml/g)	Dp macro (nm)	DRT (kg/m <sup>3</sup> )
<b>Goal</b>	-	-	700/1200°C	75-250 µm	150/200	1	<10	>20	> 0,1	>0,05	>500 nm	>2000
120711	111213	1203697	700	100-315	172/333	1,496	-	16	0,18	0,15	526,89	1230
120712	111214	1203697	700	100-315	142/277	1,522	90,4	11	0,19	0,17	586,96	1160
120716	111215	1203697	700	100-315	172/330	1,426	-	15	0,17	0,15	505,05	1230
120717	111220	1203697	-	-	-	-	-	-	-	-	-	-
120718	111216	1203697	700	100-315	91/1154	12,6	-	21	0,26	0,22	1119,1	1070
120719	111217	1203697	700	100-315	88/1083	12,33	74,5	28	0,27	0,22	1076,4	1170
120730	111218	1203697	700	100-315	6/70	11,47	-	40	0,29	0,23	1132	1250
120731	111219	1203697	700	100-315	100/264	2,533	-	36	0,21	0,12	357,19	790

### **Test 120711**

$Mn_xO_y$  compound I designed as powder 1 was utilized as raw material in this first test. The suspension was prepared in the T9 mixing tank connected with a peristaltic pump and a colloidal mill in a continuous recirculation mode. The prepared suspension was then transferred to the 6L small reactor that was directly connected to the atomization nozzle, as for test 120607. Because of a limited rheological knowledge on this new raw material, regarding atomization mechanism and spray-drying conditions of the corresponding suspension, this test did not work very well. Therefore due to high suspension viscosity, tank T9 and pipes clogged whereas the walls and also the roof of the atomization chamber were wetted. Finally a very small amount of product was recovered at the end of the test.

### **Test 120712**

In this case we used the same raw material, equipments and line configuration as those for test 120711. No major problems occurred during realization of the test. Figure 53 shows images obtained from optical microscopy for particles calcined at 700°C before and after sieving.

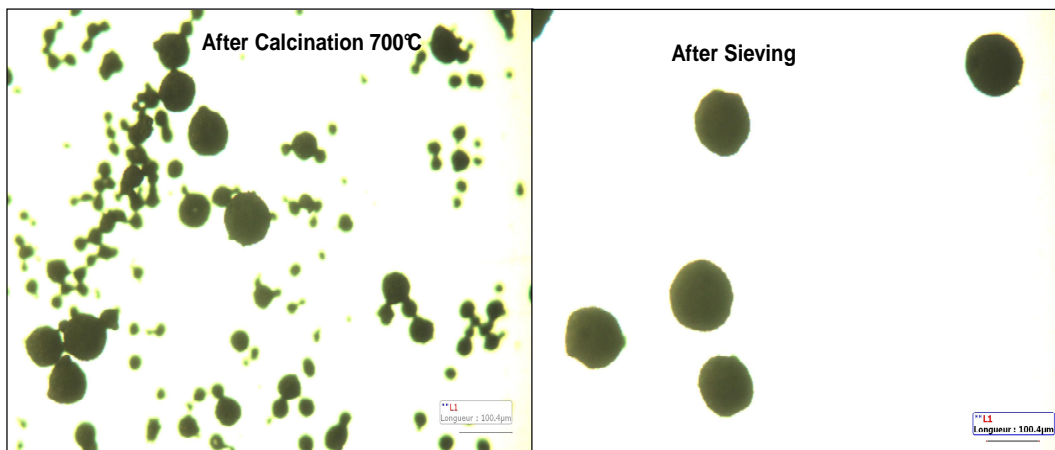


**Figure 53 - Optical microscopy images for calcined product before and after sieving (Test 120712)**

Both figures present particles with a near spherical shape and there are no major differences between big particles.

The sphericity of particles was confirmed by SEM analysis. Figure 54 shows two images of this product where it is possible to see a lot of microspheres but also some shapeless agglomerates and small particles (“satellites”).

Another relevant aspect is the presence of cavities and holes in some particles, as it can be seen on right image. This kind of microstructure is a well known trend for spray-drying and corresponds to various diffusion mechanisms and rheological considerations [64]. In this case, the force generated by the vaporization driving force is more important than the yield stress of fluid

droplets (ie structural rigidity). Thus there is diffusion and concentration of primary particles, associated with water evaporation, from the core to the shell of the particles, resulting in grain concentration at the periphery and deformation of the whole particle. This deformation results from a pressure gradient between inside and outside the particles and may generate explosion of particles giving defects, cavities, holes or a progressive distortion that generates a doughnut shape. It is generally considered for viscous suspensions that a high yield stress can give sufficient mechanical strength to the sprayed droplets, so as to decrease the mobility of primary grains and the tendency to particle deformation.

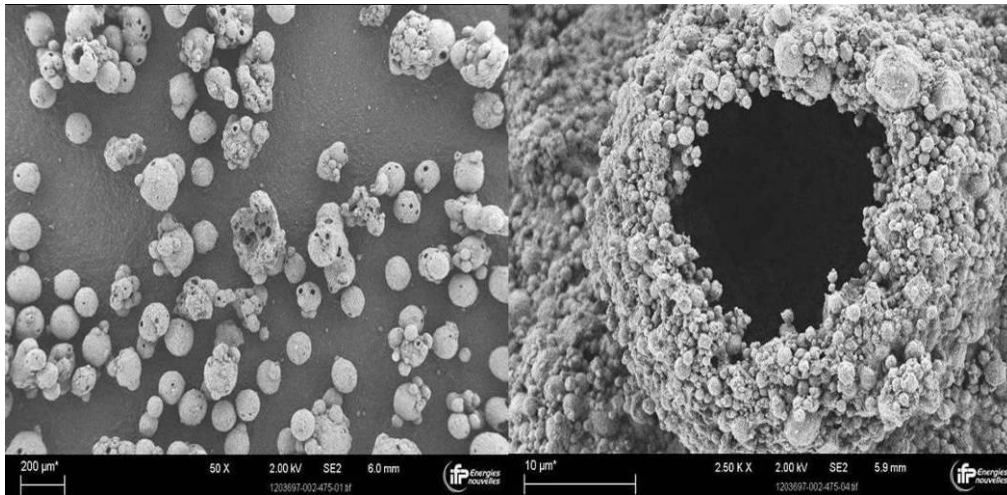


**Figure 54 - SEM photos of product 120712 (scale bar of 200 and 10 µm)**

From a morphological and a rheological point of view, figure 54 sums up the two main scenarios that can be observed during formation and drying of microspheres. While we have to manage the operating conditions on the spray dryer, for a moderate driving force, we must also determine and control the correspondence between the rheological characteristics of a suspension and the morphology of the corresponding final dried particles.

Case A: Water discharge at once during the drying process

- Good dispersion state and low yield stress
- High mobility of primary particles
- Water evaporates quickly generating deformation of microspheres
- Possible explosion of microspheres, production of hollow particles

Case B: Water drained continuously during the drying process

- Low dispersion state and high or significant yield stress
- Low mobility of primary particles
- Water evaporates quickly generating little deformation of microspheres
- No deformation of structure: dense particles without cavities (“full”)

Figure 55 intends to represent possible structures of dried spheres.

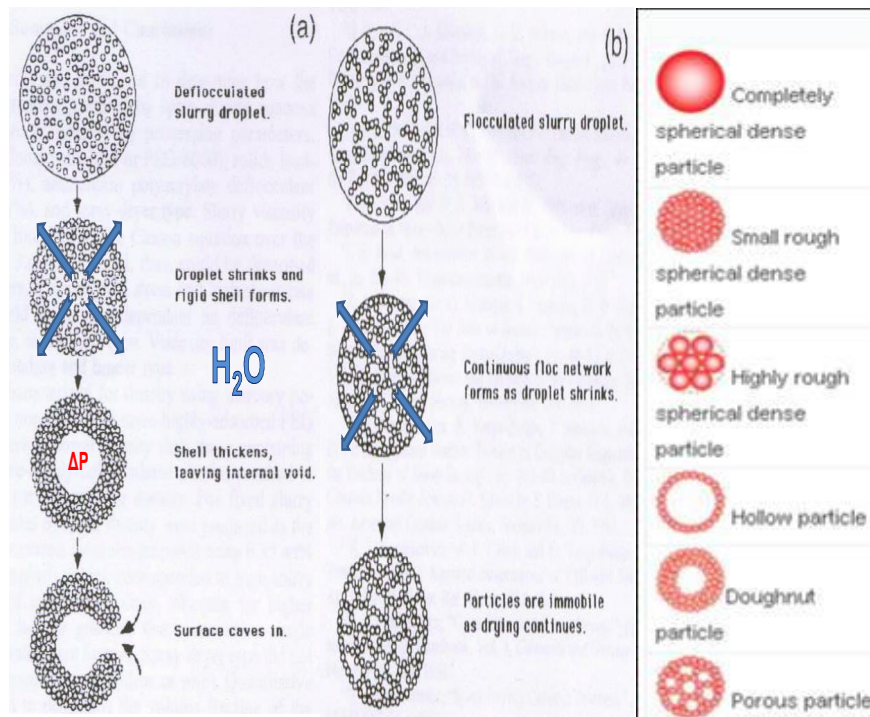


Figure 55 – Morphology of dried spheres (A: Hollow; B: Solid) and representation of possible structures.

### Test 120716

In this case we used the same raw material, equipments and line configuration as those for test 120711. The T9 tank and pipes clogged twice and the feed pipe just before the nozzle also clogged once.

As can be seen on the optical image of figure 56, this product presents some small particles (satellites) however the surface of the particles seems quite regular.

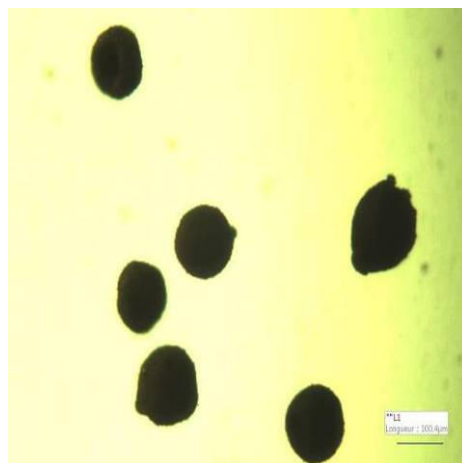
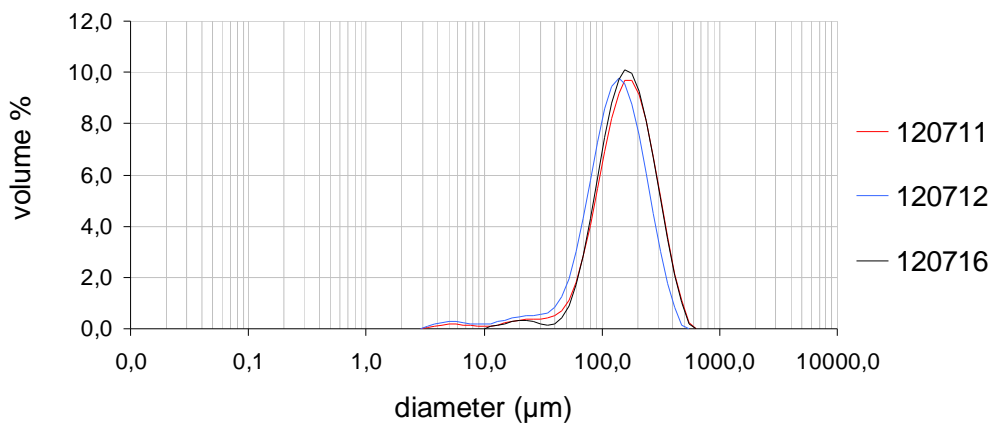


Figure 56 - Optical microscopy image for product 120716 after calcination and sieving

### **Test 120717**

In this case we used the same raw material, equipments and line configuration as those for test 120711. The T9 tank and pipes clogged three times, and it was tried to transfer the suspension toward the small 6L reactor but clogging problems appeared once again due to a very high viscosity (it was not possible to determine this apparent viscosity with our Brookfield viscometer). Finally, without valuable spray-drying experiment no product was obtained during this test.

Four tests with  $Mn_xO_y$  compound I were performed but only three final products were obtained. Between these three tests the solid content was quite similar as well as the viscosity of the prepared suspensions. The only difference came from the binder content, varying from 5 to 8 w% in the case of test 120716. Looking at figure 57 we can see that particle size distributions are very similar for the three tests and curves appear with a very classic shape with a reduced SPAN value around 1,4.



**Figure 57 - Granulometry of particles produced from tests with  $Mn_xO_y$  compound I**

### **Test 120718**

$Mn_xO_y$  compound II (solution), was utilized as raw material in this test. The experimental configuration was composed by the R50 mixing tank connected with a peristaltic pump for a continuous recirculation mode. A small amount of the prepared suspension was transferred to a 20L tank equipped with a dispersing agitator. This small tank was directly connected to the atomization nozzle by a peristaltic pump associated with a positive displacement pump in order to avoid a pulse flow at the nozzle outlet. At the beginning, due to a high solid content giving a viscous suspension and a too high inlet flow, wetting of the chamber roof occurred. At the end of the test, the feed pipe clogged three times due to nozzle fouling. A small amount of final product was recovered and it was composed by some big pasty agglomerates. This fact was maybe caused by a particularly low homogeneity and low dispersion of the organic binder, certainly induced by chemical incompatibility with the new raw material (commercial solution).

Figure 58 presents images about the morphological evolution of spray-dried particles after calcination and sieving treatments. Observing these three optical microscope images, it is possible to verify that the sieving step increases the irregularity of particles and the presence of small grains on surface. This fact may be explained by a too low mechanical strength of the particles, due to the absence of calcinations at 1200°C and may also stem from a too high sieving power.

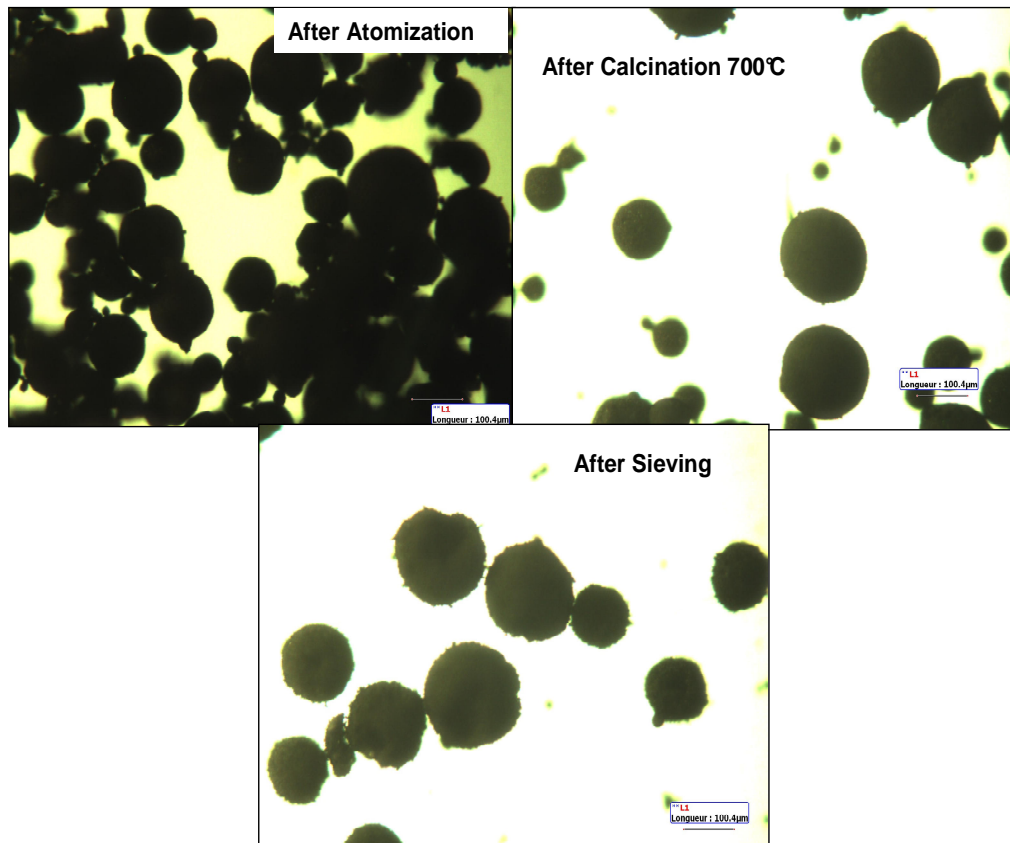


**Figure 58 - Optical microscopy images showing evolution of product 120718 during its elaboration**

As previously observed in the case of FeCuAl particles, we can verify once again in figure 58 that a lower air spray pressures results in bigger particles. In our case we assume that for a given feed flow, higher air pressures increase the energy brought to disrupt the suspension liquid film at the nozzle outlet. Therefore spraying mechanisms are modified and the diffusion cone of droplets is enlarged, which can enhance the probability of shocks between dried particles and droplets within the atomization chamber. At the end, we obtain more fragmented particles, a decrease in particle sizes, but also an increase in fines production. For an air pressure of about 2 bar we observe on figure 58 a quite large particle size distribution, confirming presence of small parts of fragmented particles

Nevertheless, as can be seen on figure 59, for a too low air pressure, the particle size distribution is enlarged because the spraying process is not constant and homogeneous. Moreover, droplet velocities are important due to inertial considerations that can generate more impact on walls

of the atomization chamber. This results in breakage and loss of big particles thus increasing the fines percentage.

So that's why for each new suspension, beyond formulation and rheological behavior, we have to well manage and adjust the operating conditions of spray-drying (such as air spray pressure)

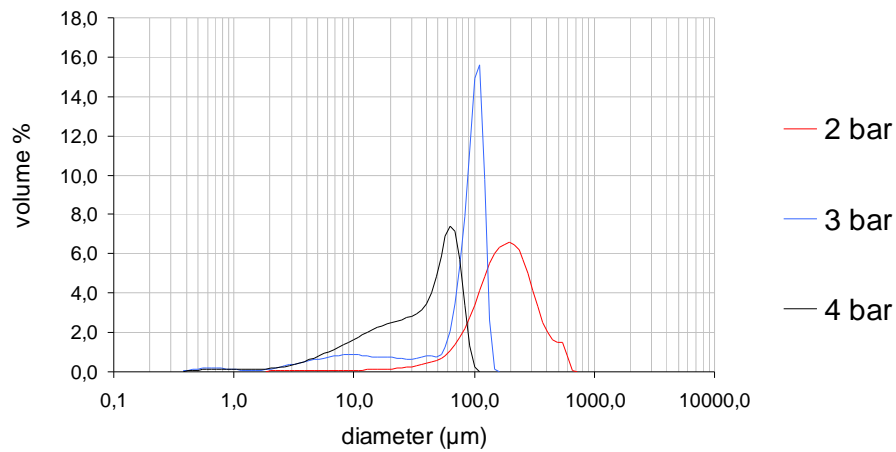


Figure 59 - Granulometry of spray-dried product 120718 for pressures of 2, 3 and 4 bar

### **Test 120719**

In this case we used the same raw material, equipments and line configuration as those for test 120718. No major problems occurred during the realization of the test. Figure 60 presents SEM images of product 120719.

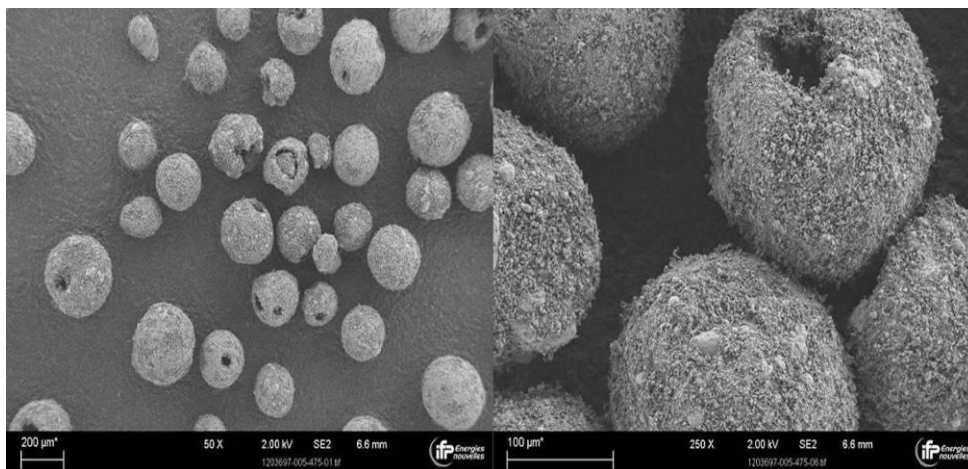
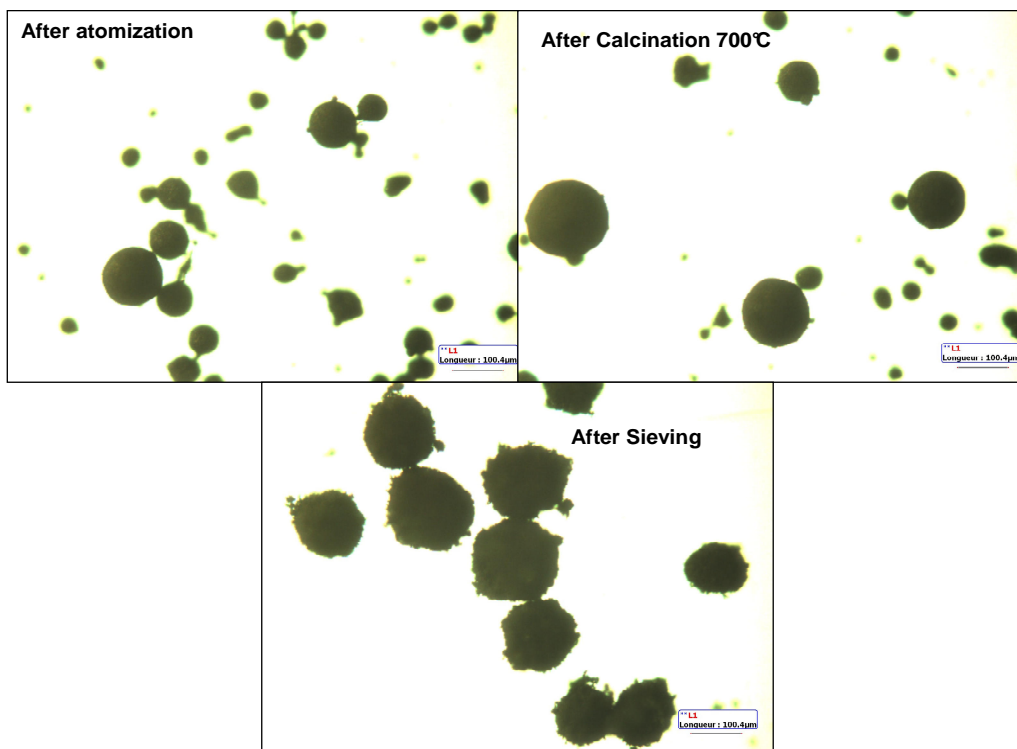


Figure 60 - Figure 45 - SEM images of product 120719 (scale bar of 200 and 100 µm)

SEM images of product 120719 show particles with a good sphericity and the required size. However like for test 120718, particles' surfaces are not very regular and they are likely hollow.

### **Test 120730**

In this case we used the same raw material, equipments and line configuration as those for test 120718. No major problems occurred during the realization of the test. Figure 61 presents optical microscopy images of the product 120730 during different stages of the process.



**Figure 61 - Optical microscopy images showing evolution of product 120730 during his elaboration**

As it was observed and discussed for test 120718, the spherical shape of particles changes dramatically during sieving and we can observe a lot of small particles “trapped” on the surface of larger ones. However, as we can see in figures 53 and 56, this deterioration does not happen with  $Mn_xO_y$  compound I, for which the same sieving equipment and input power were employed. This fact allows us to think that these products have a lower resistance than other manganese products. However, regarding the results of attrition tests (table 10), product 120719 shows a higher resistance to wear than product 120712. Finally in this case we assume that a low repartition of organic and mineral binder generates a poor cohesion for a significant fraction of particles. This fraction is easily disintegrated during sieving, thus generating thus small grains that interact with surfaces due to electrostatic effects.

With products obtained with  $Mn_xO_y$  compound II (concentrated solution), we can observe that the particle size distribution of the spray-dried products are relatively extended (figure 62). These curves show more than a single narrow peak but a bimodal particle distribution which is not the desired result. The associated SPAN value ranges for the three tests between 11,5 and 12,6, while our objective is around 1-2. Compared with the tests realized with  $Mn_xO_y$  compound I (Powder), these results indicate that without thermal treatment at high temperature, the particles are more sensitive to mechanical stress (handling, sieving). One explanation can be a lower efficiency of mineral and organic binders (peptized boehmite and PVA) which were poorly dispersed in this case. Therefore they do not enhance the green mechanical strength, nor maintain sufficient shape, structure and bulk cohesion and deterioration of non-densified particles can occur.

It is also interesting to observe that when the alumina binder content increases, the size of particles seems to decrease, which was not expected because the presence of peptized boehmite alumina binder should increase the suspension viscosity as well as the cohesion and mechanical strength of particles (attrition resistance). We assume that for the same solid content, an increase in viscosity induced consequently an increase in size of particles, but due to poor dispersion of binders (and hence a low efficiency) [15], the final particles are more easily broken during handling and sieving (more sensitivity of big particles). Figure 62 shows the particle size distribution of particles produced from  $Mn_xO_y$  compound II. Figure 62 presents the particle size distribution of particle produced from  $Mn_xO_y$  compound II.

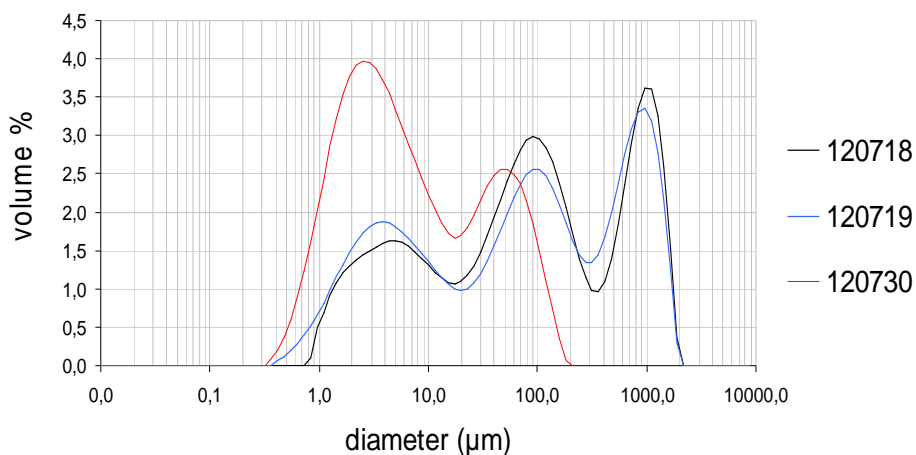


**Figure 62 - Particle size distribution of particles produced from  $Mn_xO_y$  compound II (concentrated solution)**

In figure 63 we present the evolution of tapped powder density of particles produced from  $Mn_xO_y$  compound II as a function of the alumina binder content in the feed suspension. The experimental results show an almost linear evolution of density, so when the binder content increases we assume that there is more binding phase available to keep small primary particles within the bulk

structure, thus enhancing particles packing and final density. And in the case of doughnut structure, or presence of cavities, we assume also that the shell of particles are more dense.

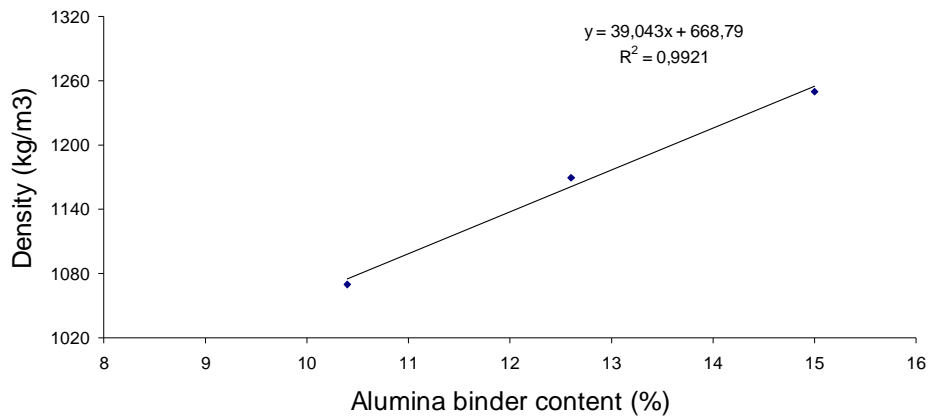


**Figure 63 - Tapped powder density of particles produced from Mn solution in function of Al binder content**

From a textural point of view, we also see that the specific surface area ( $S_{BET}$ ) is slightly higher than those obtained from  $Mn_xO_y$  compound I, mainly due to a lower primary particle size (respectively 2.6 and 4.6  $\mu m$ ) offering more available surface.

### **Test 120731**

BMP was utilized as raw material in this final test. The suspension was prepared in the small 6 L reactor like in test 120607 and the pipe clogged just once at the nozzle outlet. Surprisingly, the product collected at the end of the test was covered by some water without apparent explanation because the entire atomization chamber was dry. The suspension had a very low viscosity (25 cP) due to important pH stabilization (acid) that resulted in particles deformation during spray-drying. Figure 64 presents a SEM image of particles obtained in this test. Particles exhibit a relatively good size and have a near spherical shape, however an important fraction have a doughnut structure (appearance of a ring). The explanation is the same as that discussed earlier for test 120712, and a good representation of mechanisms involved can be seen in figures 55, 89 and 90 (appendix C). To conclude we can say that only one test was made with BMP, which does not really allow us to make conclusions and decide on the potential of BMP as a raw material.

In figure 64 we can observe a SEM image of particles from test 120731 (BMP).

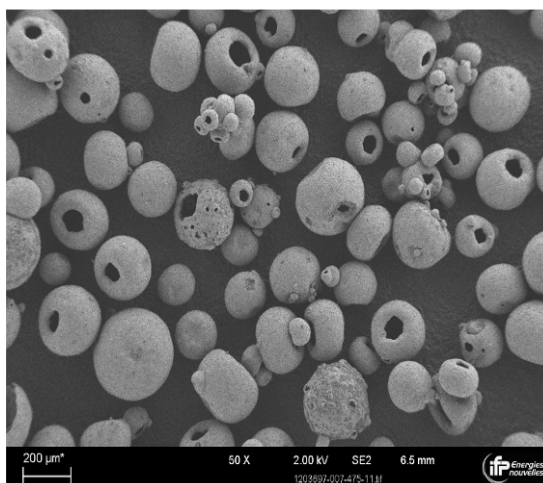


**Figure 64 - SEM images of particles from test 120731 (scale bar of 200μm)**

SEM images from each kind of manganese particles are presented in both figures 65 and 66. In figure 65 we can note that unlike in the case of FeCuAl, these products have a lot of spherical particles, however many agglomerates are formed. Another interesting point for these products is the existence of cavities in particles mainly in the case of BMP where a majority of particles have a doughnut or hollow structure (ring shape). Using  $Mn_xO_y$  compound II, we obtained an irregular and deteriorated surface after the sieving step (figure 65).

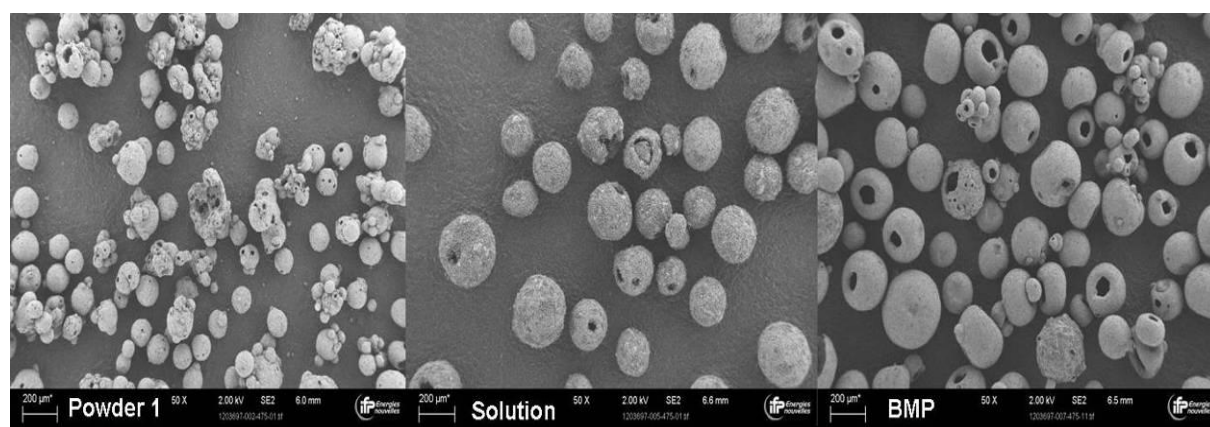


**Figure 65 – SEM images of particles elaborated respectively from  $Mn_xO_y$  compound I (powder) ,  $Mn_xO_y$  compound II (solution) and BMP (powder) and Tests 120712, 120719 and 120731 (scale bar of 200μm)**

Another point that we observe on SEM images is the existence of some cavities within the particles. Product 120719 ( $Mn_xO_y$  compound II) shows a lower number of particles with large holes. This test was performed with an inlet temperature of 180°C while products 120712 and 120731, respectively  $Mn_xO_y$  compound I and BMP, were performed with an inlet temperature of 220 and 200°C. Beyond rheological considerations on viscosity and yield stress, we assume that a higher inlet temperature leads to a quicker water evaporation from the particle in the atomization chamber. This too fast evaporation imparts a high mobility of primary particles within droplets and then causes the

creation of large cavities and holes associated with structure deformation. Figure 66 shows SEM images of particles from the different types of  $Mn_xO_y$  raw materials.

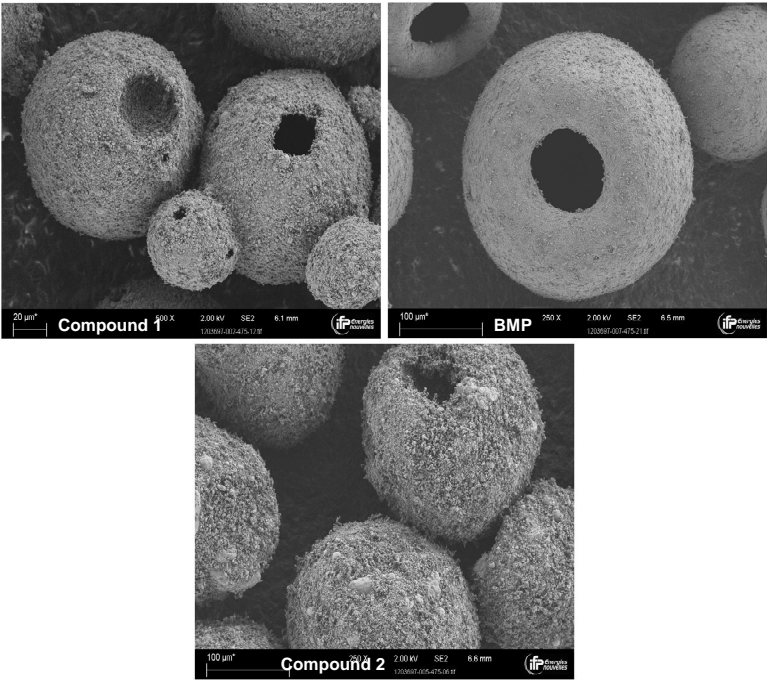


**Figure 66 – SEM images of particles from  $Mn_xO_y$  compound I ,  $Mn_xO_y$  compound I and BMP (Test 120712, 120719 and 120731 - scale bar of 100µm)**

The product obtained from BMP shows a particle size distribution with a SPAN of 2,5, with a normal curve appearance except an enlargement for small diameters corresponding to a slight deterioration of particles and to the presence of satellites on surface due to mechanical stress. Moreover it is possible to see another peak close to 1000µm diameter (figure 67). This surprising observation, especially after a sieving step (100-315µm) may result from a remaining sample analyzed just before our powder.

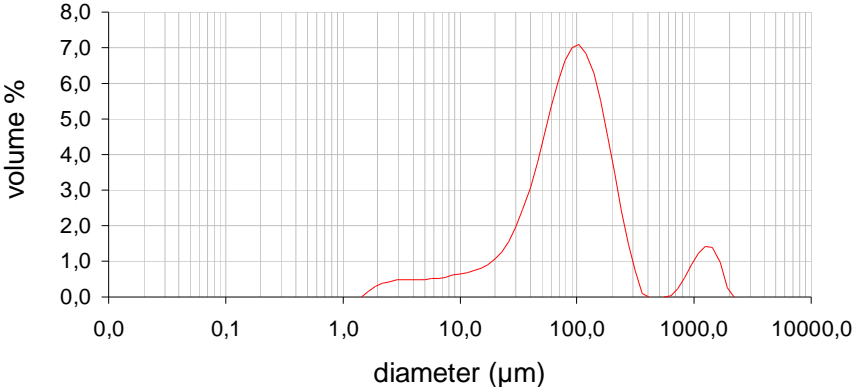


**Figure 67 - Particle Size Distribution of particles produced from BMP (Test 120731)**

In figure 68, three particle size distributions (PSD) are presented corresponding to an example of each manganese raw material we used. As was said before, particles from  $Mn_xO_y$  compound I show the best PSD with an almost normal curve aspect. The product obtained from  $Mn_xO_y$  compound II presents a bimodal distribution showing two peaks. Finally the product using BMP as raw material shows a quite good curve aspect but with presence of a surprising peak close to  $1000\mu m$ .

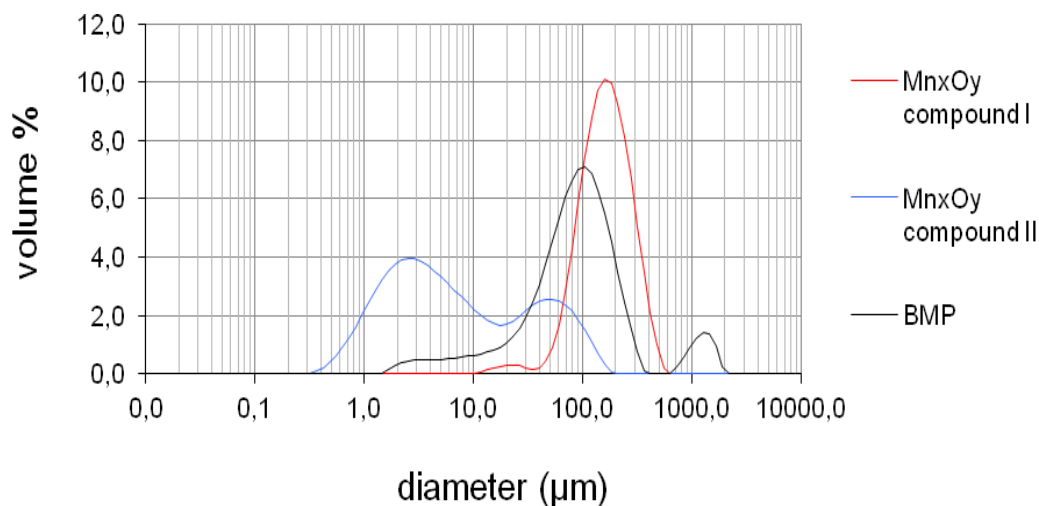


**Figure 68 - Granulometry of particles produced from Mn raw material (120716, 120730 and 120731)**

Figure 69 summarizes SEM images obtained on each kind of raw material, with three examples using FeCuAl and one example respectively for  $Mn_xO_y$  compound I,  $Mn_xO_y$  compound II and BMP. Firstly we can observe that particles obtained from manganese raw material are bigger than particles from FeCuAl and also have a more spherical shape.

We assume that the higher solid content tested for  $Mn_xO_y$  compounds are responsible of the bigger size and also that FeCuAl products might be more sensitive regarding mechanical stress during post-treatments.

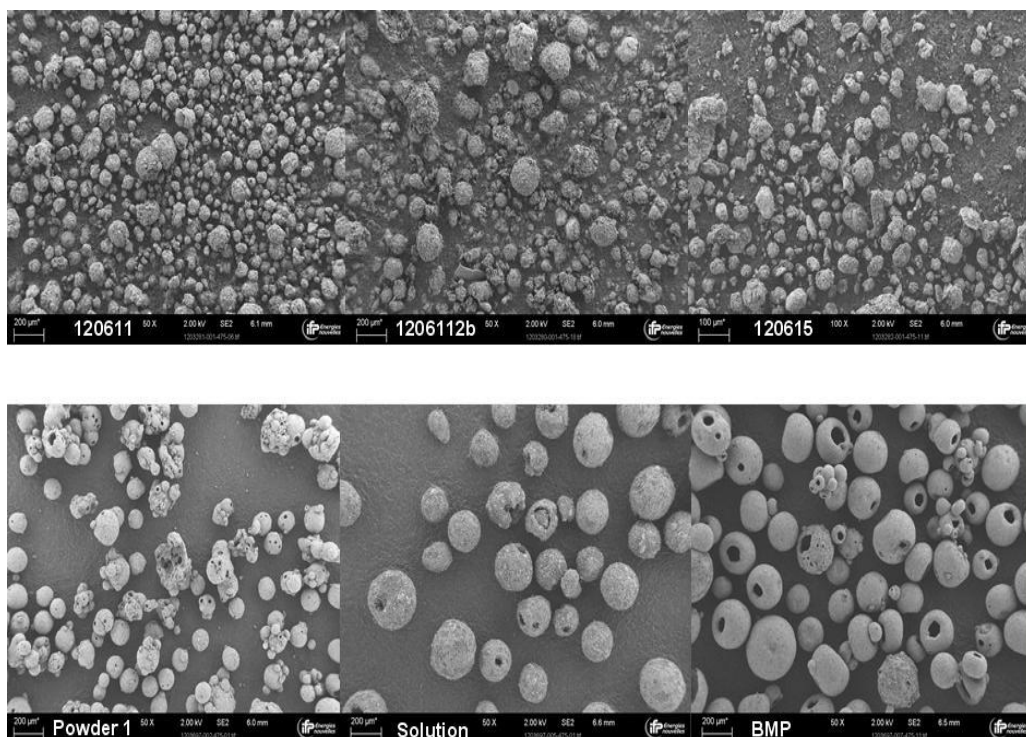


Figure 69 - SEM images of FeCuAl and Mn<sub>x</sub>O<sub>y</sub> particles summarizing trials of this work (scale bar of 200μm)

Attrition resistance analysis was only performed for three experimental tests, namely one for FeCuAl, one for Mn<sub>x</sub>O<sub>y</sub> compound I and the last one for Mn<sub>x</sub>O<sub>y</sub> compound II. Regarding our objective to get an attrition rate lower than 20%, our results were quite far, as shown in table 11. Between the three tested products, only one obtained from FeCuAl presents an interesting result, however far from our goal. Mn<sub>x</sub>O<sub>y</sub> compound I presents a lower attrition resistance than Mn<sub>x</sub>O<sub>y</sub> compound II, which was not expected due to the effect observed during sieving.

The discrepancy of results in relation to the target value can be explained by the fact that these products were not thermally treated with a complementary calcination at 1200°C, which is a classic post-treatment step really necessary to increase the bulk density and mechanical strength of particles.

Table 11 - Results of attrition Tests

Test	Raw Material	Primary particle size (μm)	Attrition rate (%)
<b>Target</b>	-	0,5	<20
<b>120612b</b>	FeCuAl	1	41,7
<b>120712</b>	Mn <sub>x</sub> O <sub>y</sub> compound I	4.6	90,4
<b>120719</b>	Mn <sub>x</sub> O <sub>y</sub> compound II	2,6	74,5

Otherwise for the superior attrition resistance of FeCuAl product compared to Mn<sub>x</sub>O<sub>y</sub> compounds we assume that it might be due to a lower primary particle size. In the case of very small primary particle size, the short distance interactions are stronger conferring a higher mechanical strength

It is also important to note that the impact of calcination at 1200°C was also evidenced concerning the evolution of density of particles. Indeed only the particles that were treated reached bulk densities higher than 2000 kg/m<sup>3</sup> (table 8) and we see that there is a density increase of about 120% when we associate a complementary thermal treatment at 1200°C to the basic calcination at 700°C.

Besides, despite the fact that all the products were not post-treated at 1200°C, manganese oxide particles show higher densities than FeCuAl particles, which can be explained by the fact that suspensions of manganese oxide have higher solid contents than those with FeCuAl.

Figure 70 presents a relation between the specific surface area (S<sub>bet</sub>) and the Alumina/binder ratio for all the products elaborated with manganese oxide as raw materials. Surface area is an important characteristic of oxygen carriers because it has a high influence on their reactivity. It is interesting to observe that for the same binder/charge ratio in test 3 (Mn<sub>x</sub>O<sub>y</sub> compound I) and in test 7 (BMP), the product obtained from the last one has a specific surface area of 36 m<sup>2</sup>/g which is almost double than that of the first one.

Regarding products obtained from manganese suspension, we observe that the surface area of particles (S<sub>BET</sub>) increases when the alumina/charge ratio increases. This can be explained by a greater contribution of the alumina precursor on the texture of the final particles. Indeed boehmite (AlOOH = hydrated alumina) is a well-known precursor of alumina (Al<sub>2</sub>O<sub>3</sub>=oxide) generating superior surface (up to 400m<sup>2</sup>/g) and porous volume (up to 1,5 ml/g).

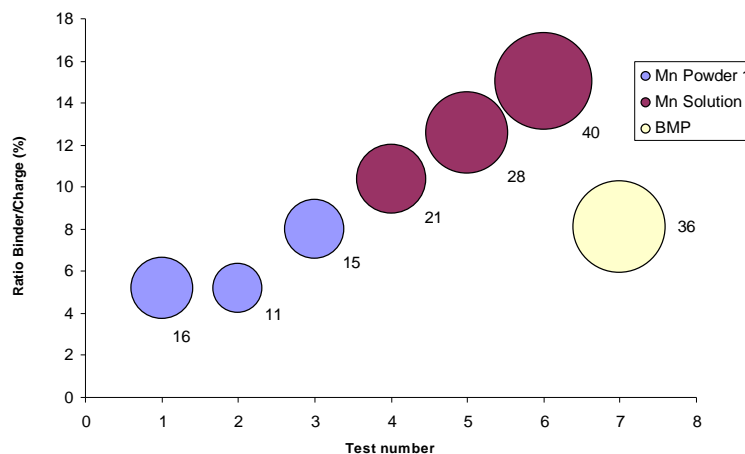


Figure 70 - Specific surface area in function of raw material used and binder on charge ratio (S<sub>bet</sub> – m<sup>2</sup>/g)

Finally, it is also interesting to note that for a high temperature thermal treatment, the textural properties of particles get considerably worse. So we see that for FeCuAl products the final porous volume and specific surface area become almost equal to zero. This observation fits well with both densification and disappearance of macroscopic cavities and holes within the final particles.

For charges based on manganese raw materials, the results show that we can produce coarse particles with a very good spherical aspect (microspheres), a diameter ( $dv_{50}$ ) between 90 and 170  $\mu\text{m}$ , and a mild bulk cohesion between the mixed phases, but with presence of some cavities and pinholes within the microstructure. The lower attrition resistance compared to the "FeCuAl" particles is mainly due to the higher particle size of the starting material (1 $\mu\text{m}$  for FeCuAl and 2,3-4,2 $\mu\text{m}$  for  $\text{Mn}_x\text{O}_y$ ). Also, the overall production yield is better when the solid content of the feed suspension is higher. Considering the spherical and size aspects, suspensions prepared with  $\text{Mn}_x\text{O}_y$  compound II seem to be very promising to optimize future experiments and to develop a performance product.

## 5 Conclusions & Prospects

---

This work aimed to produce oxygen carrier particles for the Chemical Looping Combustion technology by the spray drying process applied to various oxide suspensions.

The study was conducted in various scientific and technical fields based on chemical engineering, and materials science, including synthesis, formulation and rheology, milling, shaping, thermal treatments and material characterization.

Our experiments were based on an original approach based on bulk interaction between different mineral oxides used as active charges and a mineral alumina sol used as binding phase, in order to elaborate microspherical particles with a mean diameter ranging from 100 to 300 $\mu\text{m}$  and exhibiting both bulk cohesion and homogeneity, but also a good mechanical strength.

Four kind of active charges, mixed with different compounds, were used to formulate and prepare various aqueous suspensions. These suspensions were then spray dried to give particles that were thermally treated and analyzed with various characterizations methods such as granulometry, optical and electronic microscopy, moisture content, porosity, density and mechanical strength.

Concerning the rheological behavior, it was determined that the great majority of suspensions elaborated with our different raw materials, presents a shear thinning behavior well described by the Herschell-Bulkley equation. The flow curves were measured with all the suspensions discussed in the report but are not shown because of the lack on sensitivity of the available rheometer which resulted in incomparable results.

For FeCuAl and  $\text{Mn}_x\text{O}_y$  compounds, the results of formulation and spray drying experiments associated with post treatments show that we can produce a main fraction of coarse particles (microspheres/micro-granules) and that there is a strong impact of a solid concentration increase on the reduction of fines obtained, with a global increase in median diameter ( $dv_{50}$ ) SPAN. The more concentrated the starting suspension is, the larger the particles collected at the bottom of the spray-drying chamber are.

As expected and according to the literature, there is a significant impact of nozzle diameter and feeding flow rate. Moreover for our pneumatic atomization system, we also observed that the higher the air spray pressure, the smaller the diameter of particles (under identical spray-drying conditions). Otherwise if the feeding flow rate and nozzle diameter increase, the mean diameter and particle size distribution also increases.

It was also observed that the 1200 $^{\circ}\text{C}$  calcination step it is extremely necessary due to the increase of the density and the mechanical strength of the particles.

In conclusion, the work presented here allows us a better understanding in preparation of mixed oxides suspensions. The present results are promising to pursue research in the IFPEN CLC project, as we can see on figure 71.

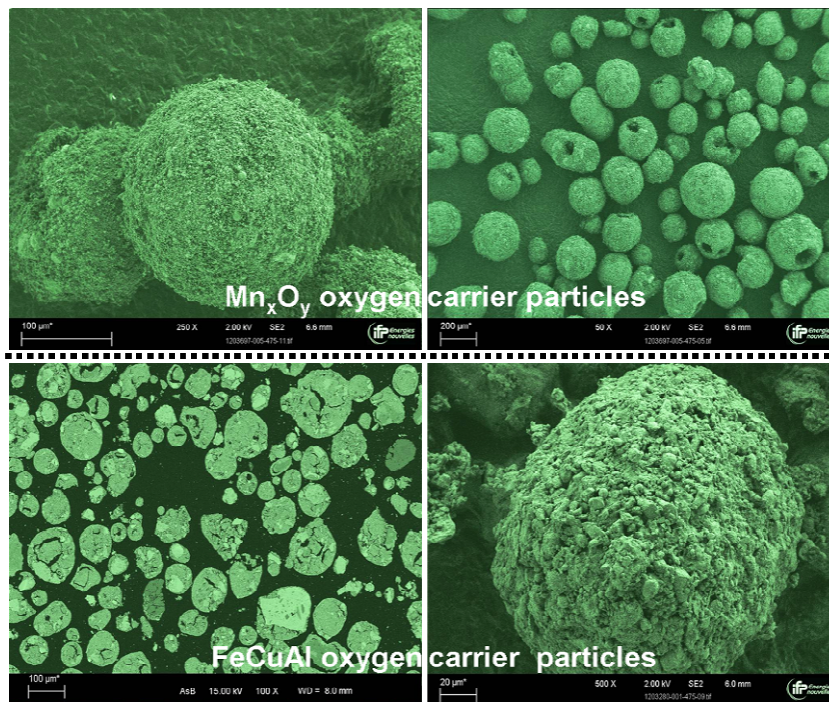


Figure 71 - SEM images representing good findings on oxygen carrier particles elaborated during this internship

For the prospects on formulation and spray drying, as a way to get an optimal combination of particles properties including particles size, morphology, textural and mechanical properties, it should be done:

- Complete product characterization, specially with attrition tests for all products;
- Treat all the products with high temperature calcination do improve particles density;
- Realize more tests with BMP and Mn<sub>x</sub>O<sub>y</sub> compound II;
- Adjust formulation, preparation and rheological behavior of suspensions to avoid clogging and formation of hollow or doughnut structure;
- Optimize spray-drying conditions to avoid a too fast water evaporation and deformation of particles (cavities and holes);
- Adapt the sequence of post-treatment operations or use sieving tools which do not deteriorate the product.

## 6 References

---

1. Archer D. (2005) *Fate of fossil fuel CO<sub>2</sub> in geologic time*, J. Geophys. Res. 110.
2. Dr. Pieter Tans, NOAA/ESRL ([www.esrl.noaa.gov/gmd/ccgg/trends/](http://www.esrl.noaa.gov/gmd/ccgg/trends/)) and Dr. Ralph Keeling, Scripps Institution of Oceanography ([scrippsco2.ucsd.edu/](http://scrippsco2.ucsd.edu/)).
3. Adanez J., Abad A., Garcia-Labiano F., Gayan P., F. de Diego L. (2011) *Progress in Chemical-Looping Combustion and Reforming technologies*. Progress in Energy and Combustion Science, Volume 38 215-282.
4. Earth System Research Laboratory – National Oceanic and Atmospheric Administration (2012) <http://www.esrl.noaa.gov/gmd/ccgg/trends/>
5. Feron, P.H.M., Hendriks, C.A. (2005) *CO<sub>2</sub> capture process principles and costs*. Oil gas science and technology Vol 60 No.3 451-459.
6. IPCC, (2005): *IPCC Special Report on Carbon Dioxide Capture and Storage*. Prepared by Working Group III of the Intergovernmental Panel on Climate Change [Metz, B., O. Davidson, H. C. de Coninck, M. Loos, and L. A. Meyer (eds.)]. Cambridge University Press, Cambridge, United Kingdom and New York, NY, USA, 442 pp.
7. Linderholm C., Mattisson T., Lyngfelt A. (2009) *Long-term integrity testing of spray-dried particles in a 10-kW chemical-looping combustor using natural gas as fuel*. Fuel Vol. 88 2083-2096.
8. Lecomte F., Broutin P., Lebas E. (2010) *CO<sub>2</sub> Capture: Technologies to Reduce Greenhouse Gas Emissions*. Paris: Éd. Technip.
9. Fang H. Haibin L., Zengli Z. (2009) *Advancements in Development of Chemical-Looping Combustion: A Review*. International Journal of Chemical Engineering Vol. 2009.
10. CO<sub>2</sub> CRC (Cooperative Research Centre for Greenhouse Gas Technologies (2011) - [http://www.co2crc.com.au/aboutccs/co2\\_capture\\_separation.html](http://www.co2crc.com.au/aboutccs/co2_capture_separation.html)
11. Johansson M., Mattisson T., Lyngfelt A. (2006) *Comparison Of Oxygen Carriers For Chemical-Looping Combustion*. Thermal Science Vol.10 93-107.
12. Hossain M. M., Lasa H. I. (2008) *Chemical-looping combustion (CLC) for inherent CO<sub>2</sub> separations—a review*. Chemical Engineering Science Vol. 63 4433-4451.
13. Abad A., Adanez J., García-Labiano F., F. de Diego L., Gayán P. (2009) *Modeling of the chemical-looping combustion of methane using a Cu-based oxygen carrier*. Energy Procedia Vol. 1 391-398
14. Fan L. S. (2010) *Chemical looping systems for fossil energy conversions*. Hoboken, New Jersey, USA: John Wiley & Sons, Inc.
15. Ishida M., Jin H. G. (1994) *A novel combustor based on chemical-looping reactions and its reaction-kinetics*. Journal of Chemical Engineering of Japan Vol. 27 296-301.
16. Fossdal A., Bakken E., Oye B.A., Schoning C., Kaus I., Mokkelbost T., Larring Y. (2011) *Study of inexpensive oxygen carriers for chemical looping combustion*. International Journal of Greenhouse Gas Control Vol.5 483-488.
17. Johansson M., Mattisson T., Lyngfelt A. (2006) *Investigation of Mn<sub>3</sub>O<sub>4</sub> With Stabilized ZrO<sub>2</sub> for Chemical-Looping Combustion*. Chemical Engineering Research and Design Vol. 84 807-818.
18. Mattisson T, and Lyngfelt A. (2001) *Capture of CO<sub>2</sub> using chemical-looping combustion*. First Biennial Meeting of The Scandinavian-Nordic Section of the Combustion Institute, Göteborg.
19. Baek J-I., Ryu J., Lee J. B., Eom T-H., Kim K-S., Yang S-R., Ryu C. K. (2011) *Highly attrition resistant oxygen carrier for chemical looping combustion*. Energy Procedia Vol. 4 349-355.
20. Cho P. Mattisson T., Lyngfelt A. (2004) *Comparison of iron-, nickel-, copper- and manganese-based oxygen carriers for chemical-looping combustion*. Fuel Vol. 83 1215-1225.

21. Lambert A., Briault P., Comte E. (2011) *Spinel mixed oxides as oxygen carriers for chemical looping combustion*. Energy Procedia Vol. 4 318-323.
22. Adanez J. (2010) *Oxygen carrier materials for Chemical-Looping processes – fundamentals*. First International Conference on Chemical Looping, IFP-EN Lyon.
23. Diego L. F., Garcia-Labiano F., Adánez J., Gayán P., Abad A., Corbella B. M., Palacios J. M.. (2004) *Development of Cu - Based Oxygen Carriers for Chemical - Looping Combustion*. Fuel Vol. 83 1749-1757.
24. Mattisson T., Järnäs A., Lyngfelt A. (2003) *Reactivity of Some Metal Oxides Supported on Alumina with Alternating Methane and Oxygen - Application for Chemical - Looping Combustion*. Energy & Fuels Vol. 17 643-651.
25. Ishida M., Jin H. (1996) *A Novel Chemical-Looping Combustor without NO<sub>x</sub> Formation*. industrial & Engineering Chemistry Research Vol. 35 2469-2472.
26. Gayán P. F. de Diego L., García-Labiano F., Adánez J., Abad A., Dueso C. (2008) *Effect of support on reactivity and selectivity of Ni-based oxygen carriers for chemical-looping combustion*. Fuel Vol. 87 2641-2650.
27. Mattisson T., Johansson M., Lyngfelt A. (2004) *Multicycle reduction and oxidation of different types of iron oxide particles-application to chemical-looping combustion*. Energy and Fuels Vol. 18 628-637.
28. Ishida M. Takeshita K., Suzuki K., Ohba T. (2005) *Application of Fe<sub>2</sub>O<sub>3</sub>-Al<sub>2</sub>O<sub>3</sub> composite particles as solid looping material of the chemical-loop combustor*. Energy and Fuels Vol. 19 2514-2518.
29. Leion H., Lyngfelt A., Johansson M., Mattisson T., Jerndal E. (2008) *The use of ilmenite as an oxygen carrier in chemical-looping combustion*. Chemical Engineering Research and Design Vol. 86 1017-1026.
30. Adanez J., F. de Diego L., García-Labiano F., Gayán P., Abad A. (2004) *Selection of oxygen carriers for chemical-looping combustion*. Energy and Fuels Vol. 18 371-377
31. Readman J. E., Olafsen A., Larring Y., Blom R. (2005) *La<sub>0.8</sub>Sr<sub>0.2</sub>Co<sub>0.2</sub>Fe<sub>0.8</sub>O<sub>3-δ</sub> as a potential oxygen carrier in a chemical looping type reactor, an in-situ powder X-ray diffraction study*. Journal of Materials Chemistry Vol. 15 1931-1937.
32. Hongguang J., Okamoto T., Ishida M. (1998) *Development of a novel chemical-looping combustion: synthesis of a looping material with a double metal oxide of CoO-NiO*. Energy Fuel Vol. 12 1272-1277.
33. Gianfresco A. (2009). *Spray Drying Engineering: Particle Stickiness In Relation With Agglomeration*. Ph.D. Thesis. Institut des Sciences et Industries du Vivant et de l'Environnement.
34. Figueiredo J. L. and Ribeiro F. R. (2007) *Catálise Heterogénea*. Fundação Caloust Gulbenkian, Lisboa, Portugal. Chapter 3.
35. Deutschmann O., Knözinger H., Kochloefl K., Turek T. (2011) *Heterogeneous Catalysis and Solid Catalysts, 2. Development and Types of Solid Catalysts*. Ullmann's Encyclopedia of Industrial Chemistry.
36. Erri P. and Varma A. (2007) *Solution Combustion Synthesized Oxygen Carriers for Chemical Looping Combustion*. Chemical Engineering Science Vol. 62 5682-5687.
37. Patel R.P., Patel M. P., Suthar A. M. (2009) *Spray drying technology: an overview*. Indian Journal of Science and Technology Vol. 2 44-47.
38. Vehring R., Foss W. R., Lechuga-Ballesteros D. (2007) *Particle formation in spray drying*. Journal of Aerosol Science Vol. 38 728-746.
39. Buchi Labortechnik AG, Training Papers Spray Drying.
40. Swarbrick J. and Boylan J. (1992) *Spray drying and Spray Congealing of Pharmaceuticals*. Encyclopedia of Pharmaceutical Technology, Marcel Dekker 207-221.
41. BETE Fog Nozzle, Inc. Spray Dry Manual (2005)
42. Gohel M. C., Parikh R. K., Nagori S. A. (2009) *Spray Drying: A Review*.
43. Komline-Sanderson (2012) - [http://www.komline.com/docs/rotary\\_atomizer.html](http://www.komline.com/docs/rotary_atomizer.html)
44. GEA Process Engineering (2012) [http://www.niroinc.com/technologies/spray\\_drying\\_tech.asp](http://www.niroinc.com/technologies/spray_drying_tech.asp)

45. Delavan Spray Technologies. SDX Spray Drying Manual
46. BUCHI (2012) - [http://www.buchi.com/Spray\\_Drying\\_Process.681.0.html](http://www.buchi.com/Spray_Drying_Process.681.0.html)
47. Taylor G. I. (1950) *The instability of liquid surfaces when accelerated in a direction perpendicular to their planes*, PRSL. Series A, Mathematical and Physical Sciences Vol. 201 192-196
48. Avvaru B., Patil M. N., Gogate P. R., Pandit A. B. (2006) *Ultrasonic atomization: Effect of liquid phase properties*. Ultrasonics Vol. 44 146-158.
49. SONAER Ultrasonics (2012) - [http://sonozap.com/Atomizer\\_Nozzles.html](http://sonozap.com/Atomizer_Nozzles.html)
50. Boel Nordic Applications. *Technology Overview*. (2012)  
<http://www.boelnordic.com/index.php/products/ultrasonic-spray-nozzle-systems/technology-overview>
51. Walzel P. (2010). *Spraying and Atomizing of Liquids*. Ullmann's Encyclopedia of Industrial Chemistry.
52. Shirley C. and Chen S. (2002) *Recent Advances on Ultrasound-Modulated Two-Fluid (UMTF) Atomization and its Applications*. Molecular and Quantum Acoustics Vol. 23 419-431.
53. GEA Process Engineering Inc. *Spray Drying Solutions – for R&D and small-scale production*
54. GEA Barr-Rossin (2012) - <http://www.barr-rosin.com/products/rosinaire-paddle-dryer.asp>
55. Strivens T. A. and Schoff, C. K. (2010) *Rheometry*. Ullmann's Encyclopedia of Industrial Chemistry
56. Malvern Instruments Ltd. *Rheology Measurements Presentation*. (2012)  
[https://www.brainshark.com/malvern/vu?pi=zGTzYmFB1z125wz0&tx=enews\\_jan12](https://www.brainshark.com/malvern/vu?pi=zGTzYmFB1z125wz0&tx=enews_jan12)
57. Abdali S. S., et al. (1992) *Entry and exit flows of Bingham fluids*. J Rheol Vol. 36 389-407.
58. APV (2000), Brochure APV Pilot Spray Drying Plant Type PSD 55.
59. Beatop Electric Limited (2012)  
[http://www.beatop.com/Laser\\_Particle\\_Size\\_Analyzer/mie\\_theory.html](http://www.beatop.com/Laser_Particle_Size_Analyzer/mie_theory.html)
60. Pye K. and Croft D.J. (2004) *Forensic Geoscience: Principles, Techniques and Applications*. Geological Society, Bath, United Kingdom
61. AZoNano (AZoNetwork) - Scanning Electron Microscope (2012) [www.azonano.com](http://www.azonano.com)
62. Encyclopaedia Britannica Online - Scanning Electron Microscope (SEM) (2012)  
<http://www.britannica.com/EBchecked/topic/526571/scanning-electron-microscope-SEM>
63. Purdue University - Scanning Electron Microscope (2012) [www.purdue.edu](http://www.purdue.edu)
64. Walker W. J. J., Reed J. S., Verma S. K. (1999) *Influence of Slurry Parameters on the Characteristics of Spray-Dried Granules*. Journal of the American Ceramic Society Vol. 82 1711-1719.

# Appendix

## Appendix A – Equipment characteristics

### Spray-Dryer APV

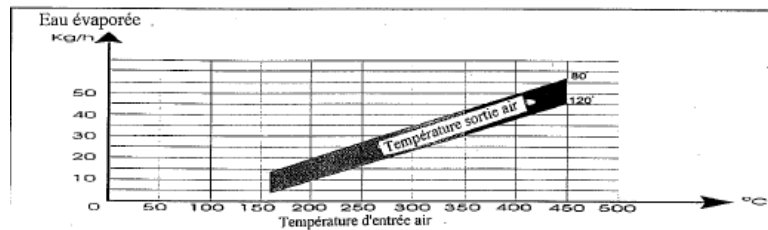
Installation Pilote de Séchage



Installation de Base PSD 55

APV Anhydro AS  
Drying & Evaporation

Installation de base PSD-55	Caractéristiques techniques
<p>* L'installation de base illustrée est équipée de l'option atomiseur centrifuge ainsi que d'une échelle et d'un garde-corps.</p>	<p><b>Dimensions</b></p> <p>Encombrement au sol : 1.55 x 2.34 m            Hauteur, installation de base : 2.70 m            Hauteur, y compris (atomiseur centrifuge) : 3.10 m            (pour la dépose de l'atomiseur) : 3.66 m            (Haut du garde-corps) : 3.75 m            Hauteur libre recommandée : 4.50 m            Diamètre de la chambre de séchage : 1.25 m            Volume d'expédition : 12 m<sup>3</sup>            Poids brut : 2200 kg            Poids net : 1500 kg</p>
	<p><b>Courant électrique</b></p> <p>Alimentation : 3 x 400 V+N+PE, 50 Hz            ou 3 x 230 V+PE, 50 Hz            -Réchauffeur d'air électrique : 48 kW            -Ventilateur aspirant : 2.6 kW</p>
	<p><b>Capacité</b></p> <p>Débit d'eau évaporée : 28 kg/h (300/90°C)            Température maximum de l'air à l'entrée : 350°C            Débit d'air régulé : 500 m<sup>3</sup>/h</p>
	<p><b>Résistance aux chocs de pression</b> : 1 bar (g)</p>
	<p><b>Niveau de bruit</b> : 87 dB (A)</p>
	<p><b>Matériaux</b></p> <p>Parties en contact avec le produit : AISI 316            Surfaces extérieures : AISI 304</p>
	<p><b>Homologation CE</b></p> <p>Réglementations : Conformité UE            *Assurance qualité : ISO 9001</p>



**Autres versions :**  
 Version en circuit fermé disponible, par ex. pour des produits contenant des solvants organiques  
 Version pharmaceutique disponible sur demande.  
 Data Sheet No. : PSD55/DSH/BASIC  
 Revision : 02.25.08.97 - BASIC FR  
 Approved by: FW  
 Date: 02.19.1997

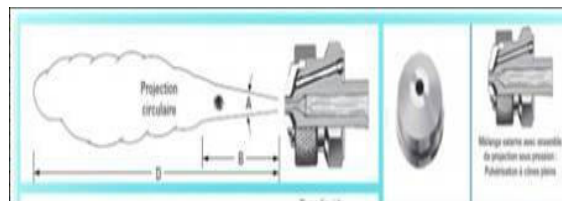


Figure 72 - Spray-Dryer APV specifications Sheet and representation of a two fluid nozzle (pneumatic) with external mix

## Appendix B - Tests Results

This section presents all results not showed in the report.

### FeCuAl Synthesis

Table 12 presents results of the three FeCuAl synthesis we realized.

Table 12 - Data concerning FeCuAl synthesis

	Temperature (°C)	pH	time (min)	NaOH Volume (L)	Mixed Nitrate salts Volume (L)	Commentaries
120416	72	3,4	72	131,5	326,9	problem with pH meter
120424	71,5	8,01	121	155,9	424	-
120509	73	8,06	108	113	308,6	-

### Granulometry of FeCuAl

#### Test 120530

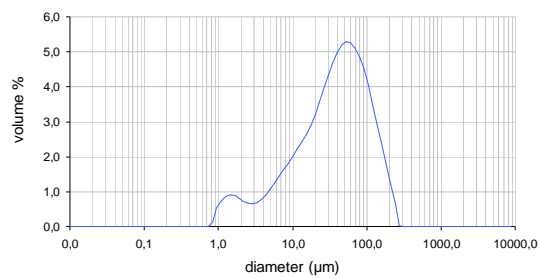


Figure 73 - Particle size distribution for product 120530 calcined at 700°C

#### Test 120607

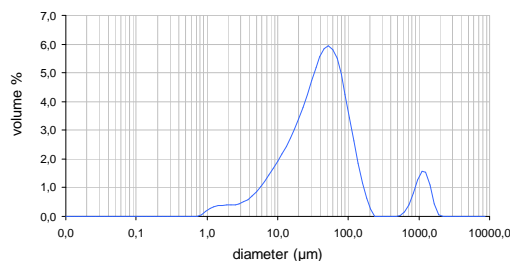


Figure 74 - Particle size distribution for product 120607 calcined at 700°C

### Test 120611

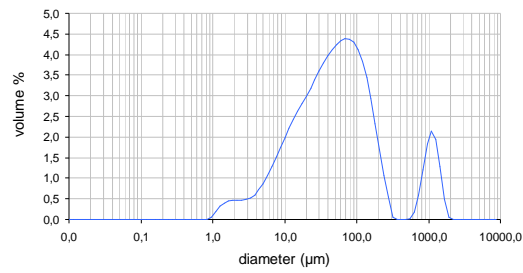


Figure 75 - Particle size distribution for product 120611 calcined at 700°C

### Test 120612b

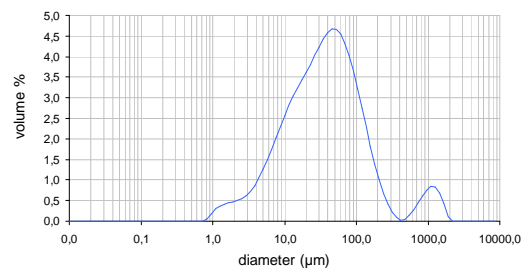


Figure 76 - Particle size distribution for product 120612b calcined at 700°C

### Test 120615

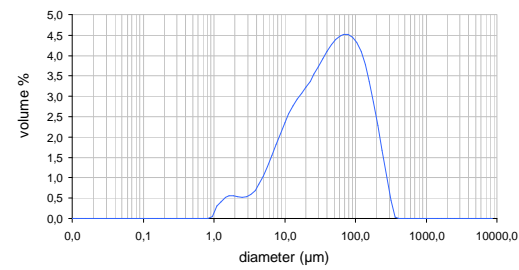


Figure 77 Particle size distribution for product 120615 calcined at 700°C

### Test 120618c

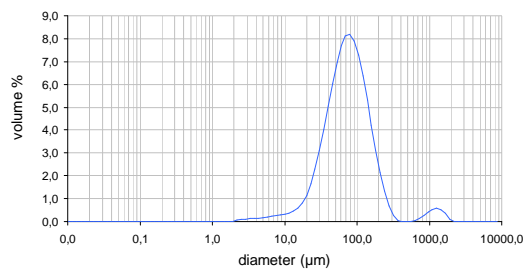


Figure 78 - Particle size distribution for product 120618c calcined at 700°C

# Scanning Electron Microscopy Analysis

## Test 120523

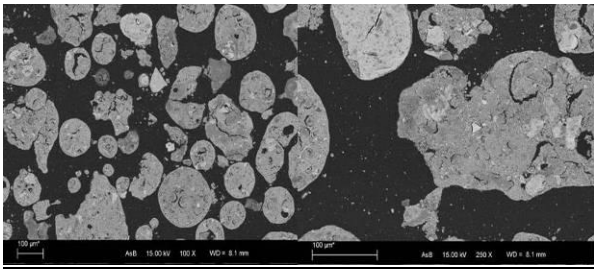


Figure 79 - SEM photos of product 120523

## Test 120524

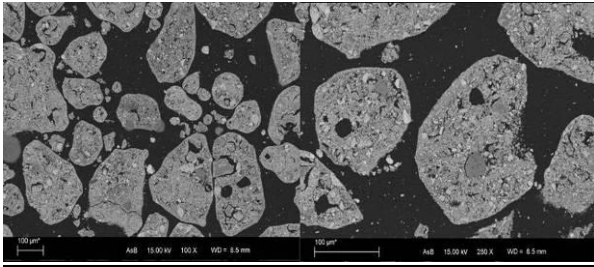


Figure 80 - SEM images of product 120524

## Test 120530

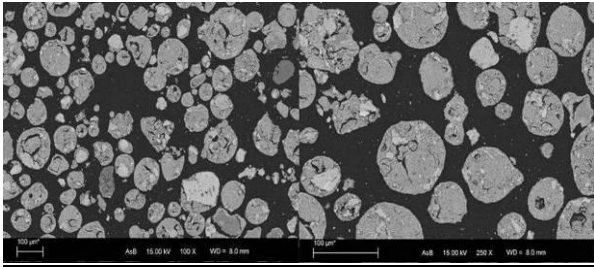


Figure 81 - SEM images of product 120530

## Test 120601

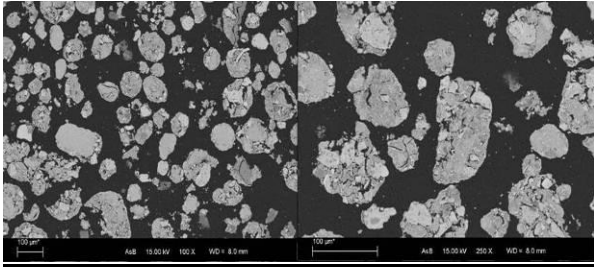
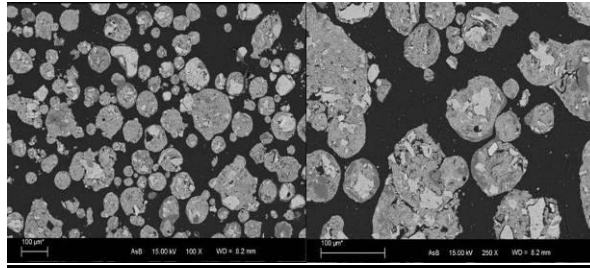


Figure 82 - SEM images of product 120601

**Test 120604**



**Figure 83 - SEM images of product 120604**

**Test 120605**

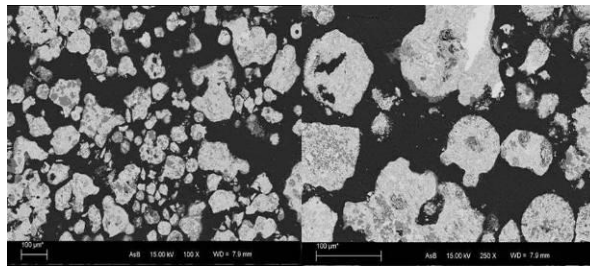


**Figure 84 - SEM images of product 120605**

**Test 120607**

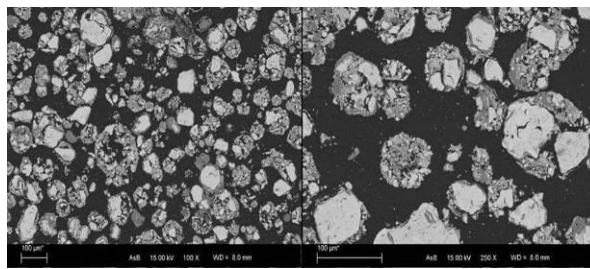


**Figure 85 - SEM images of product 120607**

**Test 120618**

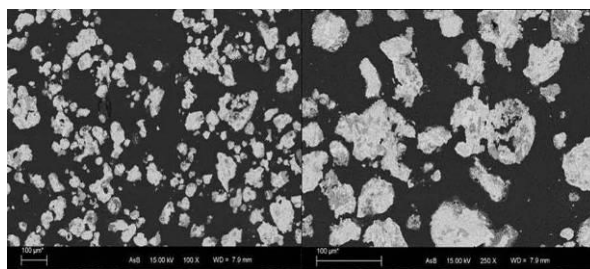


**Figure 86 - SEM images of product 120618**

**Test 120618b**

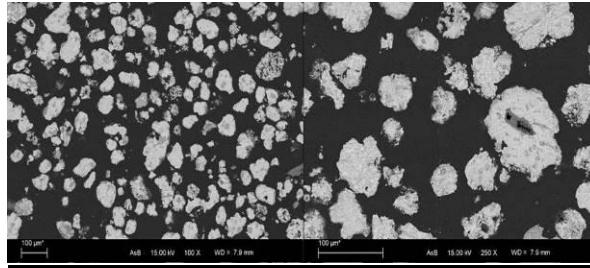


**Figure 87 - SEM images of product 120618b**

**Test 120618c**

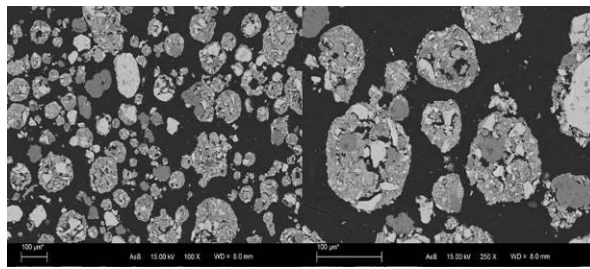


**Figure 88 - SEM images of product 120618c**

# Appendix C – Particle morphology in spray-drying

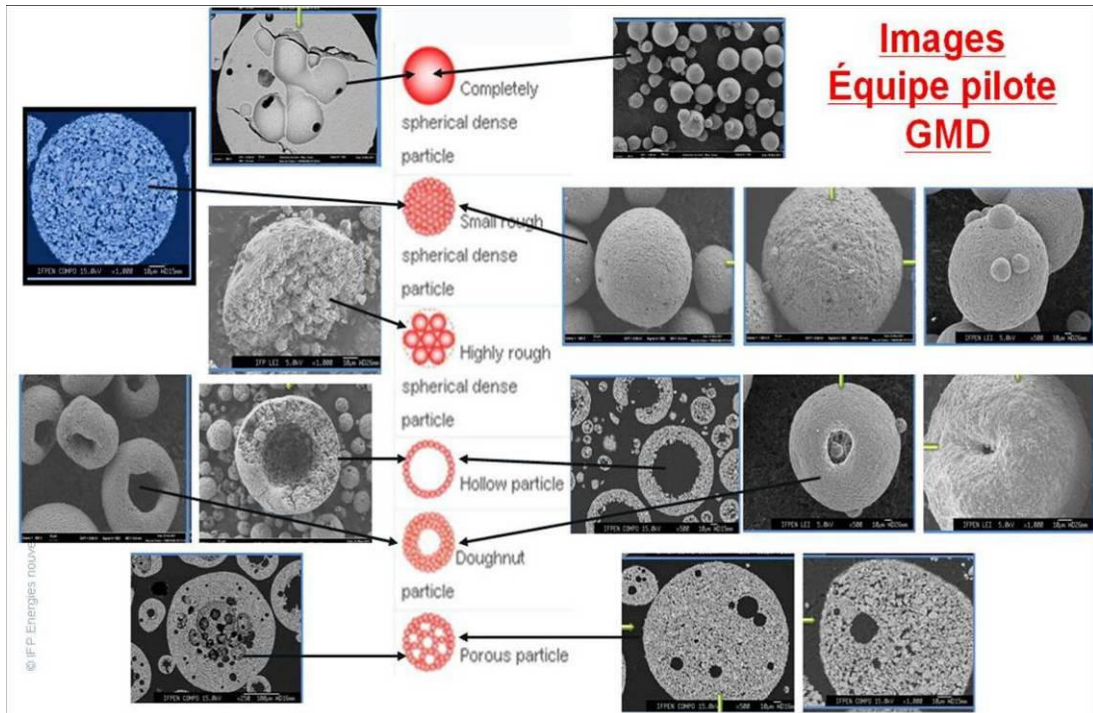


Figure 89- Examples of particle morphology obtained on IFPEN spray dryer

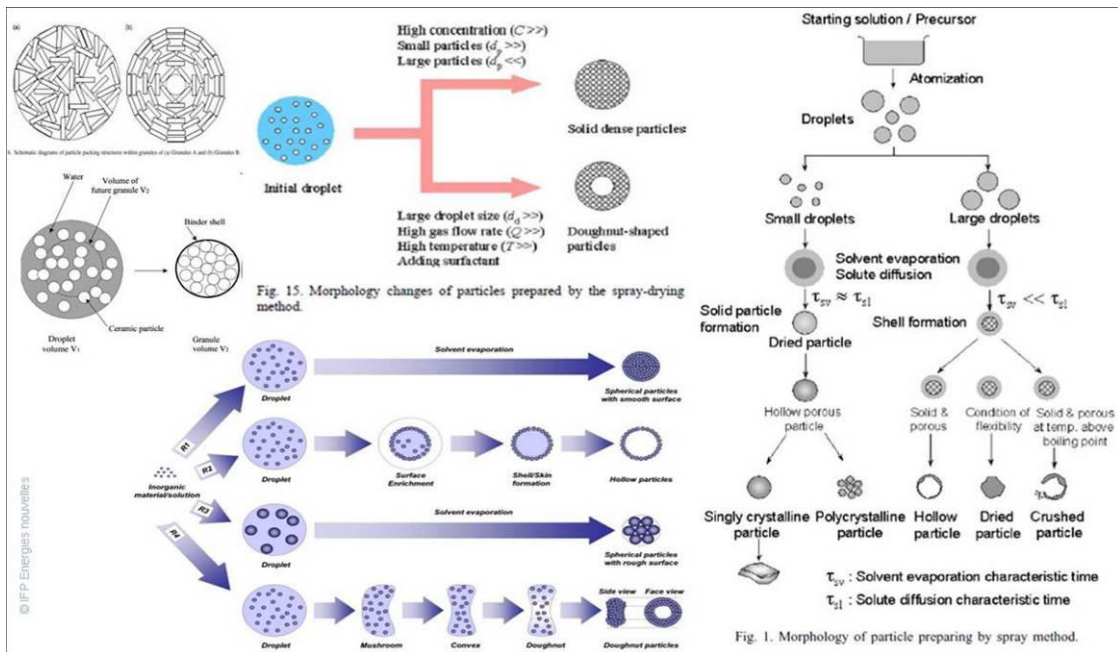


Figure 90- Elements of understanding on morphology changes that occur during spray drying